Charles University in Prague

Faculty of Mathematics and Physics

Institute of Physics of Charles University

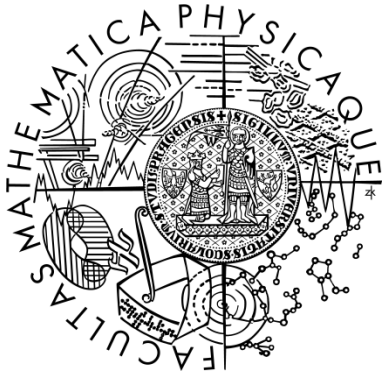

Doctoral thesis

Mgr. Věra Ňuňuková

Biophysical studies of membrane transport proteins from Nramp/MntH family and their function

Supervisor: RNDr. Roman Chaloupka, Ph.D.

Study program: Physics – Biophysics, chemical and macromolecular physics

Univerzita Karlova v Praze

Matematicko-fyzikální fakulta

Fyzikální ústav Univerzity Karlovy

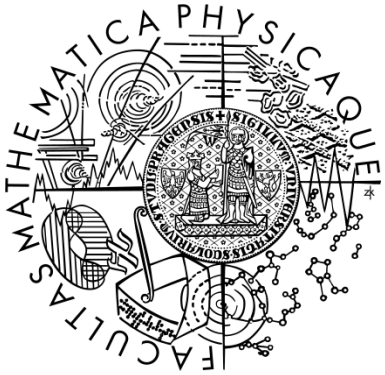

Disertační práce

Mgr. Věra Ňuňuková

Studium membránových transportních proteinů z rodiny Nramp/MntH a jejich funkce pomocí biofyzikálních metod

Vedoucí disertační práce: RNDr. Roman Chaloupka, Ph.D.

Studijní program: Fyzika – Biofyzika, chemická a makromolekulární fyzika

Acknowledgments

This work was supported by Charles University (7344/2007) to Věra Ňuňuková, Czech Science Foundation (204/07/0558) to Roman Chaloupka, Canada Foundation for Innovation (CFI: 6786) and the Natural Sciences and Engineering Research Council of Canada (NSERC: 250119) to Masoud Jelokhani-Niaraki.

Personally, I would like to firstly thank my supervisor RNDr. Roman Chaloupka Ph.D. and my consultant RNDr. Eva Urbánková Ph.D., who have given me this great opportunity to work on such an interesting and challenging project and for their advices and assistance throughout the whole study. I would also like to thank my supervisor at Wilfrid Laurier University in Canada Dr. Masoud Jelokhani-Niaraki, whose advice, patience and assistance not only in the lab was most appreciated. A big thanks to my Canadian colleagues at WLU for their company and for keeping the lab a great environment to work in. A very big THANK YOU to my family for their support and belief in me. Last but not least, thank you to Leos-my better half, for all his patience, support and understanding.

Declaration of Authorship

I hereby declare that this thesis and the work presented in it are my own and have been generated by me as the result of my own original research.

……

Mgr. Věra Ňuňuková

Table of contents

List of Abbreviations

Arg	Arginine
CD	Circular Dichroism
CMC	Critical micellar concentration
DMT	Duodenal metal transporter
DPhPC	1,2-diphytanoyl-*sn*-glycero-3-phosphocholine
DPhPG	1,2-diphytanoyl-*sn*-glycero-3-[phospho-*rac*-(1-glycerol)]
E. coli	*Escherichia coli*
ErbB	Epidermal Growth Factor Family
GlyR	Glycine receptors
GpA	Glycophorin A
His	Histidine
HPLC	High performance liquid chromatography
CL	Cardiolipin
MD	Molecular dynamics
Me^{2+}	Divalent metal ions
MntH	Proton-dependent manganese transporter
NMR	Nuclear magnetic resonance
Nramp	The natural resistance-associated macrophage protein
NRMSD	Normalized Root Mean Square Deviation
POPC	1-palmitoyl-2-oleoyl-*sn*-glycero-3-phosphocholine
POPE	1-palmitoyl-2-oleoyl-phosphatidylethanolamine
POPG	1-palmitoyl-2-oleoyl-3-phosphatidylglycerol
SDS	Sodium dodecyl sulfate
SUV	Small unilamelar vesicles
TFA	Trifluoroacetic acid
TFE	2,2,2-trifluorethanol
TMS	Transmembrane segment
Trp	Tryptophan

List of Figures

Figures in Appendices

List of Tables

Tables in Appendices

Abstract

Three synthetic peptides corresponding to transmembrane segments TMS1, TMS3 and TMS6 of secondary-active transporter MntH from *Escherichia coli* were used as a suitable alternative model enabling to study TMS structure, TMS interaction with membranes, TMS mutual interaction and also function of MntH. The secondary structure of the peptides was estimated in different environments using circular dichroism spectroscopy. These peptides interacted with and adopted helical conformation in lipid membranes. Electrophysiological experiments demonstrated that individual TMS were able under certain conditions to form ion channels in model biological membranes. Electrophysiological properties of these weakly cation-selective ion channels were strongly dependent on surrounding pH. Manganese ion, as a physiological substrate of MntH, enhanced the conductivity of TMS1 and TMS6 channels, influenced the transition between closed and open states and affected the conformation of all studied peptides. For TMS3 Mn^{2+} was crucial for formation of ion channels. It was shown that a single functionally important TMS can retain some of the functional properties of the full-length protein. These findings can contribute to understanding of structure-function relationship at the molecular level. However, it remains unclear to what extent the peptide-specific channel activity represents a functional aspect of the full-length membrane carrier protein.

Keywords: divalent metal ions, membrane transport, MntH, Nramp, patch clamp, CD spectroscopy

Abstrakt

Syntetické peptidy odpovídající svojí sekvencí transmembránovým segmentům TMS1, TMS3 a TMS6 sekundárně aktivního transportního proteinu MntH z bakterie *Escherichia coli* byly použity jako model pro studium struktury, interakce s modelovými membránami, vzájemné interakce TM segmentů a jejich funkce. Sekundární struktura byla pomocí spektroskopie cirkulárního dichroismu určována v různých prostředích. Studované peptidy interagovaly s lipidovou membránou a získávaly v tomto prostředí helikální konformaci. Elektrofyziologické experimenty dokázaly, že samostatné TMS jsou schopny za určitých podmínek tvořit iontové kanály v modelových biologických membránách. Elektrofyziologické vlastnosti těchto slabě kationtově selektivních kanálů jsou silně závislé na pH okolního prostředí. Mangan, jako fyziologický substrát MntH, zvýšil vodivost kanálů tvořených TMS1 a TMS6 a ovlivnil přechod mezi zavřeným a otevřeným stavem kanálu. Byl pozorován vliv manganu na konformaci všech studovaných peptidů. V případě TMS3 byla přítomnost Mn^{2+} pro tvorbu iontových kanálů dokonce nezbytná. Bylo dokázáno, že kanál tvořený funkčně důležitým TMS může do určité míry zachovat funkční vlastnosti celého proteinu. Tyto výsledky mohou přispět k porozumění vztahu mezi strukturou a funkcí na molekulární úrovni. I přesto však zůstává nejasné, do jaké míry peptidově specifická kanálová aktivita reprezentuje funkční aspekt celého membránového trasnportního proteinu.

Klíčová slova: dvojmocné kovové ionty, membránový transport, MntH, Nramp, patch clamp, CD spektroskopie

1. General Introduction

The focus of this study is on one bacterial member of the Nramp (**N**atural **r**esistance-**a**ssociated **m**acrophage **p**rotein) family – MntH (**Proton**-dependent **m**a**n**ganese **t**ransporter) from *Escherichia coli* (*E. coli*). The Nramp family is a group of secondary active divalent metal ion transporters, conserved throughout the evolution, playing an important role in biological processes [1-3]. So far, most information about this divalent metal ion/proton symporter was obtained using the whole-cell model system. Due to the difficulties with experimental procedures involved in membrane protein isolation purification and reconstitution, another possible approach was needed. As an alternative to this approach, synthetic peptides corresponding to transmembrane segments (TMS) were used as a model system. Three essential transmembrane segments of the secondary-active transporter were studied, focusing on the possible role of these domains in the structure and function of a full-length MntH. These segments contain important residues and understanding of their structural and functional properties could be essential for understanding of the structure-function relationship of the transporter.

This introduction gives a brief overview on general membrane transport principles, followed by the explanation of the transport of metal ions, and thereafter the Nramp family is introduced. At the end of the chapter the details about the experimental approach using transmembrane peptides as a model system are explained.

1.1 Membrane transport

In general, the passage of solutes across membranes can occur via protein-independent diffusion or protein-dependent transport processes. Protein-dependent transport includes transport via carriers or channels [4]. Channel proteins form small hydrophilic pores in the membrane, through which solutes can pass. The solutes still follow their concentration gradient without requirement of energy. This transport, due to its similarity to diffusion, is called “facilitated diffusion”. On the other hand, carriers bind the solute on one side and deliver it to the other side of the membrane, through a change of conformation of the carrier protein. Carrier binds the solute with great specificity, it is this requirement for specific binding which makes the transport selective. Transport can also occur against a concentration gradient and consequently requires energy. Mostly the solutes transported in this way are either small organic molecule or inorganic ions.

In contrast to primary active transport (driven by ATP hydrolysis), the secondary active transport is not directly coupled with ATP hydrolysis. The chemical coupling uses the free energy produced by the electrochemical potential of another solute. Pre-existing gradients which are maintained by the action of primary systems are used as driving forces. The solutes can be transported in several different ways. Some of the carriers transport a single solute across the membrane (uniport). Coupled transport, where the transport of one solute strictly depends on the transport of the second, involves either the simultaneous transfer of the second solute in the same direction (symport as for example with MntH the symport of metal ions and protons, see Fig. 1.1) or the transfer of a second solute in the opposite direction (antiport) [4].

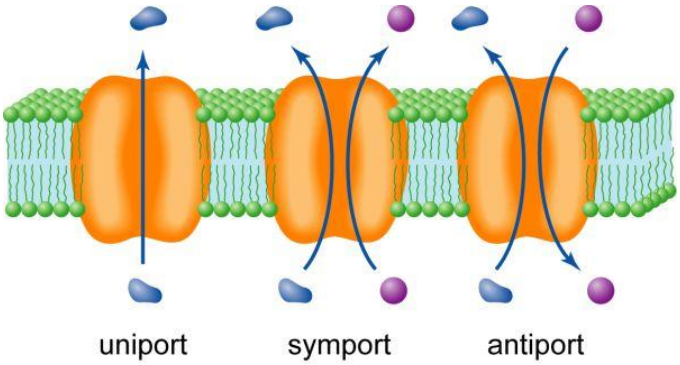

Figure 1.1: Coupled transport of solutes [4]

Membrane transport proteins belong to the group of integral membrane proteins able to span the entire phospholipid bilayer. Most integral proteins contain residues with hydrophobic side chains. These interact with fatty acyl groups of the membrane phospholipids, thus anchoring the protein to the membrane. In the most common case, the membrane spanning domains of integral proteins are α-helices or possibly multiple β-strands forming β-barrel structure within the membrane [5].

1.2 Metal ion transport

Metal ions are important for all living cells and participate in numerous metabolic junctions as cofactors of many enzymes, gene regulation, oxidative phosphorylation, free-radical homeostasis and signal transduction pathways [1,6]. There are several transport systems maintaining the homeostasis of metal ions. A high level of regulation is crucial because limited activity of a single metal ion transporter may inhibit cell growth due to the shortage of a vital metabolic element, and excess transporter activity may be toxic and lead to cell death [6]. In some of the cellular organelles and the plasma membrane, high

and low affinity transporters act in concert to maintain the right balance of metal ion concentrations [7-9].

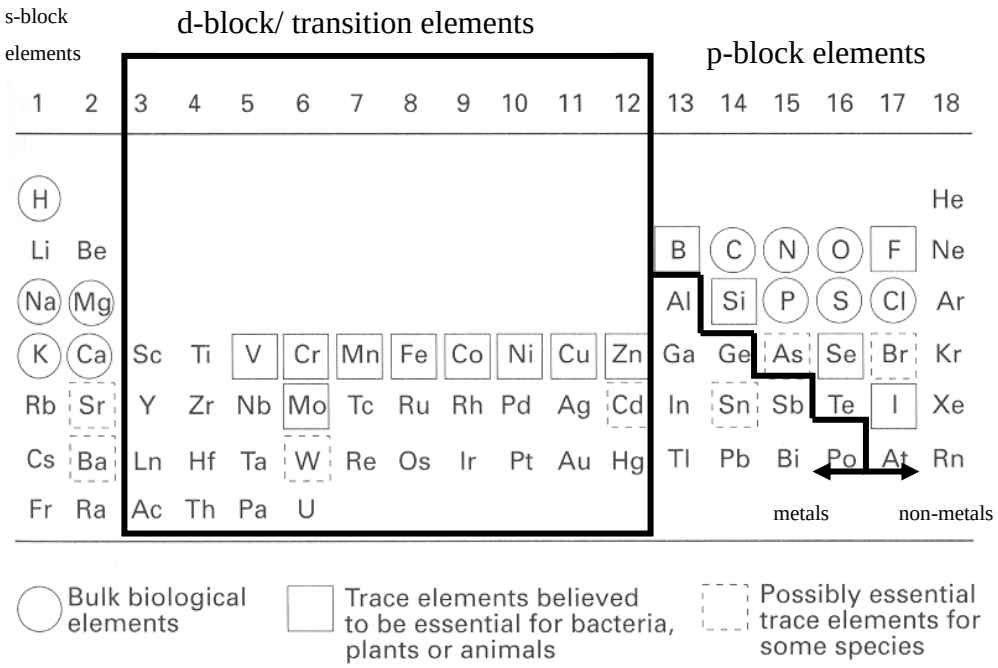

Figure 1.2 Periodic table of the metal elements [10]. The f-block elements (lanthanides and actinides) are not shown. The group of the d-block/transition elements is highlighted by a square. Most "trace elements" are found within this group (boxed). Bulk essential elements are circled. The black line is the border between metallic elements (on the left) and non-metals (on the right). This border is not strict, since the elements near it do not possess features strictly metallic or non-metallic, respectively. It is noteworthy that the elements essential for life are the lighter elements, which are also most abundant on earth [10].

Metal ion homeostasis is maintained through highly regulated processes of uptake, storage and secretion. Homeostasis of metal ions is governed by two evolutionary consequences (i) redox reactions are fundamental life processes and transition metals are essential for the function of most proteins involved in redox reactions, hence living cells compete for metal ion resources; (ii) The development of several life processes involves toxic reagents that, when present in abnormal amounts, cause damage to the very function that they serve and to proteins and nucleic acids that are present in their proximity. For example the mammalian brain utilizes components such as NO, CO and metal ions that inflict damage during their normal physiological action [6,11].

Essential elements such as copper, manganese, iron or zinc, which belong to the group of transition metals, are only needed in trace amounts (Fig 1.2). However, this does not derogate their importance [10]. Manganese ion is necessary to both free-living and

pathogenic bacterial cells for nutrient and defense purposes [12,13]. This redox active metal is a key cofactor for a wide range of metalloenzymes, including oxidases and dehydrogenases, DNA and RNA polymerases, kinases, decarboxylases, and sugar transferases [14]. It is mainly known to be involved in the oxygen production in the oxygen evolving complex in photosystem II and for its action in the dismutation of the superoxide anion as a cofactor in MnSOD (manganese superoxide dismutase). Mn^{2+} can function in place of Mg^{2+} in a variety of both structural and catalytic roles [15]. Despite its role as a nutrient it can be also toxic. In humans manganese toxicity is recognized to be a serious health hazard resulting in severe pathologies of the central nervous system. If the exposure occurs for a long period of time, the toxicity can result in a permanent crippling of the extrapyramidal system, with symptoms reminiscent of Parkinson disease [16]. The cellular requirements for manganese (submicromolar levels) are generally much lower than for iron [17]. Iron, which is symported with protons by Nramp2 [18], is an essential component of hemoglobin, cytochromes and variety of other enzymes. Together with copper, they are cofactors of a large number of metalloproteins catalyzing redox reactions. Furthemore, zinc is essential for the formation of the "zinc-finger", a structural element in proteins important for the functionality of transcription factors in transcriptional regulation. It is also a cofactor of enzymes involved in the synthesis of nucleic and amino acids [19].

A number of uptake mechanisms for micronutrients such as metal ions have evolved and many of them have been characterized in prokaryotes and eukaryotes. Metal ion transporters provide an efficient tool for competition for the limited resources, and at the same time their regulation should provide solution to the changing environment and the potential damage inflicted by abnormal concentrations. The calcium homeostasis is maintained by the coordination transport system, like Ca^{2+} ATPases [20,21,22], Na^{+}/Ca^{2+} [23,24] and H^{+}/Ca^{2+} exchangers [25,26] and several other transport systems. Iron uptake to mammalian cells involves receptor-mediated endocytosis [27]. Other important metal ions, which are essential for the life cycle of eukaryotic cells like Mn^{2+} and Zn^{2+} are transported by several families of transporters like CDF family (cation diffusion facilitator proteins) identified in bacteria, archaea and eukaryotes (reviewed in [28]), CPx-type ATPases (including P-type ATPases) transporting metal ions across the membrane [29] or ZIP family. ZIP stands for Zrt, Irt-like protein. Zrt1 (zinc regulated transporter 1) is an *S. cerevisiae* zinc transporter [30]; Irt1 (iron regulated transporter 1) functions as an iron transporter in *Arabidopsis thaliana* [31]. The ZIP family includes members from plants,

protozoa, insects, mammals and fungi, as well as from eubacteria and archaea [32]. Another important family participating in divalent metal ion homeostasis is the Nramp family briefly introduced in the next section.

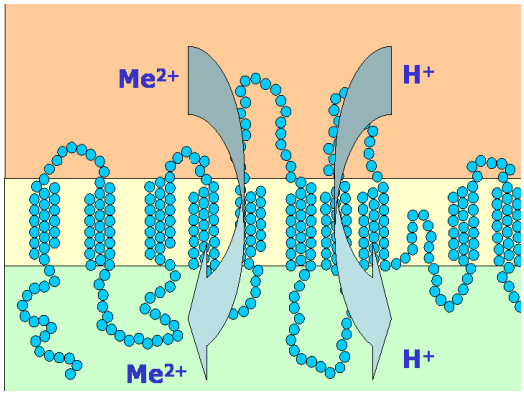

Figure 1.3 Metal symport of a member of Nramp family

1.3 The Nramp family

The Nramp family of secondary active divalent metal ion membrane transport proteins plays an important role in a variety of biological processes include metal ion homeostasis [1-3] and innate immunity [33,34]. This family has been highly conserved throughout evolution. Members of the Nramp family share remarkable protein sequence identity: yeast (28%), plant (40%), and fly (55%) with sequence identity to the mammalian proteins (46%, 58%, and 73% similarity, respectively) [35]. The Nramp proteins are electrogenic divalent metal ion/proton symporters with broad specificity for d- block transition metals, including manganese, iron, cobalt, cadmium, zinc, copper and nickel (Fig. 1.3) [1,34,36,37]. It consists of five phylogenetic groups – three bacterial groups (MntH A, MntH B and MntH C) and two eukaryotic groups (prototypical and archetypical group). The existence of bacterial Nramp homologs suggests that the Nramp family originated in prokaryotes [3,38].

Nramp proteins are present in eukaryotes, but also in yeast (Smf proteins) [39] and bacteria [36]. Except for yeast homologs, eukaryotic Nramp proteins are composed of twelve TMS (transmembrane segments) [37,39,40], whereas bacterial MntH transporters are integral transmembrane proteins predominantly with eleven TMS (Fig. 1.4).

1.3.1 Nramp1 (SLC11A1)

Nramp1 has been identified in the mouse *Bcg*/*Ity*/*Lsh* locus by positional cloning [41]. It was found to be identical to the Ity and the Lsh gene conferring resistance to infections by *Salmonella typhimurium* and *Leishmania donovani*, respectively [42]. Nramp1 is expressed in lysosomal compartment of macrophages and neutrophils and recruited to the membrane of the pathogen-containing phagosomes upon phagocythosis [43-45]. It was proposed that Nramp1 encodes an integral membrane protein that has structural homology with known prokaryotic and eukaryotic transport systems [46].

This transporter is, due to its exclusivity in metal transport (Fe^{2+}, Mn^{2+} and Co^{2+}) across the phagosomal membrane of macrophages, necessary for the defense against bacterial infection [33,47]. In humans, polymorphic variants at Nramp1 are associated with increased susceptibility to tuberculosis and leprosy [48,49].

1.3.2 Nramp2 (DMT1, DCT1, SLC11A2)

The second member of the Nramp family, Nramp2 was identified as a gene expressed in the duodenum of rats and capable of transporting divalent metal ions with an unusually broad substrate specificity (including Mn^{2+}, Zn^{2+}, Co^{2+}, Cd^{2+}, Cu^{2+}, Ni^{2+} and Pb^{2+}) [1]. Nramp2 plays several important roles in iron metabolism. It mediates metal ion transport which is H^{+}-coupled and voltage dependent. It is driven by the H^{+} electrochemical potential gradient. As opposed to *Nramp1*, which is expressed exclusively in mononuclear phagocytes such as tissue macrophages [46], *Nramp2* mRNA expression is more ubiquitous and has been detected in most tissues and cell type's analyzed [1,50,51]. However, its levels of expression are higher in the brain, thymus, proximal intestine, kidney, and bone marrow [1]. The overall identity with Nramp1 is 64%, identity of mammal Nramp2 to Nramp1 over the hydrophobic core is 78% [43]. Genetic studies in rat and mouse models revealed that Nramp2 is unconditionally required for the maintenance of life. Mutations in Nramp2 affect iron homeostasis, and cause defects in intestinal iron uptake resulting in severe iron disorders (microcytic anemia and serum and hepatic overload) [52]. Nramp2 deficient rats also show marked Mn^{2+} deficiency [53]. Study focusing on the localization of human Nramp2 showed that the protein colocalizes with markers for late endosomes/lysosomes but not with the transferrin receptor (TfR, which is

a marker for sorting and recycling endosomes and the plasma membrane) in non-intestinal cells [54]. After these results it was suggested that Nramp2 is involved in the distribution of iron in non-intestinal cells as well as in absorption of intestinal iron. Three pathways have been proposed in which Nramp2 may play a role: i) nutritional iron absorption in enterocytes, ii) recycling of iron from phagocytosed erythrocytes, and/or iii) transferrin-dependent iron uptake in erythrocytes and other cells [54].

1.3.3 Smf

There are three functionally distinct forms of the Nramp transporters in yeast – Smf1p, Smf2p, and Smf3p. They have been identified and characterized in *Saccharomyces cerevisiae*. [34,39]. These three transport proteins operate in distinct cellular compartments to differentially affect the transport and intracellular trafficking of iron and manganese ions and to lesser extent cobalt and copper [55]. Smf1p is a proton coupled metal transporter capable of translocating a wide range of divalent heavy metals, expressed on the cell surface. The proposed physiological function of Smf1p is to contribute to manganese uptake when cells are starved for this metal e.g., by depleting manganese with EGTA [55]. Smf1p together with Smf2p were shown to mediate Fe^{2+} uptake into *Xenopus laevis* oocytes [56] and contribute to copper and cadmium accumulation. Smf2p can affect cobalt levels in yeast [57] and may also participate in manganese trafficking [58]. Smf3p participate in iron metabolism in yeast as well. The major role is in controlling the cellular iron ion levels. It mobilizes vacuolar stores of iron in conditions of low iron levels [39,59].

1.3.4 MntH

MntH is a bacterial homolog of Nramp. It is a primary high-affinity Mn^{2+} transporter of *Escherichia coli* with a considerable homology to the eukaryotic Nramp proteins [60]. This homology to the eukaryotic family members and the fact that the Nramp family originated in prokaryotes (Cellier et al. 2001, Richer et al. 2003) makes MntH an attractive prototypic model of the Nramp family. Three bacterial groups MntH A-C differ in sequence (26-29 ± 3% identical) and in site-specific evolutionary rates [61]. Bacterial MntH transporters are integral transmembrane proteins predominantly with 11 TMS (Fig. 1.4). The N–terminus of the protein is located in cytoplasm and its C–terminus is exposed to the periplasmic side of the membrane as confirmed for MntH of *E. coli* [62]. The influx system of MntH

mediates the influx of Mn^{2+} with an affinity of about 0.1 μM in *Salmonella enterica ssp. typhimurium* and of 0.5 μM in *E. coli* [15]. In accordance with broad metal specificity of eukaryotic Nramp proteins, MntH of *E. coli* is also able to transport Cd^{2+}, Zn^{2+}, Co^{2+}, Fe^{2+} and probably also Cu^{2+} and Ni^{2+} [36,63]. Fe^{2+} is transported with an affinity of > 10 μM, far higher than physiological concentrations of free Fe^{2+}.

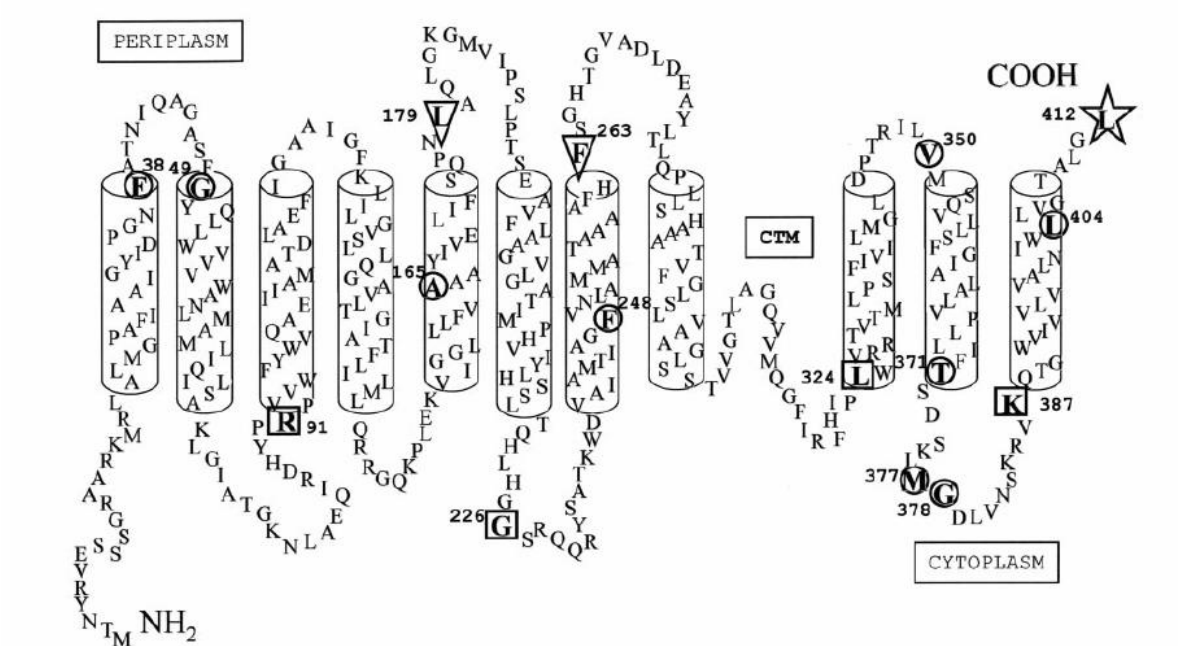

Figure 1.4 *Ecoli* MntH consensus transmembrane topology [62]

1.4 Transmembrane peptides

So far, practically all experimental information about Nramp family was acquired using the whole-cell model systems [40]. Because of difficulties with experimental procedures involved in membrane protein isolation purification and reconstitution, another possible approach was needed. This approach was to what is sometimes referred as a "divide and conquer" approach to membrane protein [64]. The fundamental explanation is to divide an α-helical membrane protein into its constituent transmembrane domains, which can normally be produced more easily and investigated in a wider range of membrane-mimetic systems than their full-length parent protein [65]. Peptide folding and insertion into membrane are nowadays widely studied using this approach.

Applicability of this approach is supported by the fact that, the folding of membrane proteins is considered as a four steps process, according to the current four-step thermodynamic model of membrane folding [66]. Previous hypothesis proposed three-step model [67], composed of interfacial partitioning, folding and insertion. A year later, two-

stage hypothesis was proposed [68]. According to this model, at first hydrophobic peptide sequence form independently stable α-helical TM domains upon insertion into bilayer. In the second step, membrane embedded helices interact with each other to establish protein's tertiary structure [65]. This hypothesis has found support from thermodynamic arguments [67-69] and also from protein fragmentation studies [70-73]. Four-step model was a combination of these two models [66].

Due to the fact that transmembrane domains could be considered as independent, peptide folding and insertion can be studied on individual transmembrane segments. Utilizing simple functional domains of the full-length membrane proteins can lead to valuable insights into their structure-function relationship. Synthetic peptides corresponding to the TMS of membrane proteins have been previously used as alternative models for studying the structure and interaction of membrane proteins with biological membranes [74].

TM peptides can be obtained by proteolytic cleavage of naturally occurring or recombinantly engineered proteins, like full-length glycophorin A (GpA) produced by tryptic fragmentation [70], or by means of chemical synthesis. This latter method, published by Galardy & Kortylewicz for the first time in 1985, is dominant nowadays thanks to advances in solid-phase peptide synthesis [75]. An alternative way of obtaining TM peptides is through biosynthesis in cell culture, especially in case of difficult chemical synthesis of exceptionally long or isotopically labeled peptides [65]. Several model systems for studying the secondary structure of TM peptides are available with their strength and weaknesses as summarized in the next subsection.

1.4.1 Model systems for studying the secondary structure of TM peptides

The majority of peptides corresponding to membrane-spanning regions are too hydrophobic to be soluble in aqueous solutions. TM peptides are usually largely unfolded and behave like random coils when dissolved as monomers in aqueous solutions [76,77]. A notable example of water-soluble TM peptide is TM helix 3 of bacteriorhodopsin. Engelman and coworkers synthesized and characterized seven peptides, corresponding to seven transmembrane domains of the full-length protein. Within these TMS the third TM helix is soluble in aqueous solutions in the absence of membrane-mimetic systems [78]. More often, isotropic solvents, such as TFE, as a simple membrane-mimetic system for peptides are used. Obvious advantages of isotropic solvents are the high solubilities of many TM peptides and the straightforward applicability of a broad spectrum of

experimental methods [65]. Molecular dynamics simulation suggest, that isotropic organic solvents such as DMSO [79] and TFE [80] induce peptide secondary structure by preferential clustering around the peptide and thus limiting water access to the peptide backbone. Formation of any type of secondary structure will be promoted by TFE as long as requirements for intramolecular hydrogen bonding are satisfied [65]. On the other hand, isotropic solvents usually disrupt the tertiary and quaternary contacts at high solvent concentrations, because their solvent shells impair such interactions. Thus, while organic solvents are frequently used in structural studies on single, monomeric peptides, they are widely considered unsuitable for investigations of helix-helix interactions and peptide oligomerization [65]. However, oligomers, composed of peptide corresponding to TM domain 4 of DMT1 and TMS4 of Nramp1, were discovered even in 100% TFE [81-84], using diffusion-ordered NMR spectroscopy. The helicity of TMS4 of Nramp1 in pure TFE was clearly dependent on peptide concentration. Even though isotropic solvents offer a good starting point for further investigations of TM peptide, the information gathered from organic isotropic solvents should be interpreted with caution when extrapolating to more complex systems [65].

Another system for studying membrane-interacting peptides is detergent micelles. Detergents are amphiphilic compounds, consisting like bilayer-forming lipids of bulkier hydrophilic headgroups and hydrophobic tail. This molecular shape impedes self-association of peptides when the detergent concentration exceeds the critical micellar concentration (CMC). SDS as the most common representative of denaturing detergents has been suggested to directly bind to helix-helix interfaces by van der Waals forces, thereby inhibiting interhelical interactions [85]. However, micelles are still used for studying peptide oligomerization innumerous studies by Lemmon and co-workers and others [86-88]. One of these studies focused on oligomerization of TMS4 of DMT1 in SDS [81,82] as an extension of their studies in 100% TFE or 40% HFIP.

Lipid vesicles are versatile model systems for studying TM peptides. Lipid bilayers offer an environment to peptides and proteins that more closely resembles natural membranes than do isotropic solvents or detergent micelles. Lipid vesicles were used to compare the dimeric structure of glycophorin A (GpA) TM domain with the corresponding structure in detergent micelles [89,90]. Although the differences in GpA dimer structure between micelles and vesicles are partially due to an insufficient number of distance constraints in the micellar system [90], three observations are worth mentioning: First, in

lipid bilayers, but not in micelles, glycine-glycine (G79, G83) contacts are obvious, which are abundant in helix–helix interfaces of membrane proteins [91,92]. Second, the bilayer-embedded dimer is stabilized by an interhelical hydrogen bond (1T87↔2I88), which does not show up in the micelle-suspended dimer [89,93]. Third, the dimer structures obtained in DMPC and POPC bilayers are indistinguishable in spite of marked differences in hydrophobic bilayer thickness. Thus, although the dimer structures in micelles and bilayers share the same overall fold, they substantially differ in their structural details. By contrast, the choice of lipid constituting the bilayer is less relevant to this dimer structure, at least for the two phospholipids used in the present example [65]. The study on GpA [90,94] and bacteriorhodopsin [76] demonstrated that the folding of individual TMS is comparable with the overall conformations of these domains in proteins.

This experimental approach could be used not only for structural studies, but also for studying functional properties of the peptide. The peptides representing TMS of nicotinic acetylcholine receptor [95], cystic fibrosis chloride channel [96] and uncoupling proteins [97] showed functional properties comparable to the native proteins. Results of these studies indicate that individual TMS can assume membrane-integrated conformations and form native-like interactions leading to formation of ion channels [74]. Another study demonstrating channel-like conductance of TM peptide was performed by Betz and co-workers [98]. In glycine receptor (GlyR) channel-like conductance profiles were studied for TM helix 2 and 4. The channel- like conductance was demonstrated for TM helix 2, but not for TM helix 4. Channel activity of TM helix 2 was corroborated and it was furthermore shown that TM helix 1 of GlyR is not conductive [99].

The most complex and challenging environment for investigating TM peptides are biological membranes. In addition to an asymmetric lipid bilayer matrix, native membranes contain many different proteins and glycoproteins which, depending on cellular compartment and cell type, can literally outweigh their lipidic components [65]. Among other complications, membranes in live cells are exposed to the action of a huge arsenal of enzymes and trafficking systems that continuously work to maintain or change membrane composition, curvature, fluidity, permeability, and so forth. Several peptic inhibitors of membrane protein oligomerization and function were reported, including peptides against ErbB2 [100], ErbB1 [101], and *Escherichia coli* methyl-accepting chemotaxis protein II (MCP-II, formerly known as aspartate receptor Tar) [102,103], for more details see review [65]. Nevertheless, to our knowledge, there has been no functional study applying the TMS

experimental approach to a secondary active transporter. However, ion channels and secondary active transporters may not be structurally so different [104,105]. It has been recently shown, that ClC-ec1 (prokaryotic homolog of ClC chloride channels) functions as an exchange pump [106]. Moreover, some unusual transport properties of Nramp proteins described previously can be interpreted in terms of channel-like mechanism [107].

1.4.2 TMS of eukaryotic homolog from the Nramp family

So far, TMS3, TMS4 and TMS6 of eukaryotic DMT1 (Nramp2) [81,82,108,109] and of eukaryotic Nramp1 [83,84,110] have been studied exclusively from the structural point of view. It has been shown that TMS4 of Nramp1 is buried more deeply in model lipid bilayers than TMS3. The insertion position of TMS4 in the model membrane is affected less by pH than the position of TMS3 [110]. These experiments have also demonstrated the importance of Asp^{192} located in TMS4 of Nramp2 for manganese binding [83]. Mutation at this position in Nramp2 (D192A) was previously shown in *in vivo* experiments to attenuate the uptake of cobalt and iron in cells [111]. For TMS6 of eukaryotic DMT1 it was shown that, the His^{267} locates near the central part of the extended segment of the peptide, while the His^{272} is involved in the α-helical folding. The mutation of H267A leads to disappearance of the flexibility in the central portion of the peptide by the formation of more helical folding. In the contrary, the mutation H272A results in an unfolding of the N-terminal helix while keeping the helical structure of the C-terminal part. No obvious difference in the structure is observed for each of the three peptides at different pH values. The specific "α-helix-extended segment-α-helix" structure of TMS6 may have an important implication for the binding of the transporter to H^+ and metal ions and the conformation change arising from the mutations of two highly conserved histidines may be correlated to the deficiency of the transport activity of DMT1[109].

Important transmembrane segments of MntH *E. coli* used in this study contain several conserved amino acid residues. It has been suggested that the most important residues for the transport function of protein are located within TMS1, TMS3 and TMS6 (helical wheel projections of TMSs are shown in Fig. 1.5) [60,63,112]. Altogether, MntH is composed from eleven transmembrane segments. The N–terminus of the protein is located in cytoplasm and its C–terminus is exposed to the periplasmic side of the membrane as confirmed for MntH of *E. coli* [62,113].

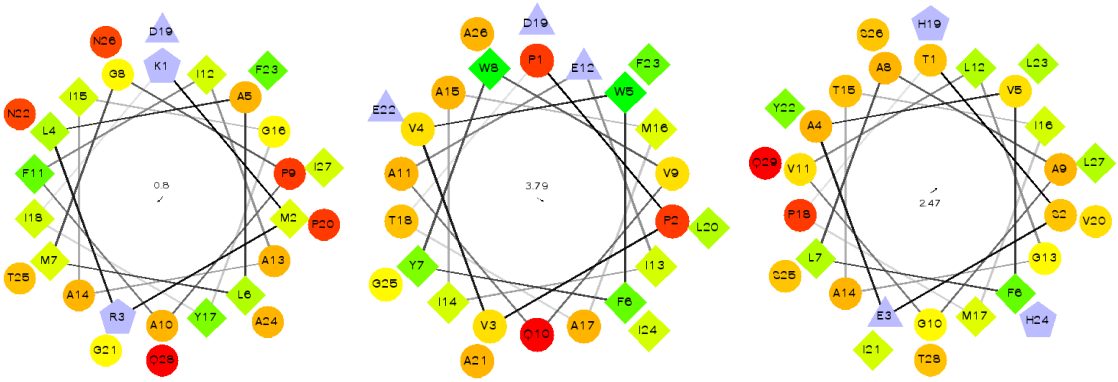

Figure 1.5 Theoretical projection of helical wheels of TMS1, TMS3 and TMS6 (projection created on http://rzlab.ucr.edu/scripts/wheel/wheel.cgi)

The first functionally important transmembrane segment is TMS1. This segment contains two important and specific conserved residues Asp[34] and Asn[37], which are necessary for binding and transport of H^+ and Me^{2+}. The TMS1 Asp residue is part of a conserved DPGN motif that has been subjected to mutagenesis in studies using MntH or Nramp2 homologs showing loss of Me^{2+} uptake caused by Gly exchange [112,114]. The carboxyl end of Nramp2 TMS1 and adjacent extra loop were implicated in Me^{2+} binding and coupling of Me^{2+} uptake to the proton-motive force [114].

TMS3 is the most hydrophobic segment. There is one positively charged residue located in the adjacent cytoplasmic loop (Arg[91]). More interesting are three negatively charged residues (Glu[102], Asp[109] and Glu[112]). All three residues play important roles in the manganese transport. Mutation of these residues caused from decrease of transport to total loss of function (E102D) [112].

Haeming and Brooker (2004) proposed in their study a hypothetical model of the metal binding site within MntH, based on the results of radioactive Mn^{2+} uptake into bacteria (Fig. 1.6). In this model, four residues, Asp[34], Asn[37], Asp[109], and Glu[112], form a site for the binding of Mn^{2+}. Pro[35], Gly[36], and Gly[115] may cause distortions in the helical periodicity of TMS1 and TMS3 that helps to form this binding pocket [112]. Even though this model seems to be preliminary, interaction of TMS1 and TMS3 was investigated in this study.

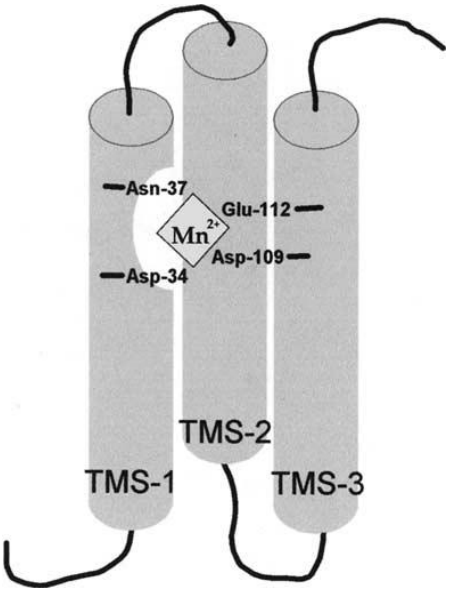

Figure 1.6 Hypothetical model for the binding of Mn2+ to MntH. In this model, four residues, Asp^{34}, Asn^{37}, Asp^{109}, and Glu^{112}, form a site for the binding of Mn^{2+}. Pro^{35}, Gly^{36}, and Gly^{115} (not shown in the figure) may cause distortions in the helical periodicity of TMS1 and TMS3 that help to form this binding pocket. [112]

The sixth transmembrane segment of both eukaryotic and bacterial Nramps is one of functionally important segments in these proteins. It has been hypothetesized, that TMS6 is essential in metal dependent proton transport in Nramps. There are several reports demonstrating the effect of the mutations of conserved histidine pair located at this TMS [111,115]. The conserved histidine residue His^{211} (in MntH from *E. coli*) is functionally important in bacterial MntH [60,63] and homologous H^{267} in eukaryotic Nramp2 [111]. According to the previous studies H211A preserved bacterial sensitivity to all the metals that were tested [63]. *E. coli* MntH transport properties were thus better preserved in the H211A mutant than in the H211Y mutant. The relatively well-preserved activity of *E. coli* MntH H211A thus suggests that the H211Y substitution impaired MntH transport due to the different acid-base properties of His and Tyr residues [63].

Modeling of Nramp homologs on the LeuT/SLC6 structure suggests that in the structure of full-length protein TMS1 and TMS6 could form a pair of discontinuous helices, each composed of an extended peptide chain interconnecting two shorter α–helices [60]. The model suggests an internal symmetry including two domains, made of TMS1-TMS5 and TMS6-TMS10, similarly folded but in inverted orientation with respect to the membrane, with discontinuous helices TMS6 and TMS1 located near the central cavity

of the protein [60]. Similar pairs of discontinuous helices constitute a characteristic feature in structures of five cation transporters [116].

The main objective of this study was to study the three interesting transmembrane segments of *E. coli* MntH and their possible interactions. It was investigated to what extent their function reflects the original function of the full-length protein. The secondary structure of these three synthetic peptides corresponding to the TMS1, TMS3 and TMS6 of *E. coli* MntH was studied in different environments. Structural studies of individual segments and two single-point mutation of TMS6 (H211A and H211R) were performed to observe their interaction with lipid membranes and their channel-forming properties in the presence and absence of metal ions. In addition, for the possible interaction between the segments themselves studies of two mixtures of TMS 1+3 and TMS 1+6 were performed.

2. Materials and Methods

2.1 Materials

All the peptides used in this study were synthesized by Vidia Inc. (Jesenice u Prahy, Czech Republic).

TMS1 peptide (H–K_{16}MRLALMGPAFIAAIGYIDPGNFATNIQ_{43}–NH_2) corresponds to residues 16–43 of *E. coli* MntH transporter (UniProtKB/Swiss-Prot database - acc. no. P0A769). Peptide mass (2991.58) checked by mass spectroscopy (2992.5 for $[M+1]^+$) and the purity assessed by HPLC to be 91.9 %.

TMS3 peptide (H- P_{90}RPVVWFYWVQAEIIAMATDLAEFIGA_{116}–NH_2) corresponds to residues 90–116 of *E. coli* MntH transporter (UniProtKB/Swiss-Prot database - acc. no. P0A769). Peptide mass (3093.7) checked by mass spectroscopy (3093.5 for $[M+1]^+$) and the purity assessed by HPLC to be 97.2 %. The peptide was practically insoluble in buffer and stock solutions were prepared in 2,2,2-trifluorethanol (TFE).

TMS6 peptide (H–T_{193}SEAVFLAAGVLGATIMPHVIYLHSSLTQ_{221}–NH_2) corresponds to residues 193–221 of *E. coli* MntH transporter (UniProtKB/Swiss-Prot database - acc. no. P0A769). Peptide mass (3026.6) was checked by mass spectroscopy (1513.8 for $[M+2]^{2+}$, 1010 for $[M+3]^{3+}$ and 757.2 for $[M+4]^{4+}$) and the purity assessed by HPLC to be 95.2%.

TMS6-OH peptide (H–TSEAVFLAAGVLGATIMPHVIYLHSSLTQ–OH) with a free C-terminus was also present in this study. Peptide mass (3025.6) was checked by mass spectroscopy (1514.1 for $[M+2]^{2+}$ and 1010.2 for $[M+3]^{3+}$) and the purity assessed by HPLC to be 94.2%.

H211A mutation (H–TSEAVFLAAGVLGATIMPAVIYLHSSLTQ–NH_2), its peptide mass (2958.59) was checked by mass spectroscopy (1480.8 for $[M+2]^{2+}$; 987.4 for $[M+3]^{3+}$ and 740.8 for $[M+4]^{4+}$) and the purity assessed by HPLC to be 93.2%.

H211R mutation (H–TSEAVFLAAGVLGATIMPRVIYLHSSLTQ–NH_2), its peptide mass (3043.65) was checked by mass spectroscopy (1523.2 for $[M+2]^{2+}$; 1015.7 for $[M+3]^{3+}$ and 762 for $[M+4]^{4+}$) and the purity assessed by HPLC to be 96.3%.

Lipids including the *E. coli* polar extract (67 % phosphatidylethanolamine, 23.2 % phosphatidylglycerol, 9.8 % cardiolipin), 1-palmitoyl-2-oleoyl-*sn*-glycero-3-phosphocholine (POPC), 1-palmitoyl-2-oleoyl-phosphatidylethanolamine (POPE), 1-palmitoyl-2-oleoyl-3-phosphatidylglycerol (POPG), 1,2-diphytanoyl-*sn*-glycero-3-phosphocholine (DPhPC) and 1,2-diphytanoyl-*sn*-glycero-3-[phospho-*rac*-(1-glycerol)] (DPhPG) were obtained from Avanti Polar Lipids, Inc. and stored as chloroform solutions at -30˚C. All other chemicals were of high-purity reagent grade and used as received.

2.2 Methods

2.2.1 Single-Channel Measurements

The patch clamp technique was first used to resolve currents through single acetylcholine-activated channels in cell-attached patches of membrane of frog skeletal muscle [117]. The method they used (described by [118]) and subsequent refinements [119] have led to techniques for high resolution recording of current in excised membrane patches in addition to those that remain cell-attached. Single channel recording gives information about unitary conductance and kinetic behaviour of ionic channels already partly investigated by classical voltage clamping and by noise analysis; it is also leading to the discovery of new classes of ion channel [120]. The single channel recording technique could be used to record channels in living organism, excised tissues, artificially grown tissues and synthetic lipids.

In our study, a stable lipid bilayer is formed on the tip of a glass micropipette. This is achieved by upward and downward movement of the patch pipette (double–dip method, Fig. 2.1) [121]. The conductance is observed after applying voltage to the measuring pipette. The pattern of successive conductance levels within a single burst of multi-level openings of TMS channel provides a possible evidence for the helix bundle (or barrel-stave; [122]) model of channel formation. A progression of conductance levels may be calculated using a simple cylinder-equivalent model for channel formation by helix bundles [123-125]. The conductance of the pore [126] is calculated using these equations:

$$G = \frac{\pi r^2}{\rho\,(l+\pi r/2)} \quad (2)$$

$$r = R\left[\frac{1}{\sin(\pi/N)} - 1\right] \quad (3)$$

Where G is the observed conductance [S], r is the radius of the pore [nm], and N is the number of aggregated helices. The radius of helix (R) is estimated as 0.5 nm; the helix length (l) for 1 residue in peptide is 0.15 nm; and the resistivity of 500 mM KCl solution calculated from limiting ionic conductance at 25 °C is 0.13 Ω m [127].

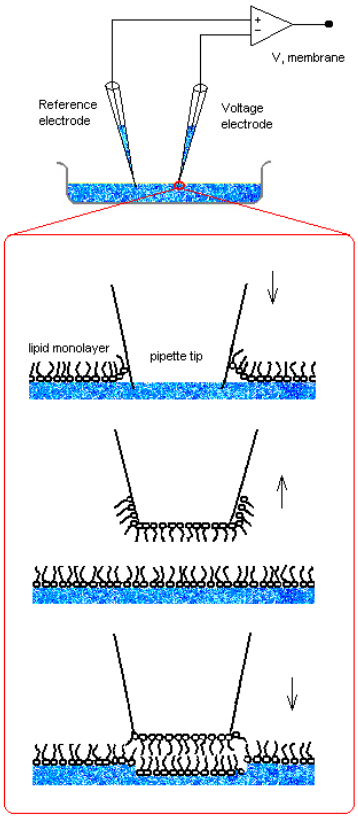

Figure 2.1 Double–dip method of forming a bilayer on the tip of micropipette

Patch–clamp experiments in this study were conducted utilizing the pipette–dipping technique as described earlier [121]. Experiments were performed using Axopatch 200B amplifier and Digidata 1322A acquisition system (Axon Instruments, USA), and the data were collected utilizing low-pass filter (1 kHz) during recording. Experiments were monitored and the data were analyzed with the pClamp 9.2 software (Axon Instruments). Patch pipettes were made of premium custom patch glass (Warner Instruments, USA), and pulled through a two-pull method by a pipette-puller (Narishige PP-830, Japan) to give approximate tip diameters of 1 μm. The pipettes were then filled with electrolyte and used immediately.

Patch clamp measurements were performed in 5 mM HEPES-citrate, 500 mM KCl, pH 5.0. Manganese (1 mM $MnCl_2$) or magnesium (1 mM $MgCl_2$) was present on both cis- and trans-sides when indicated. The peptide was initially dipped into the pipette-filling electrolyte solution (cis–side) at 1 μM final concentration. In order to create lipid monolayer, appropriate amount of lipid mixture was evaporated with a mild flow of nitrogen and re-dissolved in pentane (10 mg/ml). About 1-2 μl of the lipid solution in pentane was then carefully spread on the surface of polystyrene Petri dishes (3.5 cm and 4 cm diameter) and left to evaporate. The formation of bilayer seal was monitored as a change in resistance from ~20 MΩ when the electrode tip was placed under the lipid surface, to ~ 1-10 GΩ after formation of the bilayer seal on the tip of the micropipette. Typically at resistances higher than 10 GΩ, lipid multilayer could be stacked at the tip of the pipette and stable seals (composed of bilayer) could not be formed. Blank solutions in the absence of peptide were used for control experiments. Ion channel-like conductance was not observed in these controls. All measurements were done at room temperature (20ºC).

2.2.2 Preparation of Liposomes (SUVs*)*

Small unilamellar vesicles are single-walled vesicles of uniform diameter. SUVs were prepared from *E. coli polar lipid extract* or mixture of lipids, DPhPC/DPhPG (3:1, w/w), POPC/POPG (3:1, w/w) and POPE/POPG (3:1, w/w) respectively. The appropriate amount of lipids in chloroform solution was evaporated under a stream of nitrogen in a round-bottomed flask. The lipids were further dehydrated under vacuum overnight, and then re-hydrated with 10 mM Tris and 100 mM NaF buffer, pH 7.4, where multilamellar vesicles were formed. The mixture was sonicated with probe tip sonicator until a clear homogenous dispersion was obtained. The diameter of liposomes after sonication was estimated to be ~ 20-50 nm. The liposome dispertion was then centrifuged for 15 minutes at 14,000 rpm at 16°C temperature to remove titanium particles and other impurities. The lipid dispersion used for spectroscopic measurements was homogeneous and did not show significant light scattering in the 200-600 nm UV/visible range. The prepared SUV dispersion was stable and stored in dark at 4°C.

2.2.3 Circular Dichroism

Circular dichroism (CD) spectroscopy is a useful technique for the analysis of secondary structure of proteins and peptides in various environments. CD refers to

the differential absorption of two circularly polarized components of equal magnitude. When the light passed through an optically active sample, the left and right components are absorbed to different degrees, and so the resulting radiation would possess elliptical polarization. A CD signal will be observed when a chromophore is chiral (optically active) [128]. The CD spectrum of a protein can be divided into two main regions: the far-UV region (260-180 nm) measuring transitions involved with the amide peptide backbone and revealing important characteristics of the secondary structure of peptide, and the near-UV region (320-260 nm), which providing information about tertiary structure. Not only the microenvironment of aromatic amino acids and disulfide bonds, but the absorption and dipole orientation influences on the signal obtained in near UV [129,130]. Absorption due to the peptide bond yields two main transition peaks: a weak but broad $n \rightarrow \pi^*$ transition at around 220 nm and a more intense $\pi \rightarrow \pi^*$ transition at 190 nm [128]. Typical conformations of peptide obtained by far-UV spectroscopy are shown in Fig. 2.2. Each of these conformations gives rise to characteristic shape and magnitude of CD spectrum. A typical α-helix has a positive maximum at 192 nm ($\pi \rightarrow \pi^*$ transition) with a molar elipticity (ME) magnitude of 60,000-80,000 deg cm^2 $dmol^{-1}$ and two negative maxima at 222 nm ($n \rightarrow \pi^*$ transition) and 208 nm ($\pi \rightarrow \pi^*$ transition) with a magnitude of about -36 000 deg cm^2 $dmol^{-1}$ [131]. The CD spectrum of a β sheet has the $\pi \rightarrow \pi^*$ transition around 195-200 nm, has a magnitude of 30,000-50,000 deg cm^2 $dmol^{-1}$, and has the $n \rightarrow \pi^*$ transition at about 215-220 nm, with a magnitude of -10,000 to -20,000 deg cm^2 $dmol^{-1}$. The spectrum generally correlated with the random conformation has a large negative maximum band around 200 nm, with the magnitude of -20,000 deg cm^2 $dmol^{-1}$, and a small positive peak or a shoulder with a small negative value at 220 nm [131].

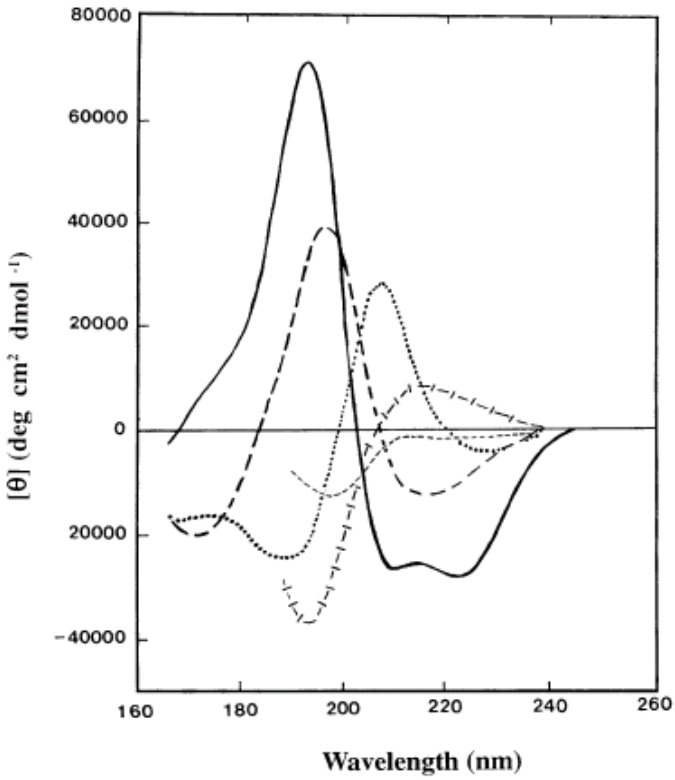

Figure 2.2 Far-UV CD spectra of typical conformations. The spectra are denoted by: (—) α-helix,(– – –) β-sheet, (••••) type I β-turn, (-ı-ı-) poly (Pro) II helix, (----) irregular structure [128].

The experimentally obtained spectra are converted from elipticity (θ) in millidegrees to molar elipticity ([θ]) according to this equation (4):

$$ME = \frac{millidegrees}{\#\ of\ AA \times conc[mol] \times cell\ length[cm] \times 10} \quad (4)\ [129]$$

After this conversion, the secondary structure of the protein is estimated, using deconvolution methods with a specific protein database. These methods compare the CD spectrum with CD spectra of known proteins from the different database. There are a few suitable programs for this analysis: BELOK (two-step ridge regression), BPNN (backpropagation neural network), CCA (convex constraint analysis), CONTIN-LL (ridge regression), K2D (learning neural network), SELCON3 (Self-Consistent Method), SSE (secondary structure estimation) and VARSLC and CDSSTR (variable selection) [132,133].

In our study, CD spectra were recorded on an AVIV 215 spectropolarimeter (Aviv Biomedical, USA). For all far-UV measurements a rectangular quartz cuvette of 1 mm

pathlength was used. Spectra were collected from 260 to 190 nm at 0.5 nm intervals with a 0.5 nm/s scanning speed at 25°C temperature. For each sample four scans were averaged and blank spectra obtained under identical conditions were subtracted. Samples were equilibrated at room temperature for ~15 min prior to measurement. All measurements were carried out in 10 mM Tris, 100 mM NaF (pH 7.4). Trifluoroethanol (TFE - 25% or 50% v/v), 1 mM SUVs or SDS were present, when indicated. The final concentration of peptide in the sample in all measurements was 20 μM.

The results are expressed as the mean residue ellipticity. The contents of secondary structures were calculated according to the Sreerama–Woody method on the DICHROWEB website (http://www.cryst.bbk.ac.uk/cdweb/html/home.html) using CONTIN–LL algorithm (with a 42–reference set) [134]. It is important to note that the deconvolution analysis method used is a rough estimate of structural composition, since the reference data set used for calculating secondary structure content is primarily based on known structures of soluble globular proteins and not membrane proteins. It has been shown that reference databases derived from soluble proteins do not always produce accurate results when applied to membrane protein CD analysis [135].

2.2.4 Reverse-phase High performance liquid chromatography (RP-HPLC)

High performance liquid chromatography is a technique that has arisen from the application of theories and instrumentation originally developed for gas chromatography to liquid chromatography [136]. HPLC is frequently used to separate, identify, and/or quantify virtually any sample based on their idiosyncratic polarities and interactions with the column's stationary phase. HPLC utilizes different types of stationary phase (typically, hydrophobic saturated carbon chains), a pump that moves the mobile phase(s) and analyte through the column, and a detector that provides a characteristic retention time for the analyte (Fig. 2.3). Analyte retention time is dependent on the strength of its interactions with the stationary phase, the ratio/composition of used solvents, and the flow rate of the mobile phase [137].

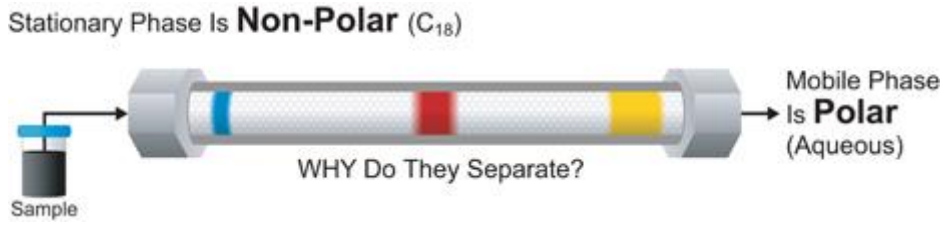

Figure 2.3 Reversed-Phase HPLC column (www.waters.com)

RP-HPLC is a system where the column stationary phase matrix is non-polar and the mobile phase is a polar mixture of water plus polar organic solvents such as methanol and acetonitrile. RP-HPLC has both analytical and preparative applications in the area of biochemical separation and purification. RP-HPLC separates molecules on the basis of differences in their hydrophobicity and amphiphilicity. The components of the analyte mixture pass over stationary-phase particles bearing pores large enough for them to enter, where interactions with the hydrophobic surface removes them from the flowing mobile-phase stream. The strength and nature of the interaction between the sample particles and the stationary phase depends on both hydrophobic interactions and polar interactions. As the concentration of organic solvent in the eluent increases, it reaches a critical value for each analyte which desorbs it from the hydrophobic stationary-phase surface and allows it to elute from the column in the flowing mobile phase. Since this elution depends on the precise distribution of hydrophobic residues in each species, each analyte elutes from the column at a characteristic time, and the resulting peak can be used to confirm its identity and estimate its quantity [137].

The HPLC system used in this study was composed of a Waters 2996 photodiode array detector with a Waters 600 pump, a Waters 600 controller and a Waters 717plus Autosampler. The analytical column used for all experiments was from Phenomenex.

Samples were degassed in a bath sonicator prior to transfer to the autosampler. Typical injection volume was 10-15 µl. RP-HPLC analyses were performed on an analytical Luna C5 column (250×4.6 mm inner diameter, 5 µm particle size, 100 Å pore size). The initial solvent composition was 75% A and 25% B (solvent A: 0.05% TFA in H_2O, solvent B: 0.05% TFA in acetonitrile). The final solvent composition was 0% A and 100% B. The runtime was 40 minutes at a flow rate of 0.5 ml/min. Equilibration time between two runs, where initial conditions of solvents were restored was 12 min. Retention times were recorded at room temperature.

3. Results

3.1 *TMS1*

The first and probably the most interesting transmembrane segment, TMS1, corresponds to residues 16–43 of *E. coli* MntH transporter. This segment contains the "Nramp signature", a highly specific and conserved sequence motif DPGN at its C-terminus. Within this segment, there is a negative charge (Asp^{33}) near the C-terminus and 3 positively charged amino acids are located near the N-terminus adjacent to the cytoplasmic loop (Arg^{15}, Lys^{16}, Arg^{18}). To explore the secondary structure of this TM domain, its CD spectra are measured as a single peptide and in mixture with other TM segments, TMS3 and TMS6 in various environments, such as aqueous solutions, the membrane mimetic solvent TFE and the detergent SDS, as well as small unilamellar phospholipid vesicles.

3.1.1 CD analysis

The CD spectra of TMS1 in buffer showed dominantly unordered structures. The spectra of mixtures of peptide segments in aqueous solution were comparable to that of TMS1 (Fig. 3.1). The overall shapes of the spectra with two negative maxima at ~ 220 nm and ~ 198 nm imply a dominantly random coil conformation with some ordered structures. As exhibited in the CD spectra, no significant conformational change was observed in the presence of manganese ions, the substrate of the full-length MntH protein (Fig. 3.1).

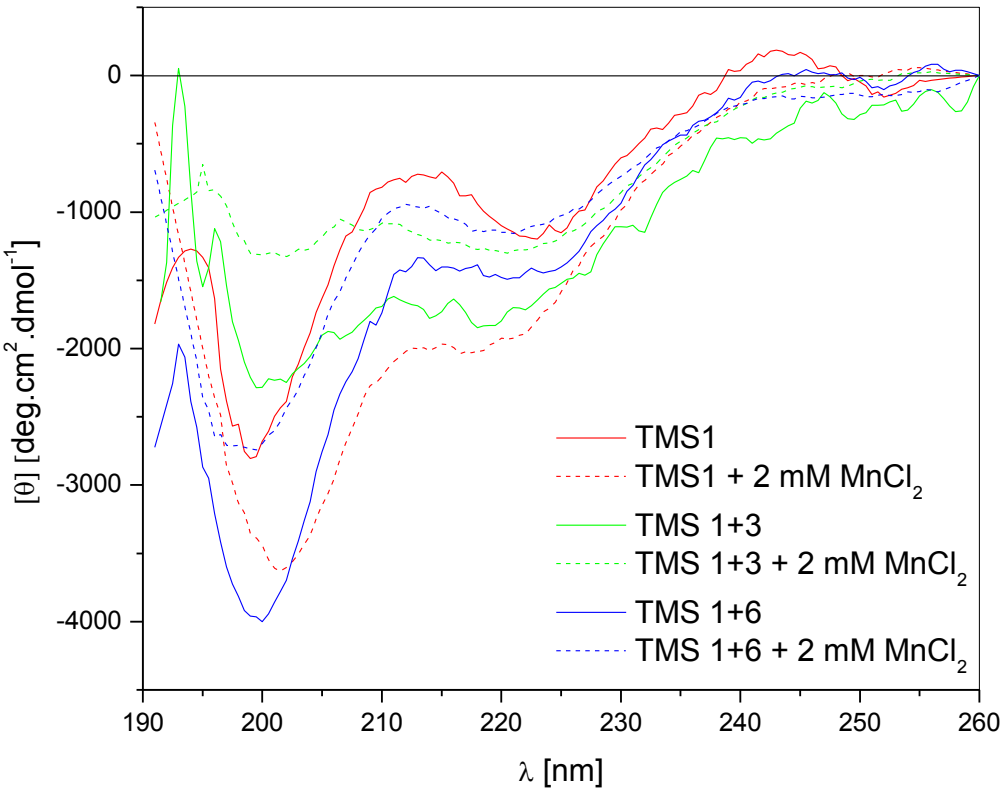

Figure 3.1 CD spectra of TMS1 and mixtures TMS 1+3 and TMS 1+6 in buffer in the presence and absence of manganese ions.

In contrast to the spectra in buffer, CD spectra in SDS micelles were significantly changed. As seen in Fig. 3.2A TMS1 and peptide mixtures became dominantly helical in SDS micelles, known to induce and stabilize secondary structures. According to Zhong & Johnson, α-helical structure is more likely to be induced at or above critical micellar concentration of SDS [138]. The CD spectra of TMS1 in SDS were concentration dependent with the $\theta_{222}/\theta_{208}$ ratio changing from 2 (below CMC) to 1.5 (above CMC). These results could imply self-association of the peptide as was shown in coiled-coils. Coiled coils are common structural motifs, consisting of two to five amphipatic α-helices wrapped around each other to form supercoils [139]. The spectrum of TMS1 in SDS micelles had the characteristics of an α–helical conformation with two negative maxima at 222 and 208 nm and a positive maximum at 193 nm (Fig. 3.2A). The CD spectra of TMS1 in aqueous solutions of TFE (from 25% to 50%) also depicted α-helical conformations with $\theta_{222}/\theta_{208}$ ratio of ~ 0.9 (Fig 3.2B). The observed α–helical content of TMS1 in SDS (above CMC) was comparable to that of TMS1 in TFE/water environment (Table 1 in

Appendix1). The effect of manganese metal ions on TMS1 conformation in SDS was insignificant, however in TFE this effect was more conspicuous (2.8% vs. 12% increase of helicity).

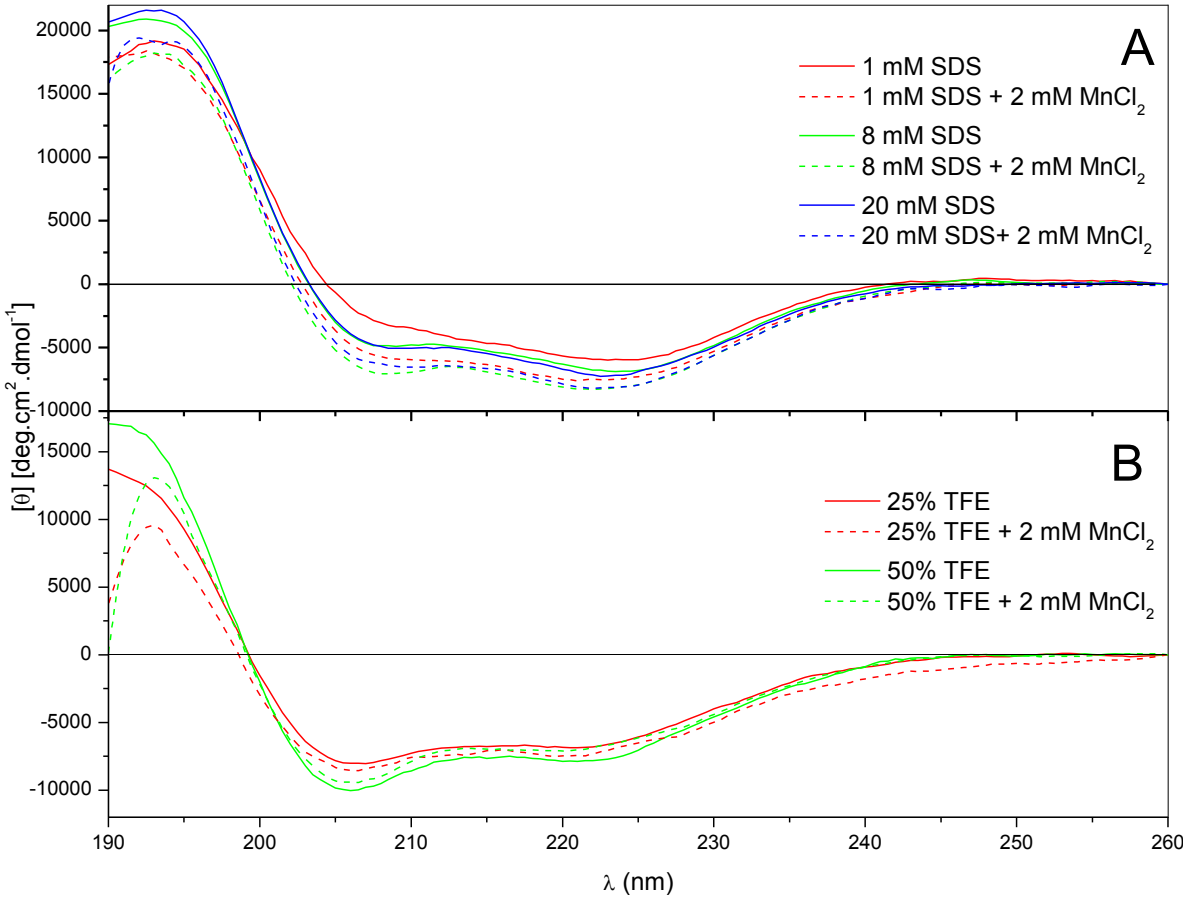

Figure 3.2 CD spectra of TMS1 in different concentration of (A) SDS and (B) TFE

The conformation of TMS1 was further explored in different lipid vesicles. CD spectra of TMS1 in SUV of following lipid compositions: POPC/POPG, DPhPC/DPhPG, POPE/POPG (all in molar ratio 3:1) and *E. coli* polar lipid extract (67% PE, 23.2% PG and 9.8 % CL) are shown in Fig. 3.3. These lipid membranes represent both liquid and gel phases of bilayers. Under our experimental conditions DPhPC/DPhPG was in the gel phase, the same lipid system was also used in the single-channel measurements.

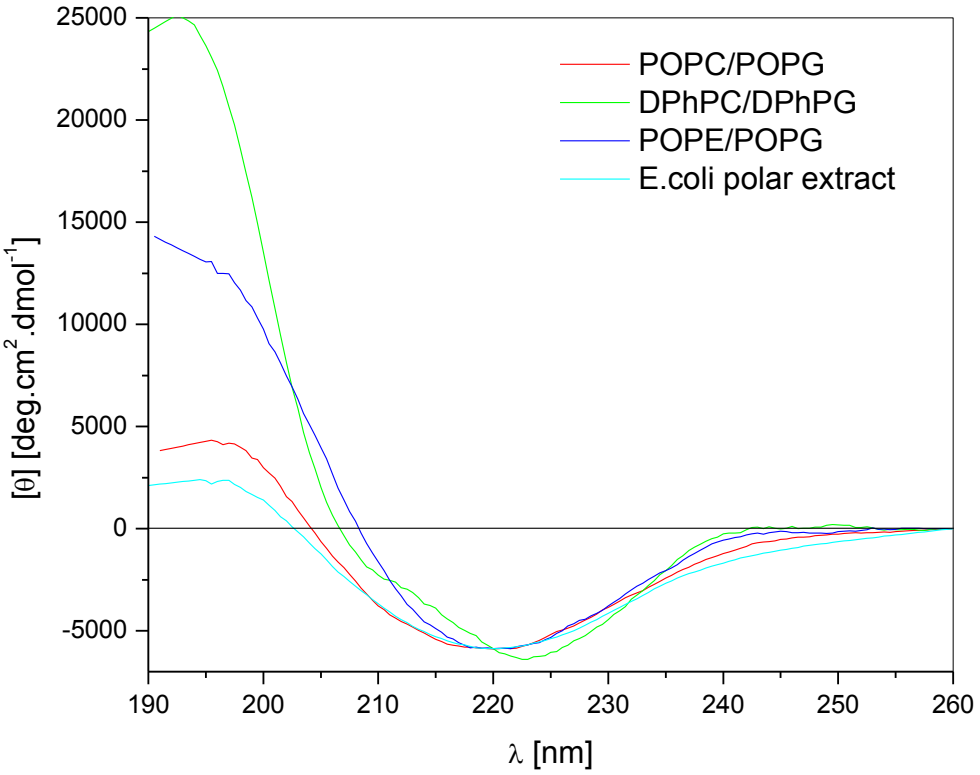

Figure 3.3 CD spectra of TMS1 in lipid vesicles of different lipid composition. Spectra are normalized at 220 nm.

TMS1 in DPhPC/DPhPG showed the most α-helical and ordered structure. The character of the spectra was different for other lipid environments. There were two negative maximum bands one at 222 nm and the second weaker shoulder-like one at 208 nm, as well as one positive maximum band at 193 nm. The spectra implied the association of helices and possible penetration of TMS1 into the DPhPC/DPhPG bilayer. However, for other three lipid systems the α-helical content was less than 15%. The difference in secondary structure may be due to the different physical properties of the lipid vesicles under our experimental conditions. As previously mentioned, DPhPC/DPhPG was in gel phase and all the other lipid systems were in liquid phase. Based on the CD spectra shown in Fig. 3.3 the conformation in POPC/POPG and *E. coli* polar lipid extract vesicles is comparable. Even though POPE/POPG vesicles are closer in composition to the *E. coli* polar lipid extract, the normalized mean residue elipticity at 220 nm of the peptide in POPE/POPG is almost three times higher than in POPC/POPG and *E. coli* polar lipid extract. Possibly the secondary structure of TMS1 is more dependent

on the physical characteristics (phase) of the lipid vesicle, rather than the composition of lipid vesicles.

3.1.1.1 Effect of metal ions on TMS1 conformation

The secondary structure of TMS1 was also studied in the presence of divalent metal ions as possible substrates. The effect of manganese as the physiological substrate for MntH protein was studied under the previously stated experimental conditions. It was shown that manganese ions had no significant effect on the conformation of TMS1 in aqueous solutions (Table 1 in Appendix 1). According to the deconvolution analysis, in 25% TFE α-helicity in the presence of manganese ions was slightly increased. The same effect was observed in 50% TFE.

In different concentrations of SDS the effect of manganese ions is similar. It increased the α-helical content on average by 2.5%, whereas the β-strand content was decreased.

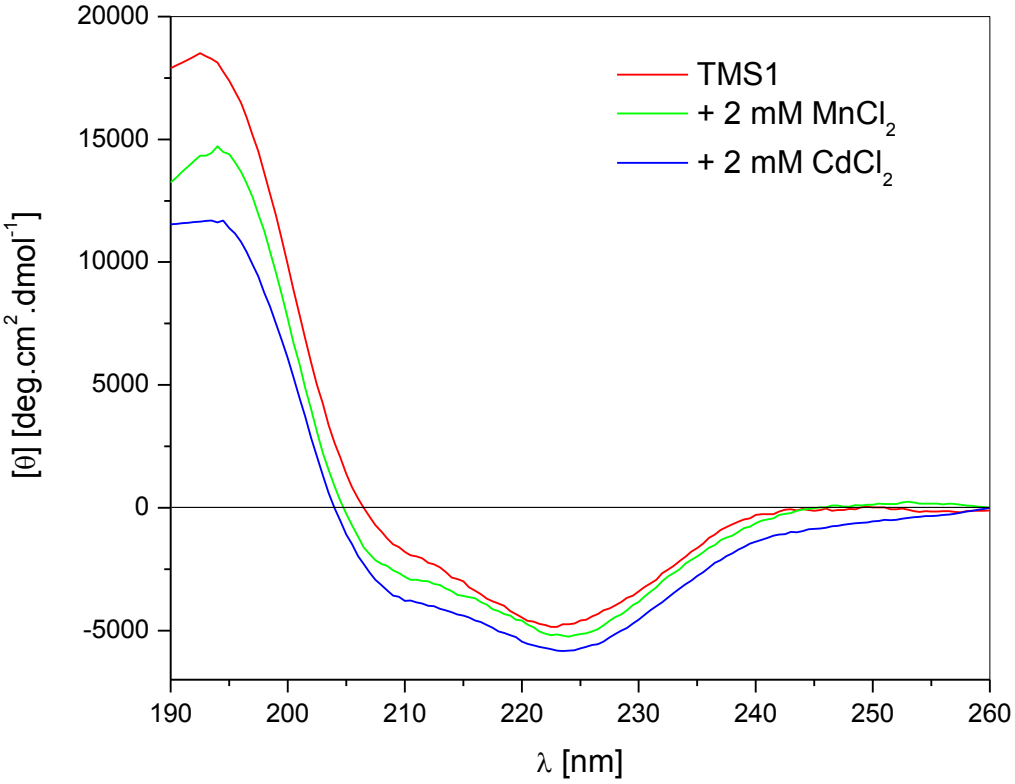

Figure 3.4 CD spectra of TMS1 in DPhPC/DPhPG vesicles in the presence of manganese and cadmium ions

The influence of cadmium on the secondary structure was also monitored in SUVs. Both metal ions should reduce the negative charge on the membrane surface. The effect of metal ions was different in each lipid vesicles (Table 3.1). The increase of α-helical content was observed in DPhPC/DPhPG vesicles only (Fig. 3.4). Both metal ions increased the α-helix content by ~ 2%. On the other hand, β-strand content significantly decreased by ~ 5% in the presence manganese ions and ~ 6% percent in the presence of cadmium ions. A very different effect on the structure was observed in POPC/POPG vesicles. The spectra showed less ordered structures in the presence of both metal ions. The percentage of turns in this environment slightly increased (Fig. 1 in Appendix 1). In the presence of manganese ions the α- helical content slightly decreased. However, for cadmium ions there was no change in the α-helical content. A similar situation was observed in the *E. coli* polar lipid extract vesicles. The α-helix content was decreased in the presence of manganese ions (~ 2%) and was not changed in the presence of cadmium ions. The structure of TMS1 became slightly more unordered in the presence of these ions (Fig. 2 in Appendix 1). In contrast, different effect of metal ions was detected in the POPE/POPG vesicles. The secondary structure became more unordered for both metal ions (5–7 %). Overall, the ellipticity of the segment was weak (Fig. 3 in Appendix 1).

Table 3.1 Deconvolution analysis of TMS1 spectra in lipid vesicles

	Secondary structure [%]			
	α−helix	β−strand	Turns	Unordered
DPhPC/DPhPG	18.7	36.8	16.7	27.8
+ 2 mM $MnCl_2$	20.7	32.2	18.3	28.7
+ 2 mM $CdCl_2$	20.7	31.3	19.9	28.1
POPC/POPG	13.5	33.4	22.9	30.3
+ 2 mM $MnCl_2$	12.8	32.0	23.6	31.7
+ 2 mM $CdCl_2$	13.7	29.7	23.6	33.0
E. coli polar lipid extract	12.7	33.1	22.4	31.7
+ 2 mM $MnCl_2$	10.6	32.5	23.3	33.7
+ 2 mM $CdCl_2$	12.3	33.7	22.0	33.0
POPE/POPG	10.4	37.9	22.7	29.0
+ 2 mM $MnCl_2$	9.0	31.6	22.9	36.5
+ 2 mM $CdCl_2$	6.2	39.1	21.1	33.5

3.1.2 Electrophysiological studies using patch clamp

The channel–forming properties of peptides were studied in phospholipid bilayers (DPhPC/DPhPG 3:1 molar ratio) formed at the tip of micropipettes at 20 °C (room temperature). Electrophysiological studies were performed on a lipid system with sufficient mechanical strength. Blank solutions were prepared as negative controls to eliminate the possibility of leakage artifacts. No ion channel-like conductance was observed in these controls. Ion channel activity of alamethicin and gramicidin was also monitored in this lipid bilayer system as positive control. Both of these well-known ion channel peptides showed the expected conductance values comparable to the previously published results [121].

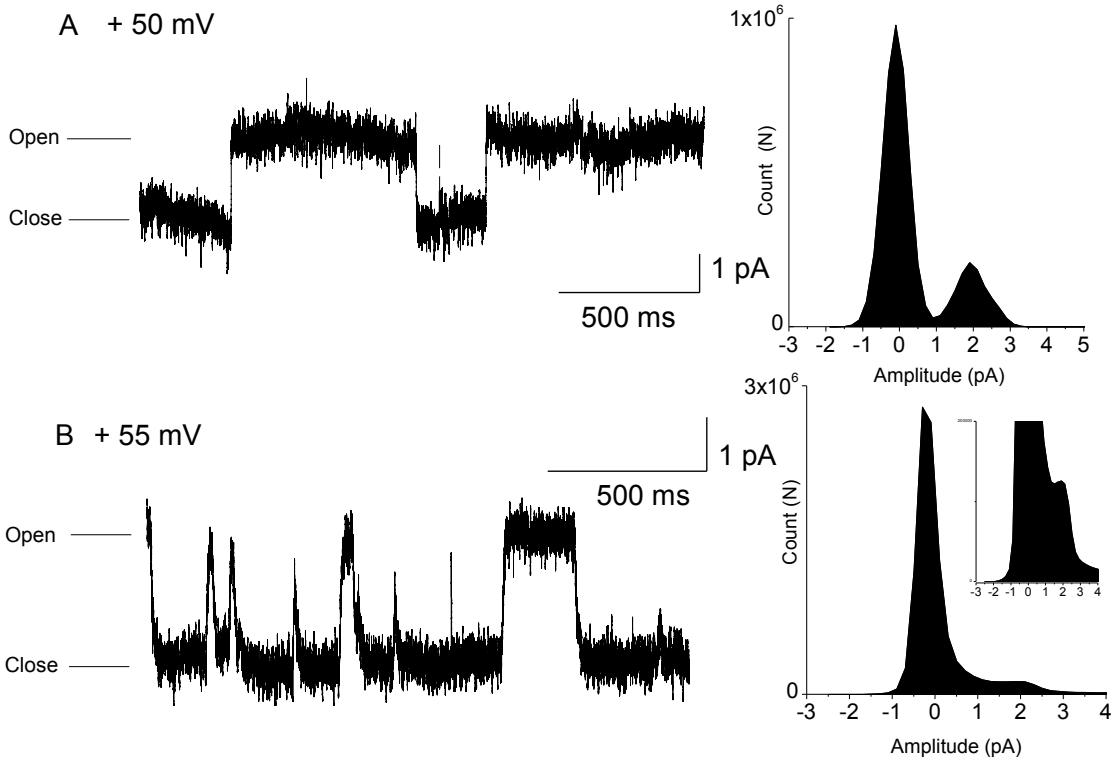

Figure 3.5 Representative current patterns of TMS1 (in 5 mM HEPES pH 5.0, 500 mM KCl, on both sides of the micropipette) (A) in the absence of 1 mM $MnCl_2$ (+50 mV) (B) in the presence of 1 mM $MnCl_2$ (+55 mV)

In HEPES-citrate buffer at pH 5.0, the presence of manganese had no significant impact on the probability of occurrence of channels formed by TMS1 (36% in the presence of manganese, 38% in the absence) (Fig. 3.5). In both cases single-channels were observed, with conductance values of 23.1 ± 10.7 pS and 25.4 ± 7.9 pS, respectively. Comparing these conductance values to the other transmembrane segments (TMS3, TMS6 see sections 3.2.2 and 3.3.2), TMS1 showed the lowest conductance. The ion conducting unit of TMS1 ion channel could be modeled by a helical bundle composed of several peptide molecules. The measured conductance values and their comparison with the calculated values derived from the cylindrical-bundle pore model [126] imply the formation of oligomeric helical bundle conducting unit composed of three helices. Possible association of the TMS1 helices is also supported by the CD spectra of this peptide in DPhPC/DPhPG lipid vesicles exhibited in Fig. 3.4.

3.2 TMS3

TMS3 is the most hydrophobic segment among all studied segments in this study. This segment contains three negatively charged residues (Glu^{102}, Asp^{109} and Glu^{112}) in the transmembrane part, close to periplasm and one positively charged arginine (Arg^{91}) in the adjacent cytoplasmic loop. It also contains two tryptophan residues inside the transmembrane part closer to cytoplasm. The presence of Trp residues is important for fluorescence experiments. These residues could have some functional or structure stabilizing roles in the whole protein. The TMS3 sample contained ~ 3.5% TFE, due to the insolubility of the segment. This concentration of TFE does not interfere with our spectroscopic or electrophysiological measurements.

3.2.1 CD analysis

To observe the secondary structure of TMS3, CD analysis was performed in different environments. The CD spectra of TMS3 measured in TFE from 3.5% to 50% are shown in Fig. 3.6. TMS3 in 3.5% TFE showed mostly β-strand structure, with a positive maximum ~ 200 nm and a negative maximum at 230 nm. With increasing percentage of TFE the α-helical content was increased. In 25% TFE the first negative maximum was at 221 nm, the second negative maximum was observed at 210 nm. Moreover, in 50% TFE TMS3 showed a representative α–helical structure with two negative maxima (222 nm and 208 nm) and one positive maximum around 193 nm (Fig. 3.9).

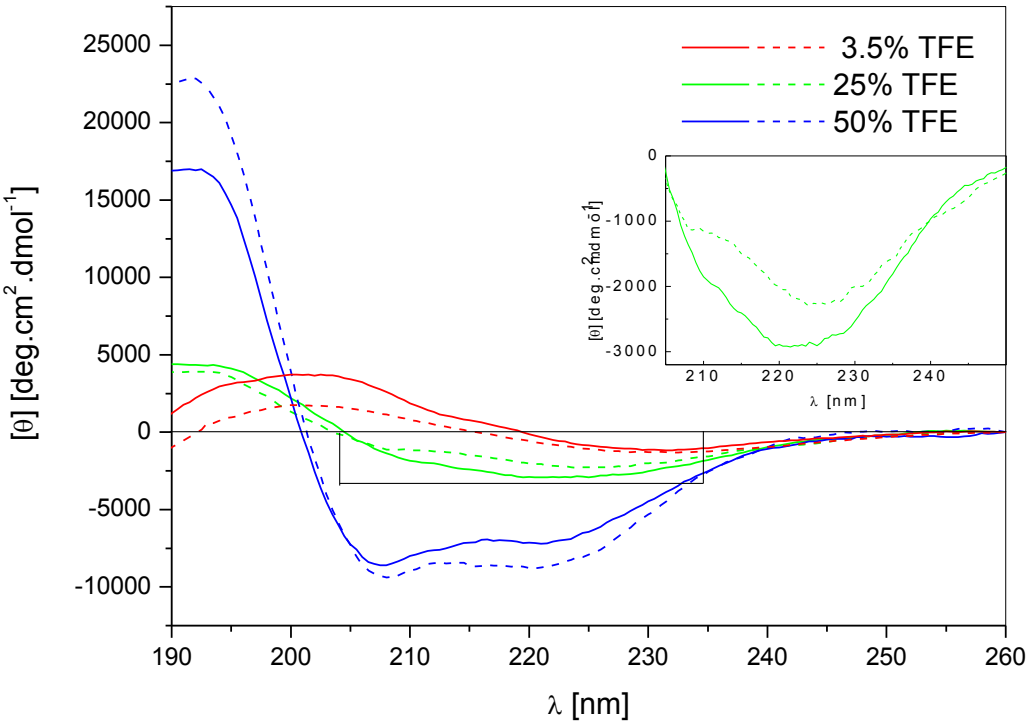

Figure 3.6 CD spectra of TMS3 at different concentrations of TFE

CD spectra of TMS3 at different concentrations of SDS had an α-helical characteristic with two negative maxima at 222nm and 208 nm and one positive maximum ~193 nm (Fig. 3.7). Surprisingly, according to the deconvolution analysis, the spectra measured in SDS below CMC were more helical compared to those above CMC (by almost 10%). However, the α–helical content below and at CMC was comparable (51.5% and 52% respectively). The spectrum above critical micellar concentration had 41.1% α–helical content (Table 3 in Appendix 2).

Similar to TMS1 in the previous section, the ability of TMS3 to penetrate in the lipid vesicle and the secondary structure in different SUVs were studied. TMS3 was mixed directly with lipid vesicles.

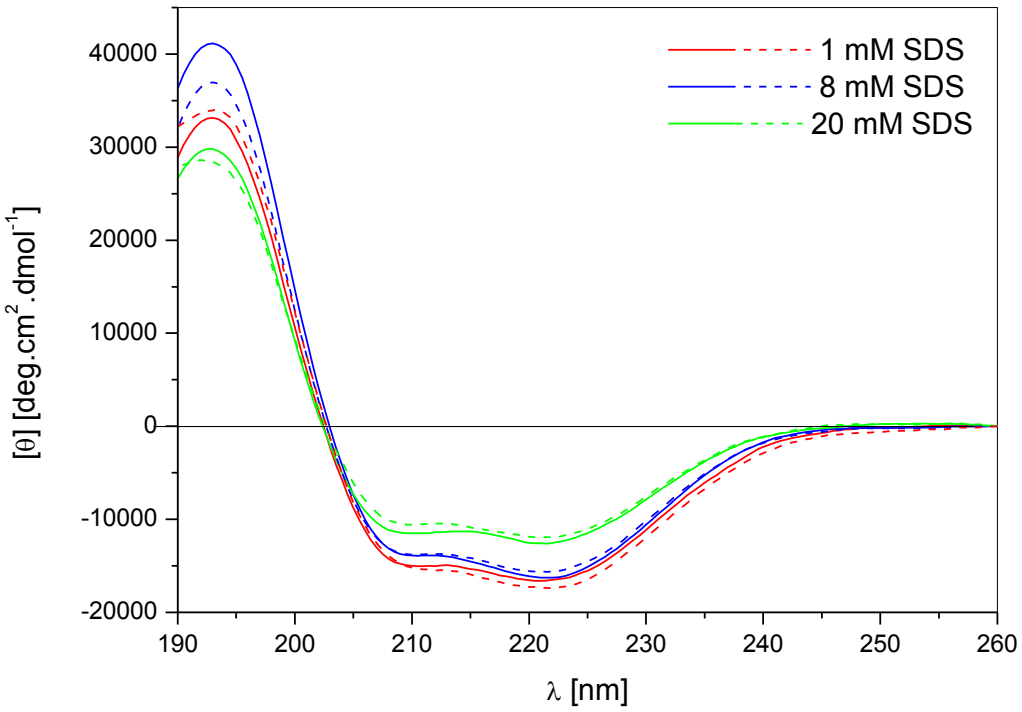

Figure 3.7 CD spectra of TMS3 at different concentrations of SDS in the absence (solid lines) and presence of manganese ions (dashed lines)

CD spectra of TMS3 in lipid vesicles of different lipid compositions are shown in Fig. 3.8. In two lipid systems (DPhPC/DPhPG and POPC/POPG) the segment was mostly β-sheet (39% for DPhPC/DPhPG and 37% for POPC/POPG, Table 3.2) and unordered structure with very low elipticity. In comparison to other studied segments, TMS3 was the least α-helical structure in DPhPC/DPhPG. Whereas the secondary structure of TMS1seemed to be more dependent on the physical characteristics (phase) of the lipid system, TMS3 was influenced more by the composition of lipid vesicles. Phosphatidylcholine (PC) based lipid systems do not induce an α-helical structure in TMS3. PC is a zwitterionic lipid and PG has a negative charge. On the other hand PE lipids are also uncharged. The overall charge of lipids plays an important role in the secondary structure of the segment in different lipid systems. But the different properties of these lipid systems are the reason why the secondary structure of mostly negatively charged TMS3 showed more α-helical structure in PE based lipid systems. Phosphatidylethanoamine in comparison to phasphatidylcholine has two double bonds, which makes PE more rigid than PC.

In *E. coli* polar lipid extract vesicles the α-helicity of TMS3 increased in comparison to phosphatidylcholine lipids by more than 10% to ~ 20%. The β-strand conformation is still significantly higher than α-helix in this lipid environment.

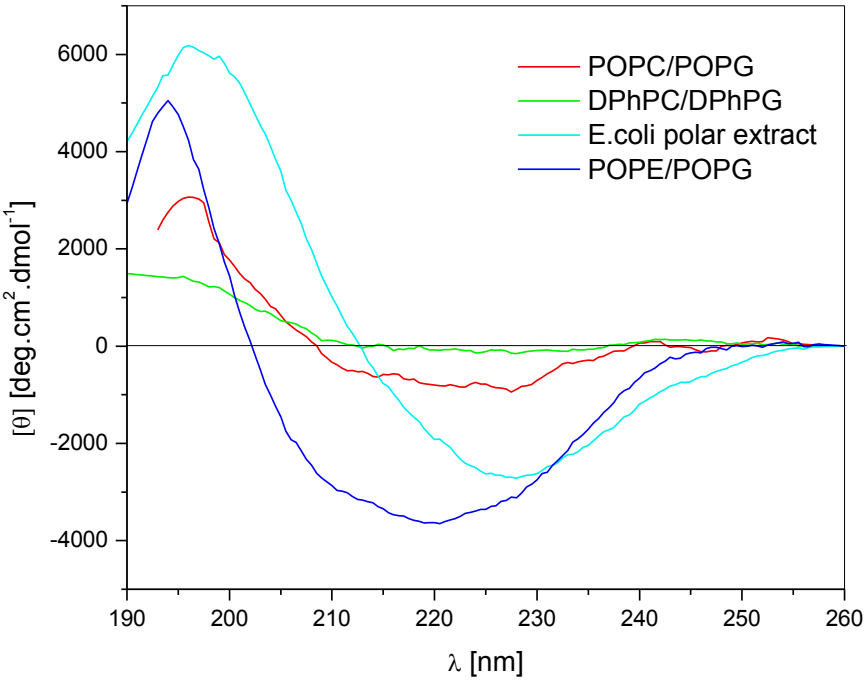

Figure 3.8 CD spectra of TMS3 in various lipid vesicles

A spontaneous insertion of TMS3 into lipid bilayer surface was detected in *E. coli* SUVs [140]. The CD spectrum of TMS3 was a combination of β-sheet and α-helix, with a negative maximum at 228 nm and a positive maximum at 196 nm (Fig 3.8). TMS3 is believed to partially penetrate into the *E. coli* polar lipid extract vesicles. Heating of the sample to 40°C neither induced helicity nor promoted the penetration (Fig. 11 in Appendix 2). The peptide in the second lipid system composed of POPE/POPG showed a higher α-helical content, than the PC environment. The spectrum is different from *E. coli* polar lipid extract, with a negative maximum at 220 nm and a positive maximum at 194 nm. Comparing to *E. coli* polar lipid extract vesicles (containing PE, PG and cardiolipin) the spectrum of the peptide is more unordered (Fig 3.8, Table 3.2). Cardiolipin could have a role in inducing the secondary structure in this system.

3.2.1.1 Effect of metal ions on TMS3 conformation

Similar to TMS1, the secondary structure of TMS3 was also studied in the presence of divalent metal ions. It was shown that manganese ions had no significant effect on the conformation of TMS3 in TFE. In 3.5% and 50% TFE manganese slightly induced helicity (Table 3 in Appendix 2). According to the deconvolution analysis TMS3 did not gain structure in 25% TFE, even tough the shape spectra of TMS3 changed (Fig. 3.6). The presence of 2 mM $MnCl_2$ in all SDS measurements results in minor decrease of α–helical content by 2.3 ± 1.4%. In contrast to TMS1, the overall characteristic of the spectra in different concentrations of SDS was not changed (Fig 3.7, Table 3 in Appendix 2).

Table 3.2 Deconvolution analysis of TMS3 spectra in lipid vesicles

	Secondary structure [%]			
	α−helix	β−strand	Turns	Unordered
DPhPC/DPhPG	5.5	39.4	22.0	32.8
+ 2 mM $MnCl_2$	13.5	36.8	22.6	32.5
+ 2 mM $CdCl_2$	10.1	33.3	24.3	32.1
POPC/POPG	7.3	37.0	22.7	33.0
+ 2 mM $MnCl_2$	8.6	35.6	23.5	32.4
+ 2 mM $CdCl_2$	9.7	34.2	24.2	32.0
E. coli polar lipid extract	19.6	34.9	23.1	22.3
+ 2 mM $MnCl_2$	15.5	32.6	23.5	28.3
+ 2 mM $CdCl_2$	18.1	30.9	22.8	28.1
+ 2 mM $CaCl_2$	10.0	34.6	23.7	31.6
+ 2 mM $MgCl_2$	17.2	29.4	25.2	28.3
POPE/POPG	13.5	33.1	22.5	30.8
+ 2 mM $MnCl_2$	14.0	32.8	22.0	31.0
+ 2 mM $CdCl_2$	20.3	28.1	22.4	29.2

Metal ions have more significant influence on the secondary structure of the TMS3 in lipid vesicles. TMS3 in DPhPC/DPhPG vesicles seemed to gain more α-helical content (α-helix increased by 8% in the presence of manganese and by ~5% in the presence of cadmium ions). Fig. 9 in Appendix 2 shows that the CD spectra in the presence of metal ions are changed. In POPC/POPG vesicles the presence of metal ions increased the elipticity of spectra (Fig. 9 in Appendix 2). The maximum of the spectra was not clearly detected due to the scattering of the sample below 193 nm. The secondary structure became slightly more ordered in the presence of manganese and cadmium ions (Table 3.2).

Various divalent metal ions (manganese, cadmium, magnesium and calcium) were used to investigate the effect of these ions on the secondary structure of TMS3 in *E. coli* polar lipid extract (Table 3.2). In contrast to the effect of the metal ions in all other lipid systems, these metal ions did not increase the α- helical content of the peptide segment (Fig. 10 in Appendix 2). Inversely, some metal ions made the secondary structure of TMS3 more unordered. Manganese ions did not significantly influence the structure. A slight increase of β-sheet structure was observed at the expense of decrease in of α–helical content (~ 4%) (Table 3.2). Significant difference in the shape of the spectra was observed in the presence of cadmium and magnesium ions. In the presence of these two metal ions, the negative maximum at 228 nm changed to two negative maxima at 224 nm and 209 nm. The maximum slightly red shifted to 195 nm. The most significant distortion of secondary structure was observed in the presence of calcium ions (Fig. 10 in Appendix 2).

In POPE/POPG vesicles the presence of metal ions slightly increased the α-helicity of the segment. The CD spectra of TMS3 in the presence of manganese ions had a shoulder at 210 nm. In the presence of cadmium ions this shoulder shifted to 209 nm. The overall elipticity of the spectra was higher (Fig. 12 in Appendix 2). In POPE/POPG, the α-helix content for TMS3 was 13.5%, and this value increased to ~ 20% in the presence of cadmium ions (Table 3.2).

3.2.2 Electrophysiological studies using patch clamp

All the patch clamp measurements were performed under the same conditions as those used for TMS1. Channel-like activity was observed for TMS3 only in the presence of manganese ions. In the absence of 1 mM $MnCl_2$, on both sides of the pipette, no channel–like activity was observed. This implicates that for channel activity of TMS3 the presence of manganese is essential. It is not clear, whether the effect of manganese ions on TMS3 channel opening is specific (i.e. Mn^{2+} interacts directly with the peptide) or non-specific.

The channels were voltage-dependent and showed multiple conductance levels (Fig. 3.9). The conductance of ion channels was 30.95 ± 6.8 pS for the first open state, 48.3 ± 4.6 pS for the second state and 84.7 ± 13.5 pS for the third state. This measured conductance values and their comparison with calculated values derived from cylindrical-bundle pore model [126] imply the formation of conducting units composed by three to four helices forming a pore of ~ 0.1 nm diameter.

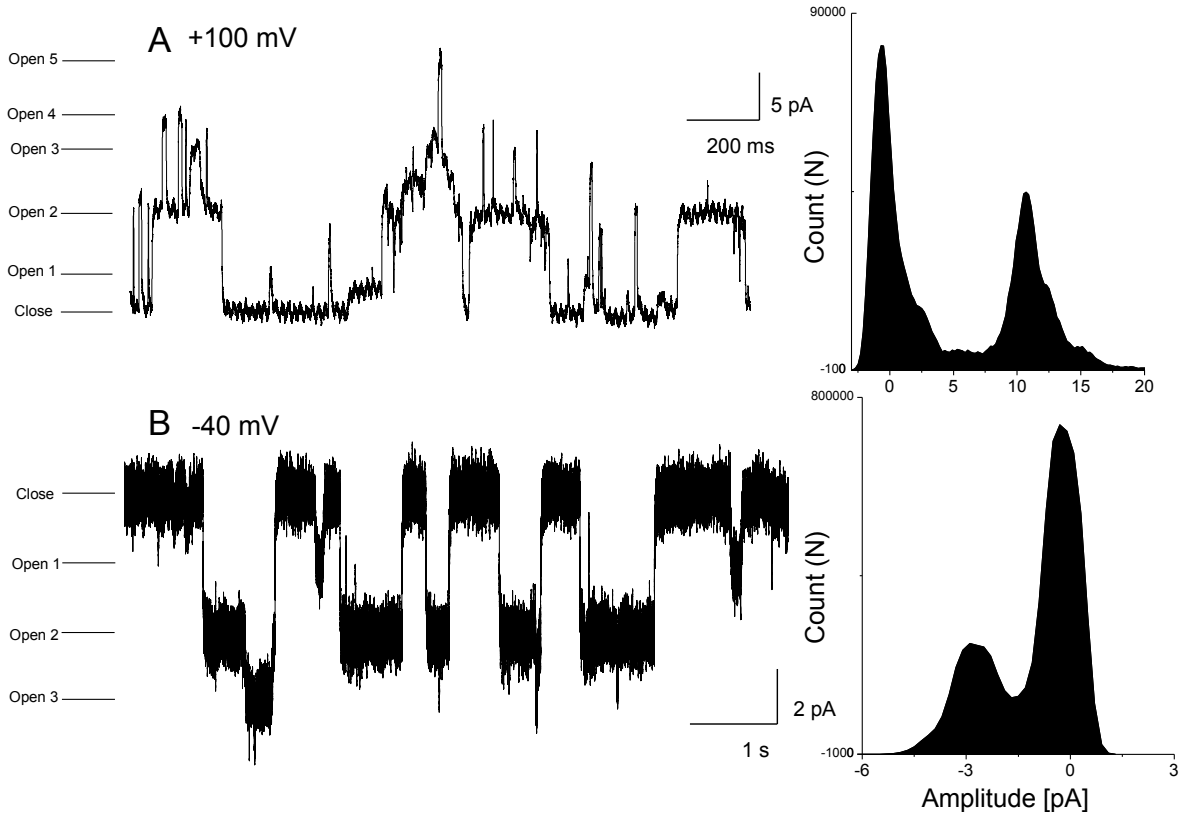

Figure 3.9 Representative current patterns of TMS3 (in 5 mM HEPES pH 5.0, 500 mM KCl, 1 mM $MnCl_2$, 1% TFE on both sides of the micropipette) at (A) positive applied voltage (+100 mV) (B) applied voltage (-40 mV)

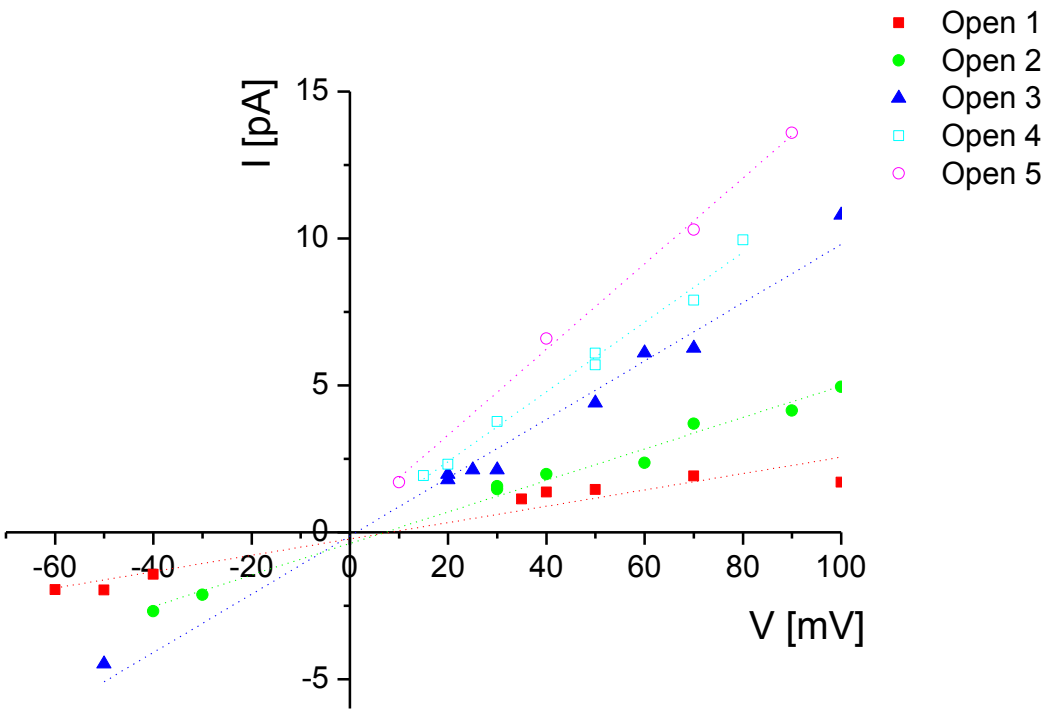

Figure 3.10 Current–voltage (I–V) relationships of ion channels formed by the TMS3

Measurements of reversal potential, in the presence of asymmetric KCl concentrations across the bilayer (0.5 M KCl on cis–side, 0.1 M KCl on trans–side), were intended for determination of ion selectivity. Reversal potential for TMS3 was -7.8 ± 1.5 mV. The permeability ratio from the Goldman–Hodgkin–Katz equation is P_{Cation}/P_{Anion} = 1.6 [126]. This result indicates that TMS3 is a slightly cation selective ion channel. The current-voltage relationship is linear, thus the channels formed by TMS3 showed an ohmic behaviour. There is no voltage-dependence in the open-closed pattern of the individual channels (Fig. 3.10), however the appearance of different conducting states was voltage dependent.

3.3 *TMS6*

The sixth transmembrane segment of both eukaryotic and bacterial Nramps is one of functionally most important segments, being involved in the transport and in the coupling of both substrates. There have been several reports demonstrating the effect of the mutations of conserved histidine pair located at this TMS [111,141]. The conserved His^{211} (in MntH from *E. coli*) is functionally important in both bacterial MntH [60,63] and eukaryotic Nramp2 (His^{267} in rat Nramp2) [111].

The TMS6 segment contains one negatively charged glutamic acid (Glu^{195}) at the adjacent periplasmic loop. Two histidine residues are located within the transmembrane part (His^{211}, His^{216}). There is one additional histidine residue at the border with cytoplasm, which is not part of our synthesized peptide. For this study two versions of TMS6 segment were prepared, one with the free C-terminus (TMS6-OH) and second one with amide-protected C-terminus (TMS6). Also two mutant versions of TMS6, H211R and H211A, were synthesized to investigate the influence of H^{211} on the physiochemical properties of this peptide. The comparison of secondary structure in aqueous buffer, TFE and the lipid systems will be shown in the following section.

3.3.1 CD analysis

Circular dichroism of the peptides was studied in the same experimental conditions as TMS1 and TMS3. Ellipticities of CD spectra in aqueous buffer were weak (Figure 3.11). For TMS6-OH and H211R, these spectra showed dominantly random coil conformations with a negative band at 198 nm. The characteristics of CD spectra of H211A and TMS6 were rather different. The spectrum of H211A had two negative maxima at 222 nm and 201 nm. TMS6 had one negative maximum at 220 nm and a shoulder at 204 nm. Both peptides were without any visible maximum above 190 nm (Fig. 3.11). This conformational difference of H211A can be attributed to the higher hydrophobicity of the peptide (alanine is more hydrophobic than histidine), which can cause partial association of the peptide. The amide-protected terminus of TMS6 could also lead to association and stabilization of helices in the buffer (Fig 3.11). TMS6 showed more ordered structure in aqueous buffer than TMS6-OH Table 3.3.

Table 3.3 Deconvolution analysis of TMS6 peptides spectra in buffer

	Secondary structure [%]			
	α−helix	β−strand	Turns	Unordered
TMS6-OH	6.5	37.3	21.8	34.5
+ 2 mM $MnCl_2$	9.0	33.2	24.0	33.9
TMS6	6.2	39.6	20.6	33.6
+ 2 mM $MnCl_2$	9.8	40.6	27.8	21.8
H211A	6.8	36.6	22.9	33.8
+ 2 mM $MnCl_2$	4.5	41.3	20.6	33.6
H211R	7.8	34.1	23.6	34.4
+ 2 mM $MnCl_2$	6.4	36.7	21.9	35.0

The CD spectra of all the peptides were also measured in the TFE-containing buffer (Fig. 13 in Appendix 3). CD spectra of the TMS6-OH and TMS6 in 50% TFE confirmed the helix–forming tendency of this peptide domain. Overall, the spectra in these milieus exhibited α-helical conformations (Fig. 13 in Appendix 3). Similar results were obtained also for both H211A and H211R peptides. These results imply that in the less polar hydrophobic environments TMS6 of *E. coli* MntH has a high potential to form helical structures.

At different concentrations of SDS the secondary structure of each peptide and degree of induction of α-helix was different. (Fig. 14, Table 4 in Appendix 3). TMS6-OH gained α-helical structure with increasing concentration of SDS (from 18% in 1mM SDS to 31% in 20 mM SDS). Both mutant peptides showed more helicity than TMS6-OH, with the highest α-helical content at CMC (54% for H211A, 51% for H211R). Increase in the concentration of SDS resulted in the decrease in the helical content of H211A (~10%) and a slight decrease in the helical content of H211R (Table 5 in Appendix 3).

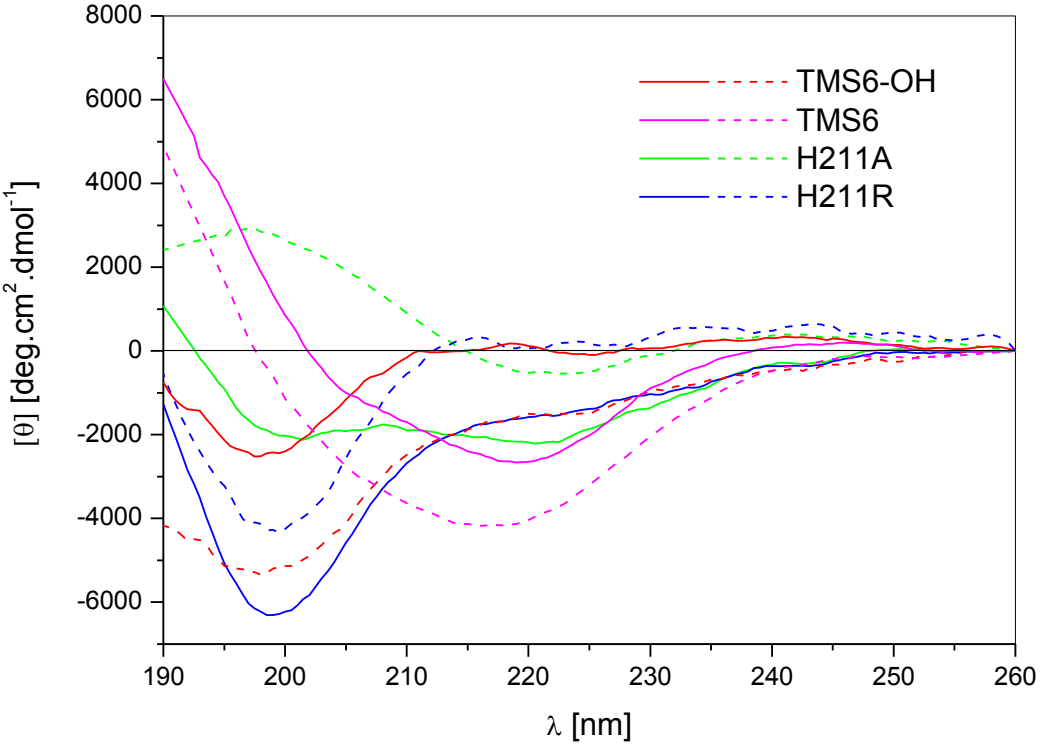

Figure 3.11 CD spectra of the peptides in aqueous buffer. Solid lines show spectra without manganese and dashed lines show spectra in the presence of 2 mM $MnCl_2$. The spectra represent the average of two independent experiments.

The secondary structure of the peptides was also studied in various lipid vesicles. CD spectra of all four variation of TMS6 peptide in DPhPC/DPhPG SUVs exhibited remarkable changes when compared to those measured in buffer (Fig. 3.12). CD spectra of TMS6 peptides in DPhPC/DPhPG vesicles showed two negative maxima at 222 nm and 210 nm and a positive maximum at 193 nm, implying the formation of a helical conformation of the peptide. The helicity of peptides in lipid vesicles increased comparing to buffer environment by ~ 10% for TMS6-OH, ~ 15% for H211A, ~ 23% for TMS6 and more than 30% for H211R. These significant conformational changes are indicative of spontaneous insertion of the peptides into the lipid bilayer. Comparing the free and amide-protected TMS6 in diphytanoyl vesicles, CD spectra of amide-protected TMS6 showed more secondary structure than TMS6-OH. According to the deconvolution analysis α-helix content of TMS6 was ~ 30% and ~ 16% for TMS6-OH. The amide-protected terminus promotes helicity in DPhPC/DPhPG lipid system. The estimated secondary structure content is shown in Table 3.4. The order of α-helicity in DPhPC/DPhPG vesicles decreased as follows: H211R > TMS6 > H211A > TMS6-OH.

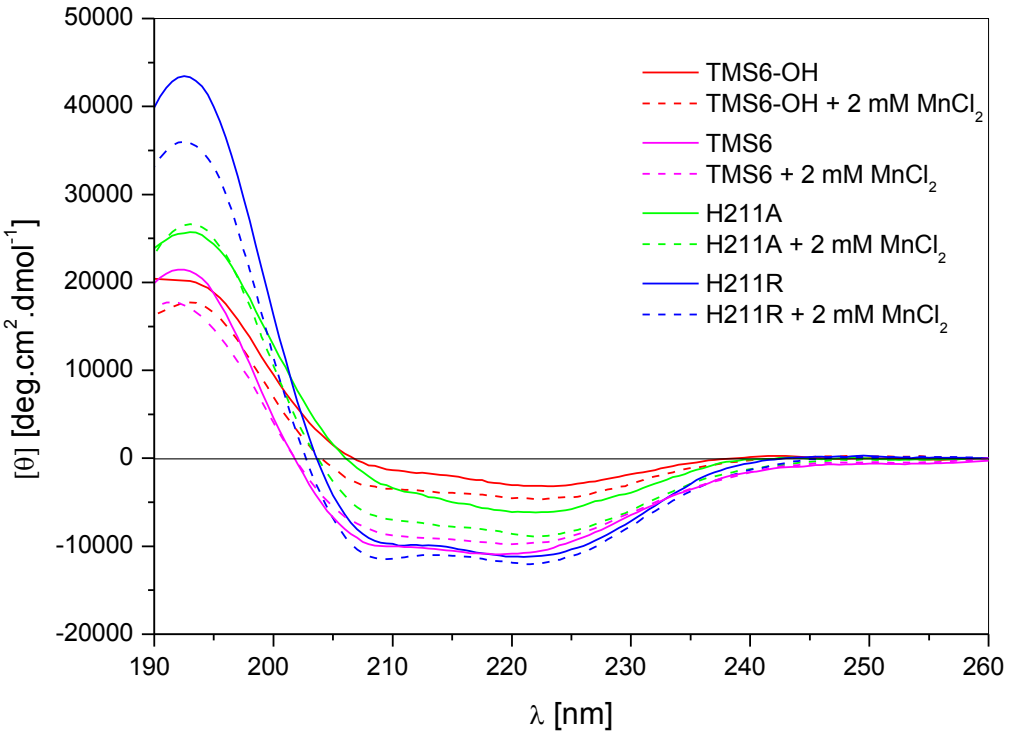

Figure 3.12 CD spectra of the peptides in the presence of DPhPC/DPhPG vesicles. Solid lines show spectra without manganese and dashed lines show spectra in the presence of 2 mM $MnCl_2$.

CD spectra of TMS6, TMS6-OH and mutants in POPC/POPG vesicles were significantly different from those in diphytanoyl vesicles (Fig.15 in Appendix 3). TMS6 in POPC/POPG vesicles had the highest helical content (α-helix ~ 31%) from all studied peptides. In contrast, TMS6-OH had the lowest α-helical content – only ~ 8%. Similar to previous lipid environment the amide-protected terminus in TMS6 was promoting the helicity of the peptide. The spectra of H211A mutant was rather different comparing to the others with only one major negative maximum at 222 nm. This mutant had mostly β-sheet structure (Fig.15 in Appendix 3).

The last SUVs used to study the secondary structure of peptides were *E. coli* polar lipid extract vesicles. Interestingly, TMS6-OH had comparable α-helical content to POPC/POPG (~ 8%) in these vesicles. These peptides showed lower helicity in lipid vesicles in their liquid phase, and almost double the α-helical content in SUVs in gel phase (DPhPC/DPhPG). In *E. coli* polar lipid extract the highest helicity was observed for mutant H211A (~ 24%) (Table 6 in Appendix 3). The CD spectra of TMS6 and H211R were comparable.

Table 3.4 Deconvolution analysis of TMS6 peptides spectra in DPhPC/DPhPG vesicles

	Secondary structure [%]			
	α-helix	β-strand	Turns	Unordered
TMS6-OH	15.8	38.4	16.6	29.2
+2 mM $MnCl_2$	19.5	33.0	18.8	28.8
TMS6	30.4	23.2	19.5	26.9
+2 mM $MnCl_2$	27.0	25.3	19.5	28.2
H211A	22.3	34.9	15.7	27.1
+2 mM $MnCl_2$	31.7	25.9	17.5	25.0
H211R	42.6	23.1	13.1	21.2
+2 mM $MnCl_2$	43.8	18.4	15.6	22.3

The secondary structure of TMS6 with amide-protected terminus was more helical than TMS6-OH in all lipid environments. The amide-protected terminus seems to promote helicity more or less in all studied lipid vesicles. Interestingly the influence of the amide-protection seems to be more pronounced for PC based lipid vesicles. Whereas the biggest increase of α-helical content was observed for POPC/POPG vesicles (by ~ 24%).

3.3.1.1 Effect of metal ions on conformation of TMS6 peptides

The presence of manganese divalent ions influenced the secondary structure of the peptides in buffer (Fig. 3.11). The most remarkable change was observed for H211A. It seems that in the presence of Mn^{2+} in aqueous solution the mutant H211A tends to associate and form ordered β-structures.

In both helix-promoting solvents TFE and SDS the α–helical structure of the studied peptides became more pronounced in the presence of manganese ions. The only exception was TMS6 in 50% TFE; in this case no difference in the spectra was observed (Fig. 13 in Appendix 3).

Except for TMS6, all peptides studied in SUVs gained helical structure in the presence of manganese ions (Fig. 3.12, Table 3.4). The most significant increase of α-helicity in the presence of manganese ions was observed for H211A in DPhPC/DPhPG vesicles (by ~ 9%); it was accompanied by a decrease of β-strand structure.

The effect of manganese ions and cadmium ions was studied in *E. coli* polar lipid extract vesicles. Similar to the previously mentioned lipid system manganese ions slightly increased α-helix content of TMS6-OH, the increase of helicity is more pronounced in the presence of cadmium ions. On the other hand, TMS6 and both mutations showed decrease in helicity in the presence of both divalent metal ions (Table 6 in Appendix 3). All studied peptides became less ordered in the presence of Mn^{2+}.

3.3.2 Electrophysiological studies using patch–clamp

All the patch clamp measurements were performed under the same experimental conditions as those using TMS1 and TMS3. Both TMS6 and TMS6-OH channel–like conductance had clear transitions between the open and closed states, when observed under acidic pH (pH 5.0 cis- and trans-side) conditions in the presence and absence of manganese ions (in 40% of trials with $MnCl_2$ and 56% of trials without $MnCl_2$ for TMS6 and in 42% and 35% of trials, respectively for TMS6-OH). The presence of manganese was not necessary for ion channel formation but influenced ion channel characteristics.

The free-terminus TMS6-OH in the absence of manganese showed a multi-state channel activity (Fig. 3.13A) with two dominant conductance states. The two open conductance states had the conductance values of 273 ± 64 pS and 464 ± 96 pS, respectively. The closed state occurred rarely. Values of the first open state were comparable to the first open state of the amide-protected TMS6 (Fig. 3.14A). Ion channels of TMS6 recorded in the absence of manganese (Fig. 3.14A) showed a multi-state ion-channel activity, with three dominant conductance values of 293 ± 151 pS, 798 ± 184 pS and 1243 ± 378 pS (Fig. 3.14A).

Both TMS6 peptides showed multi-state channel activity in the presence of 1 mM $MnCl_2$ at pH 5.0. TMS6-OH showed four clearly defined dominant conductance states (Fig. 3.13B). The first conductance state was comparable to those observed without manganese ions, 250 ± 20 pS. Similar to TMS6-OH, amide protected TMS6 showed four conductance states with one sub-state observed near the first open state. The conductance

of the first state in TMS6 was lower compared to TMS6-OH, 81 ± 56 pS. The second state in TMS6 had conductance comparable to the first state of TMS6-OH 214 ± 144 pS.

Analogically to TMS1 and TMS3, the conductance states in the presence of manganese were used to estimate the number of helices forming the conducting units using the helical bundle model [126]. The conductance values of TMS6-OH imply that the conducting unit is formed of four to six helices. Comparably the conducting unit of the amide-protected TMS6 segment is formed of five to six helices.

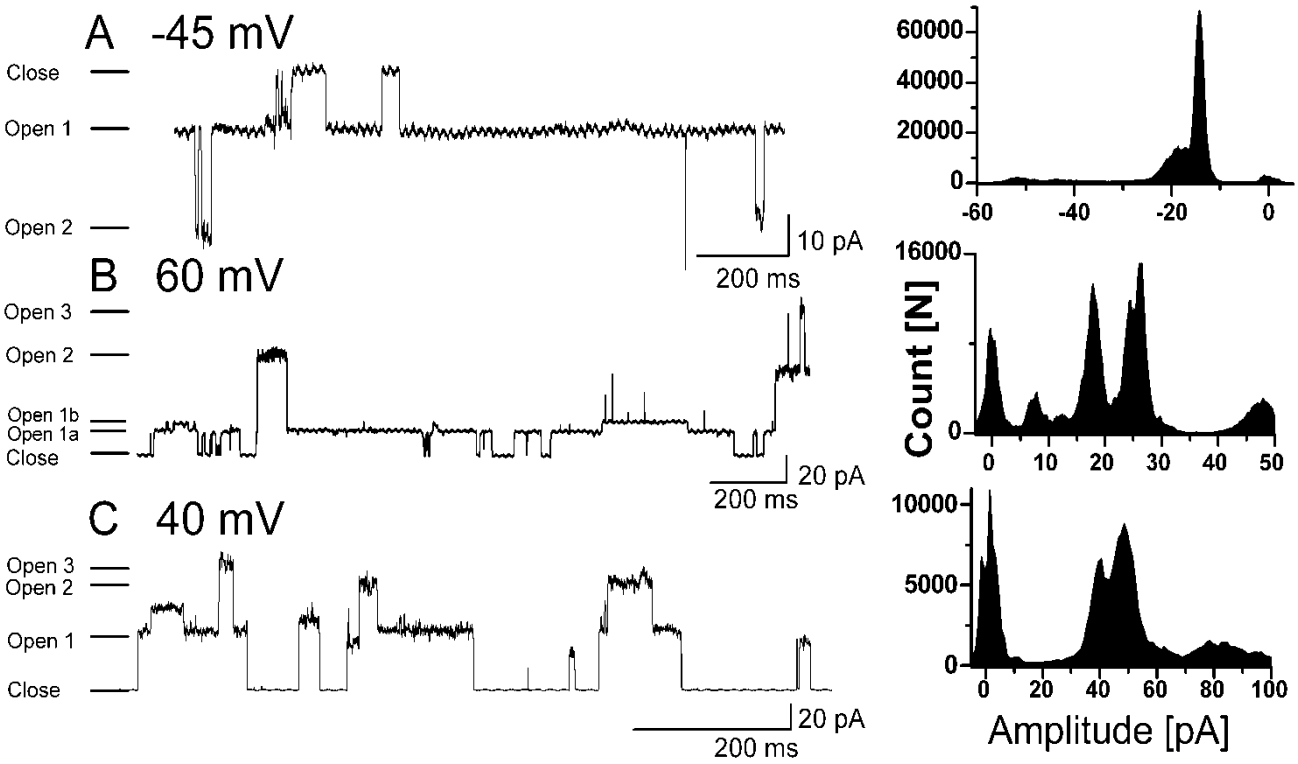

Figure 3.13 Representative current patterns of TMS6-OH (in 5 mM HEPES pH, 500 mM KCl,) at (A) pH 5.0 on both sides of the micropipette, (B) pH 5.0 on both sides of the micropipette with 1 mM $MnCl_2$, (C) pH 5.0 on trans-side and pH 7.4 on cis-side both sides with 1 mM $MnCl_2$

TMS6-OH was further studied under asymmetrical conditions (pH 7.4 on the cis-side and pH 5.0 on the trans-side). This peptide showed multi-state channel activity under these experimental conditions (Fig. 3.13C). The reversed case (pH 5.0 cis and pH 7.4 trans) did not yield stable membranes and consequently, no channel–like activity was observed. In addition, in order to study the effect of other physiologically relevant ions, similar experiments with TMS6-OH were also performed for magnesium ions (contrary to Mn^{2+}, Mg^{2+} is not substrate of full-length MntH protein). In the presence of 1 mM $MgCl_2$ at pH 5.0, TMS6-OH did not show any multi-state channel-like activity, but displayed weak single-channel activity, however, only rarely (in 18% of the experiments).

To further characterize the observed ion channels formed by TMS6 and TMS6-OH, current–voltage relationships were investigated under both symmetrical conditions for TMS6 and TMS6-OH and asymmetrical conditions for TMS6-OH (Fig. 3.15). In comparison to symmetrical conditions, the average conductance of TMS6-OH ion channels were significantly higher (symmetrical: 360 ± 130 pS and asymmetrical: 990 ± 160 pS). Interestingly, the reversal potential under asymmetrical conditions was zero (Fig. 3.15D), which excluded the possibility that the channels are proton selective. In that case reversal potential would be close to the Nerst potential for difference of 2.4 pH units, i.e. -140 mV. The presence of manganese ions seemed to have smaller effect on the channel activity than the pH conditions. The conductance of the TMS6-OH channel in the presence of Mn^{2+} ions under symmetrical pH conditions was higher (360 ± 130 pS) than the conductance in its absence (273 ± 64 pS). On the other hand, the first conductance level of TMS6 channel was lower in the presence of manganese (81 ± 56 pS), than in its absence (293 ± 151 pS).

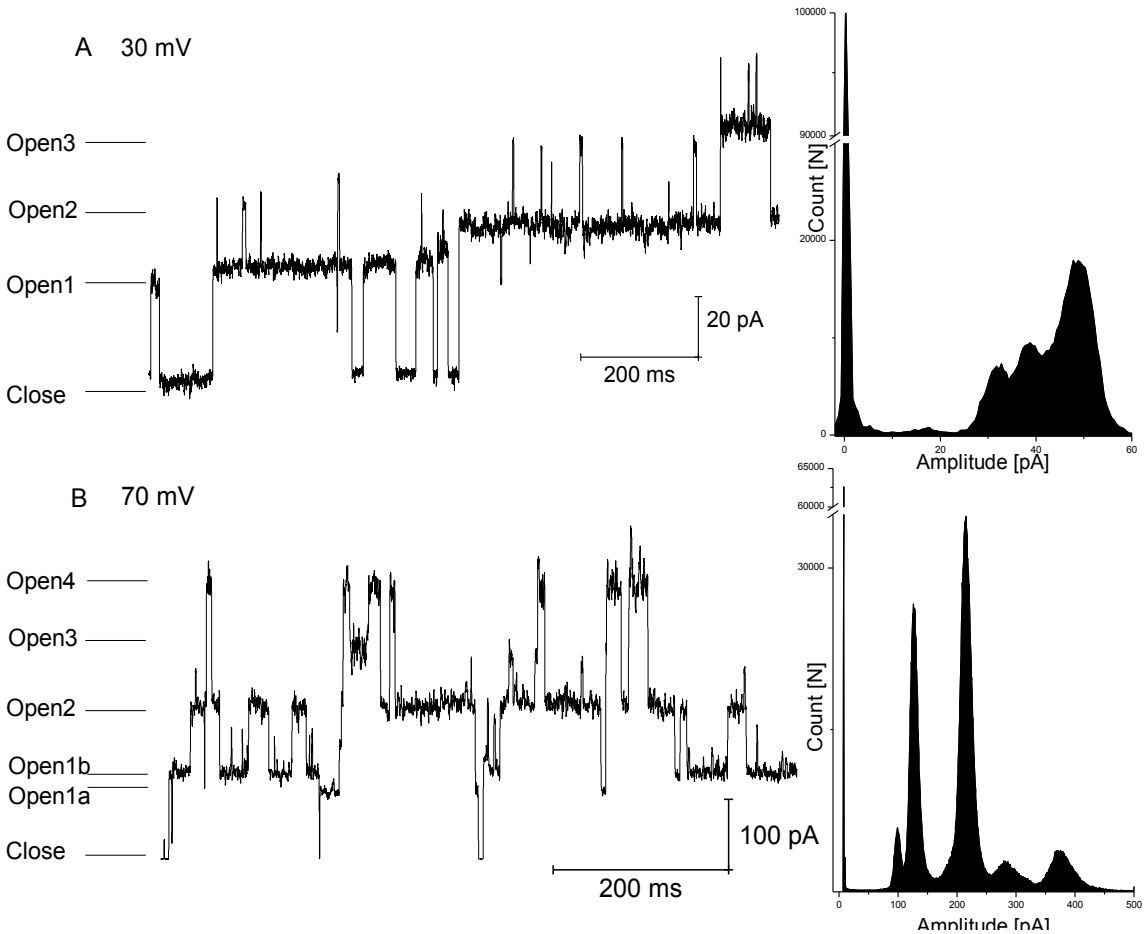

Figure 3.14: Representative current patterns of TMS6 (in 5 mM HEPES pH 5.0, 500 mM KCl, on both sides of the micropipette) (A) in the absence of 1 mM $MnCl_2$ (+30 mV) (B) in the presence of 1 mM $MnCl_2$ (+70 mV)

We also examined the channel–forming properties of both TMS6 peptides containing the mutation at His^{211}. Replacing His^{211} with alanine caused decrease in the channel–like activity. In H211A channel–like activity was rarely observed (in 13% of the experiments) in the presence of manganese ions. No channel–like activity was observed when His^{211} replaced with arginine.

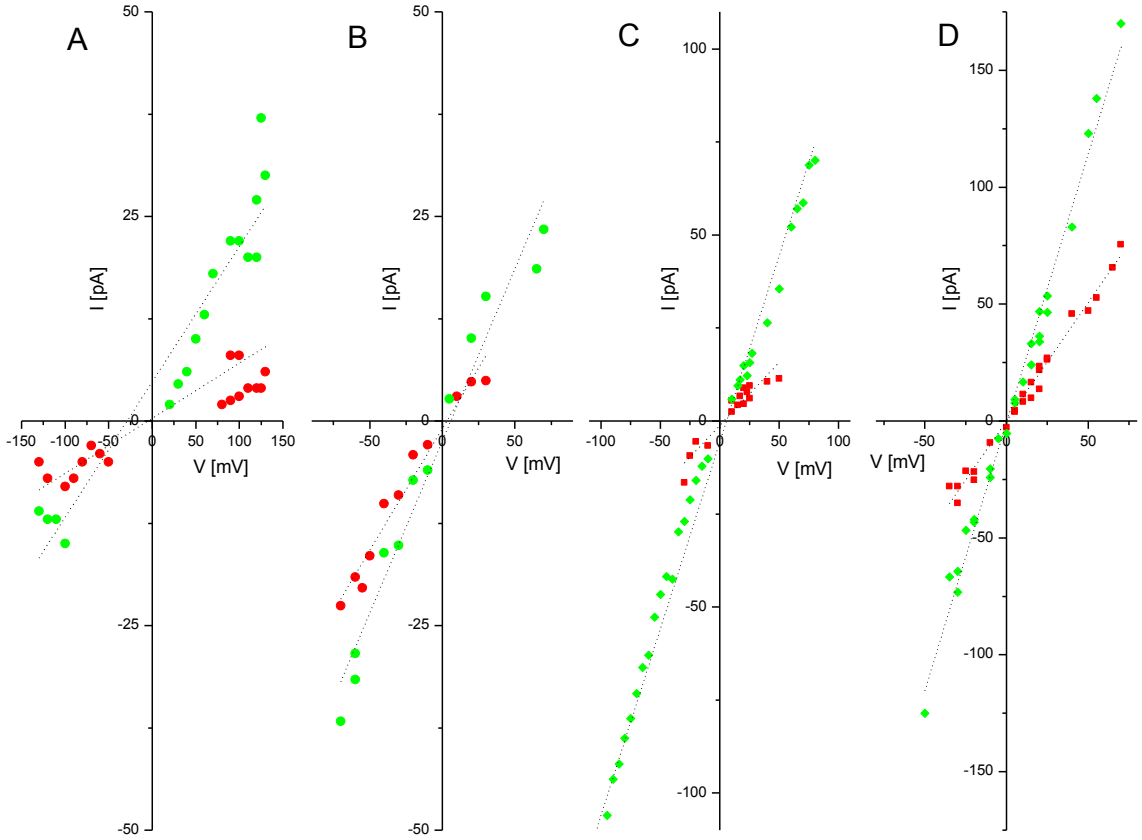

Figure 3.15 Current-voltage (I-V) relationship of ion channels formed by TMS6 peptides. Red circles represent open state O_1 and green circles open state O_2. (A) TMS6 pH 5.0 with 1 mM $MnCl_2$ on both sides (B) TMS6-OH pH 5.0 on both sides (C) TMS6-OH pH 5.0 with 1 mM $MnCl_2$ on both sides (D) TMS6-OH pH 5.0 on cis-side and pH 7.4 on trans-side, both sides with 1 mM $MnCl_2$, dotted lines show linear fit.

Measurements of reversal potential, at asymmetric KCl concentrations across the bilayer (0.5 M KCl on cis-side, 0.1 M KCl on trans-side, pH 5.0 on both sides), were performed for determination of ion selectivity of TMS6-OH. It was found that the reversal potential in the presence of manganese ions (V_{rev}= -11.5 ± 1.1 mV) did not differ significantly from the value measured in its absence (V_{rev}= -11.9 ± 3.2 mV). Thus, the permeability ratio calculated according to Goldman–Hodgkin–Katz equation [126] is almost identical in the presence (P_{Cation}/P_{Anion} = 2.02) and absence of manganese (P_{Cation}/P_{Anion} = 2.06). This finding denotes that the ion channels formed by TMS6-OH are weakly cation selective and may have comparable average diameters in the absence and presence of Mn^{2+} ions.

3.4 *Peptide mixtures*

In this section, interaction of TMS1 and TMS3, together with TMS6 was investigated for two reasons. (1) There is a hypothetical model of metal binding site within the MntH [112]. This model proposed formation of a binding pocket between four residues in TMS1 and TMS3. (2) Modeling of Nramp homologs on the LeuT/SLC6 structure suggests that in the structure of full-length protein TMS1 and TMS6 could form a pair of discontinuous helices, each composed of an extended peptide chain interconnecting two shorter α–helices [60].

3.4.1 CD analysis

The mixtures of segments were also studied under the same conditions as individual TMS. The spectra of the secondary structure of mixtures in buffer are shown in Fig. 3.1. The mixture of TMS 1+6 had comparable structure to TMS1 (Fig. 3.1, Table 2 in Appendix 1). TMS 1+3 mixture showed a dominantly random structure in aqueous solution, with some ordered structures (Fig. 3.1, Table 2 in Appendix 1). In comparison to the spectra of single peptides TMS1, TMS3 and TMS6, there is no visible sign of interaction between TMS1 and TMS3 or TMS1 and TMS6 in aqueous buffer. Moreover, no interaction leading to formation of any stable heterodimeric species was observed in the RP-HPLC profile (See section 3.1.2, Fig. 3.7, Table 3.2).

In TFE, the secondary structures of peptide mixtures were a combination of α-helix and β–strand (Fig. 4 in Appendix 1). The helical content for TMS 1+3 is slightly higher than for TMS 1+6 (24% and 20%, respectively). Both mixtures showed typical α-helix double negative maxima at 222 nm and 208 nm and a positive maximum around 192 nm (Fig. 4 in Appendix 1). In SDS the secondary structure was very different for each mixture (Fig. 3.16). TMS 1+6 showed α-helical structure at/above the CMC. At concentration below the CMC the spectrum is a combination of α-helix and β-strand with negative maximum at 222 nm, a shoulder at 208 nm and a positive maximum at 193 nm. The α-helical content increased with the increasing concentration of SDS in the sample from 23% (below CMC: 1 mM SDS) to 30% (at CMC: 8 mM SDS) and 32.5% (above CMC: 20 mM SDS). The β–strand content was decreasing with the growth of the α-helical content. The spectral characteristics of TMS 1+3 were influenced by the conformation of TMS3 at different concentrations of SDS. The most α-helicity in the mixture of TMS1 and TMS3 was observed below CMC (α-helix content ~ 42%). At CMC the α-helicity dropped to

20% whereas above CMC the helicity increased to 35%. TMS 1+3 showed two negative maxima at 222 nm and 208 nm with positive maximum at 193 nm for all three spectra, but the intensity of elipticity was the weakest at CMC. TMS1 and TMS3 did not show any interaction at the CMC, slight interaction was observed for TMS1 and TMS6. The combination of all three segments together showed some interaction under these experimental conditions (Fig. 5 in Appendix 1).

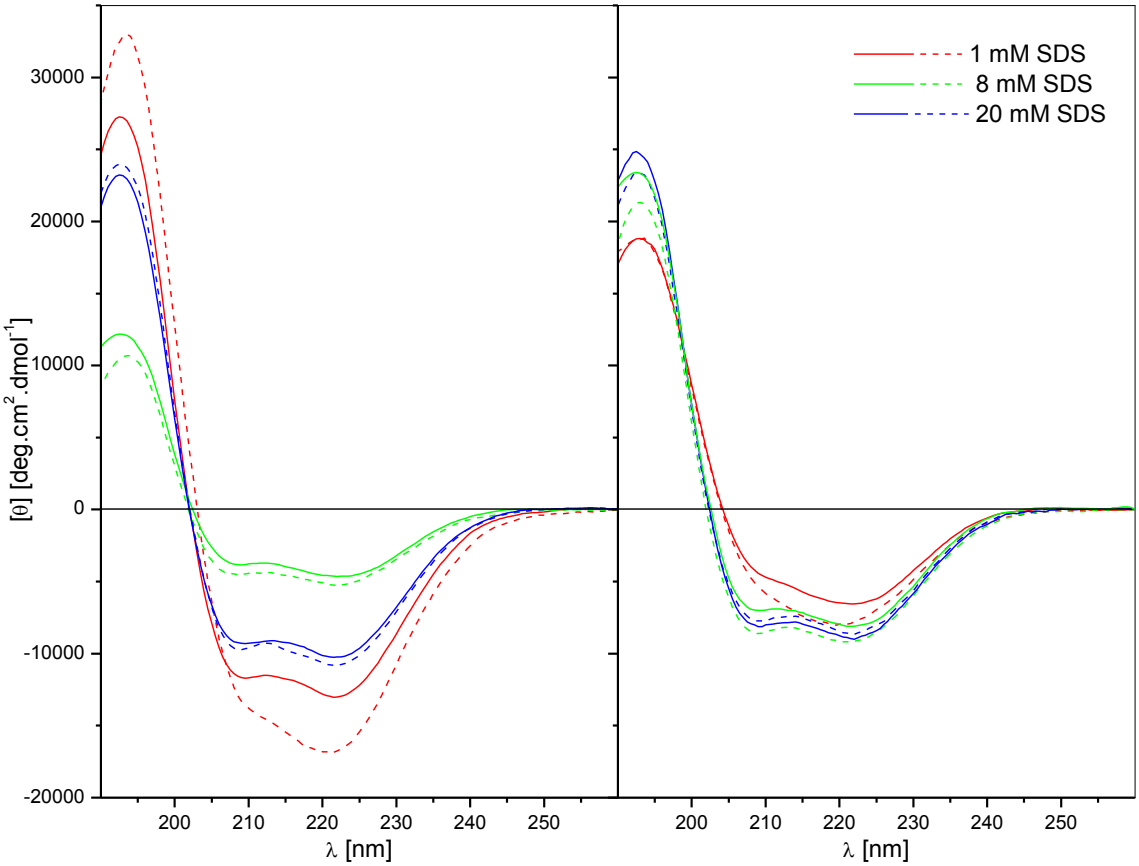

Figure 3.16 CD spectra of peptide mixtures in SDS; TMS 1+3 (left) TMS 1+6 (right)

Interaction of transmembrane segments was studied in lipid systems in order to determine the possible connection to the functional properties. The CD spectra of TMS mixtures normalized at 220 nm in different lipid systems are shown in Fig. 6 and Fig. 7 in Appendix 1, and the deconvolution analysis is shown in Table 2 in Appendix 1. The CD spectra of the mixtures of segments in DPhPC/DPhPG vesicles were compared with the calculated values. The calculated values were obtained from the addition of values for single segments of TMS1 and TMS3, TMS1 and TMS6 (Fig. 3.16). The change of spectra in DPhPC/DPhPG vesicles implies interaction between segments TMS1 and TMS3, and

between TMS1 and TMS6 as well. This interaction was even more emphasized in the presence on manganese ions (Fig. 3.17). Both TMS1 and TMS6 segments have one negatively charged residue and two positively charged ones, these positively charged termini may help the insertion and interaction in the lipid vesicles. In POPC/POPG vesicles TMS1 and TMS6 showed significant difference between the experimentally obtained and calculated spectra. On the other hand, in comparison to DPhPC/DPhPG vesicles, interaction between segments TMS1 and TMS3 in POPC/POPG was less pronounced (Fig. 8 in Appendix 1). The interaction between TMS1 and TMS3 in POPC/POPG was comparable to the interaction in POPE/POPG vesicles. No significant difference was observed in *E. coli* polar lipid extract for TMS1 and TMS3 or TMS 1 and TMS6 segments. The interaction of segments is dependent on the surrounding environment of the transmembrane segments. The interaction of segments was observed in membrane mimetic environment; on the other hand the interaction in lipid vesicles was strongly dependent on the composition of the vesicles.

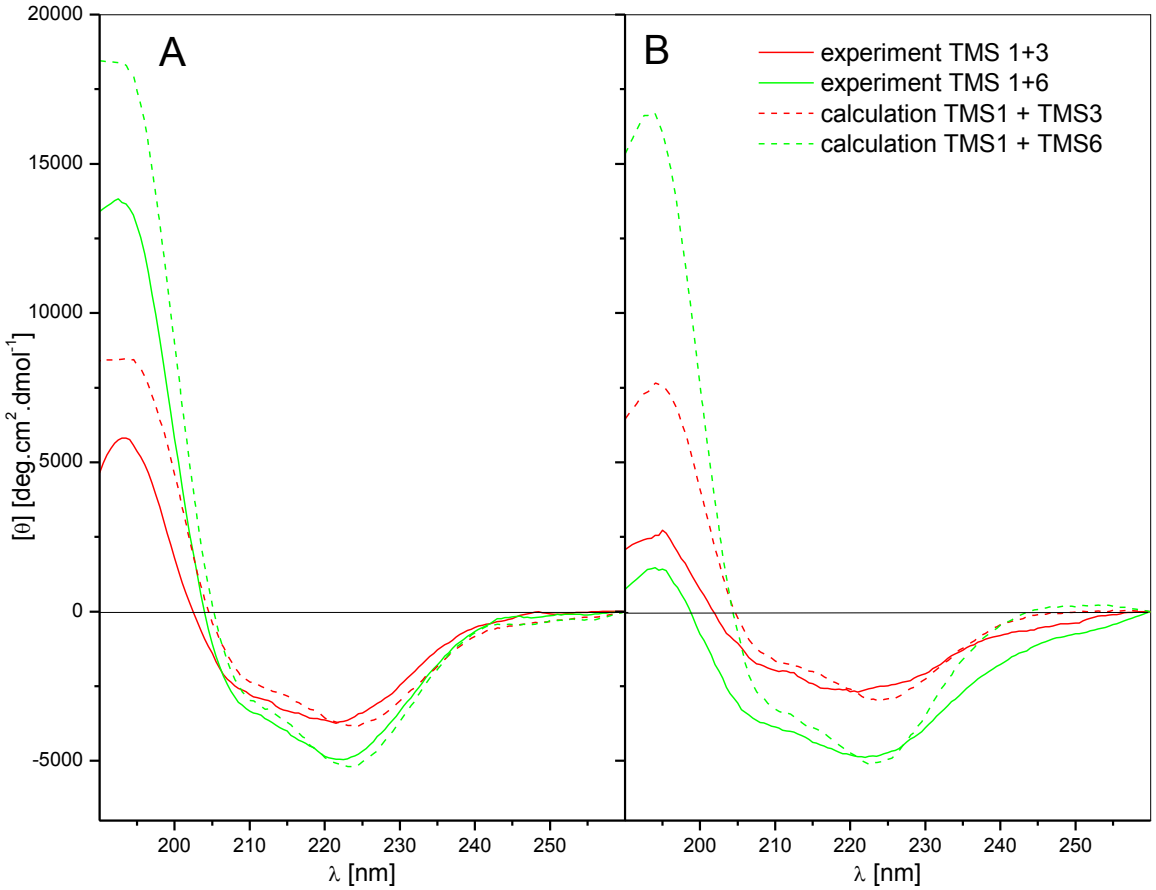

Figure 3.17 Comparative spectra of experimental vs. calculated data for mixtures of segments TMS1, TMS3 and TMS6 in DPhPC/DPhPG vesicles, (A) in the absence and (B) in the presence of 2 mM $MnCl_2$. Calculated data are normalized at 220 nm.

3.4.2 Electrophysiological studies using patch–clamp

In contrast to the individual TMS, in case of TMS 1+3 under the same experimental conditions, channel activity was rarely observed (in 23% of trial), mostly two-state channels with very low conductance (maximum ~ 10 pS). The mixture of TMS 1+6 under the same experimental conditions showed no channel activity. The disability of peptide mixture to form stable channels contrary to individual peptides might be due to the interaction of TMS in DPhPC/DPhPG vesicles in the presence of manganese (Fig. 3.17).

3.4.3 RP-HPLC analysis

According to the HPLC chromatograms mixtures of TMS 1+3 and TMS 1+6 do not interact together to form a detectable stable species in aqueous environment. The retention times reveal that TMS1 was the least hydrophobic peptide segment (lowest retention time). The highest retention time and therefore the highest hydrophobicity was observed for TMS3 (Fig. 3.18).

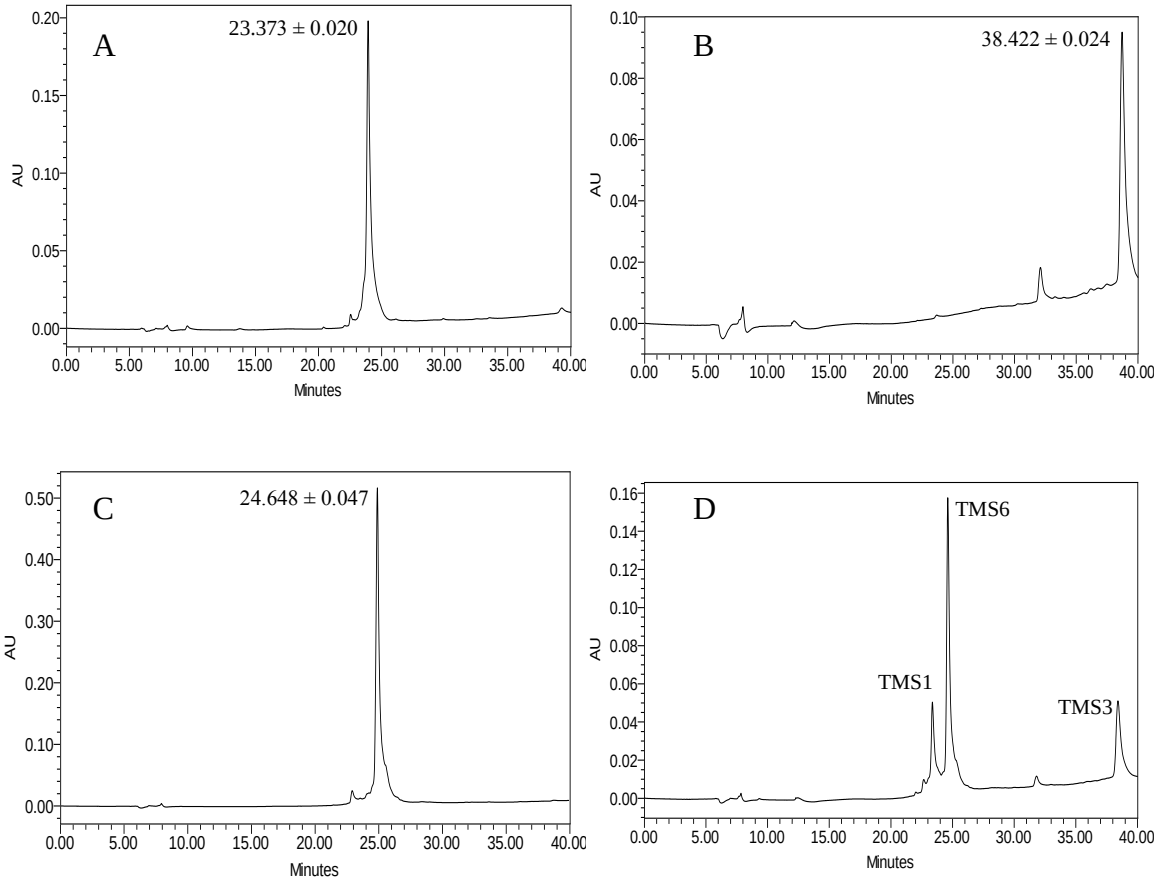

Figure 3.18 HPLC data of peptides (A) TMS1 (B) TMS3 (C) TMS6 and (D) mixture of TMS 1+3+6

4. Discussion

In order to obtain more information about individual transmembrane segments of *E.coli* MntH transporter (and consequently also about full-length protein), we studied secondary structure and interaction of synthetic peptides corresponding to the selected TMS in different environments (including buffer, detergent micelles and SUVs) using CD spectroscopy. Their functional properties were studied using patch clamp measurements.

As demonstrated by the far-UV CD spectra, generally the peptide structures in lipid vesicles compared to buffer, changed from unordered to more ordered and in some cases helical conformations. This conformational change indicated the insertion of peptides into the lipid bilayer and their interaction with lipids. Alternatively, in 50% TFE the peptides were dominantly monomeric, thus TFE promoted the formation of independent helical conformations (Fig. 3.2, Fig. 3.6 and Fig. 13 in Appendix 3). In comparison the secondary structure of peptides in all studied lipid vesicles (Fig. 3.3, Fig. 3.8 and Fig. 3.12) implies that peptide interaction with lipid membranes can lead to partial association of transmembrane segments. This is clearly substantiated by switching of the ratio of $\theta_{208}/\theta_{222}$ from values more than 1 (in 50% TFE) to less than 1 (in lipid vesicles). The same reversal of negative maxima ratio has been previously observed in coiled-coil motifs and oligomerization of helical peptides in lipid membrane milieus [142]. The change of CD spectra in lipid vesicles therefore supports the change in conformation of peptides following their interaction with the lipid bilayers. The structural information obtained from CD spectroscopy experiments supports the results obtained in previous study investigating TMS3 of eukaryotic Nramp in lipid vesicles. The perturbation of TMS3 to lipid packing was pH dependent. Overall, the helical content for TMS3 was low for pH 7, but in PC lipids under acidic pH the peptide was predominantly helical. The folding of the peptide is dependent on composition of phospholipids [110].

The ability of TMS1, TMS3, TMS6 and TMS6-OH to form conducting channels shows that at least these peptides are able to fully cross the membrane under our experimental conditions. Full insertion of peptides in the lipid membranes could be partly induced by the membrane potential, missing during CD experiments. The ion conducting units of peptides ion channel could be formed by a helical bundle composed of several peptide molecules corresponding to the transmembrane segments of MntH. The possible

association of the peptide helices is also supported by the CD spectra of this peptide in lipid membranes exhibited in Fig. 3.3, Fig. 3.8 and Fig. 3.12). The pH dependence of TMS6 ability to form ion channels is correlated to the secondary structure alternation of the orthologous segment from rat Nramp2 induced by pH changes [109].

Even though single peptides TMS1, TMS3 and TMS6 were able to form stable ion channels at least in the presence of manganese ions, the TMS mixtures did not show strong channel activity. It is suggested that the interaction of peptides followed by the conformational change of the segment mixture prevents the mixture from either fully spanning the lipid bilayer or forming appropriate conducting units within the membrane (Fig. 3.17). TMS 1+6 mixture in DPhPC/DPhPG vesicles showed similar helicity to TMS1, higher than TMS6 itself but contrary to the individual TMS, this mixture was not able to form an active ion channel. However, the ability to form ion channels need not to be directly correlated with the helix-forming propensity of the peptides or their affinity for lipid membranes as shown for individual TMS of UCP2 [97]. The helicity of TMS1+3 was in-between the helicities of the single peptides, and the channels of very low conductance were observed only rarely.

The ability of TMS3 to form Mn-dependent channels is quite interesting finding. TMS3 in MntH is putatively taking part in metal binding [112]. It is highly probable that the conducting units are oligomers of the peptides and therefore the transport pathway is different from that of intact monomeric protein. It has been already found in other proteins, that some of their transmembrane parts are able to behave like channels [96,97] and even to retain partly the substrate specificity of their original protein. At present, it is not clear, how universal this phenomenon could be and whether it is connected to the evolution of membrane proteins. There is no direct proof of this phenomenon, since there are not many known 3D structures of transport proteins. Regarding the known variable stoichiometry of Nramp/MntH proteins, the fact that TMS3 is able to create ion channels in membrane might support the possibility of a multimeric functional form for these proteins.

Even though the α-helicity in DPhPC/DPhPG vesicles for TMS6 is almost twice as high as for TMS6-OH, this difference has no significant influence on the ability of the peptide to form ion channels. Another interesting finding is the disability of H211R to form any channels. H211R attains the most helical conformation in DPhPC/DPhPG lipid vesicle milieus. Hence, the ability to form conducting channels is not directly related to α-

helical content in the peptides. It seems improbable that the peptide interacts better with the lipid membranes just due to the positive charge of its Arg residue (the membranes contain PG headgroups and are negatively charged). Addition of the divalent cation like manganese, which should reduce the negative surface charge on the membrane surface, increased the helicity of peptides but did not influence the order of their helical contents. Interestingly, the lack of correlation between helical content and channel-forming ability was observed in [97] as well.

The channel-forming properties of TMS6 further underline the importance of two conserved histidine residues for the full-length protein function. It has been previously reported that mutation of the homologous conserved histidine residues to Ala, Cys or Arg results in reduced or complete loss of function of Nramp2 *in vivo* [111]. Our findings at the level of individual TMS are in agreement with this study suggesting that His^{267} of the full–length Nramp2 plays an important role in the pH regulation of metal transport by this protein. The same authors suggest that protonation and/or deprotonation could favor conformational changes facilitating the transport function of Nramp2 [111]. Moreover, according to this study it seems unlikely that in full-length Nramp2, this pair of histidine residues could either bind metal ions directly or simply be part of a relay or channel enabling proton movement across the membrane [111].

Likewise, homologous His^{211} located within TMS6 of *E. coli* MntH was shown to regulate pH dependent metal uptake [60,63]. This residue was found to be accessible to solvent in full-length MntH, supporting a direct role of His^{211} protonation/deprotonation in transport cycle [60]. At the level of individual TMS, the mutation of His^{211} to Arg clearly prevented the peptide to form ion channels and even in the case of the mutation to Ala the stable channels were rarely formed. The channel activity of TMS6 suggests that His^{211} protonation/deprotonation could rather induce conformational changes facilitating transport function in this transmembrane segment (see Chapter 3.3.2).

Manganese ion (Mn^{2+}), as one of the metal substrates of MntH protein, induced minor changes in the CD spectra, mostly causing increase in helicity. Interaction of TMS 1+3 and TMS 1+6 in lipid vesicles was emphasized in the presence of manganese ions. From the patch clamp data, the effect of Mn^{2+} on ion conductance with TMS1 and TMS6 is not clear. In contrast, obvious effects of manganese ions on ion conductance have been observed for TMS3 [140]. As supported by the CD data, manganese ions can directly

interact with the peptide and therefore affect the association/dissociation properties of peptide oligomers. On the other hand, manganese ions interact with the lipid headgroups and thus influence the properties of the membrane and, indirectly, the conformation of peptide channels - possibly the membrane insertion step.

The selectivity of measured peptides TMS3 and TMS6-OH channels, with slight preference of cations (K^+) over anions (Cl^-), resembles the properties of yeast homolog Smf1p. Smf1p was reported to form an ion channel conducting monovalent cations (Na^+, K^+, Li^+) [56]. However, protons do not seem to be among the specific substrates of the peptide channel. TMS3 has three negatively charged residues, but the sequence of TMS6-OH does not provide obvious reasons for preference of cations, as there is only one negative residue (glutamate near the N-terminus of the peptide), and the two protonated histidines (at pH 5.0) are located near the center of the transmembrane part. The negatively charged lipid headgroups (PG in our case) could be in both cases involved in the channel structure (toroidal model as it for some small peptides [143]). It cannot be excluded that the lipids could play a structural and/or functional role in the whole protein as well as it was shown for cardiolipin and ADP/ATP carrier [144].

The formation of ion channels in lipid membranes by a transmembrane segment of secondary active transporter can naturally provoke questions about the relevance and implications of such a finding for the full-length transport protein. Several studies demonstrated that the individual TMS of transmembrane ion channels of known 3D structure can assume membrane-integrated conformations almost identical with the overall conformation of full-length proteins [76,90,94] and form native-like interactions leading to formation of ion channels [74] showing functional properties comparable to the native proteins [60,97,145]. Furthermore, there is a growing evidence that ion channels and active transporters might have common features [105,106]. It has been suggested that at least some of the secondary active transporters could contain a channel inside their structure, either with a single-file of binding sites [104], or with multiple gates rather than a single gate [146]. In addition, proteins from the Nramp family show striking properties, which can be described in terms of channel-like models. Metal-independent proton transport and proton-independent metal transport were described under specific conditions [1,141]. A spontaneous recurrent mutation G185R converts Nramp2 functionally into a calcium channel [147]. Moreover, metal-dependent proton slip can be also interpreted in terms of a channel-like mechanism [107].

5. Conclusion

The main objective of this study was to study the secondary structure and interactions of synthetic peptides corresponding to three selected transmembrane segments of *E. coli* MntH in model membranes and to investigate their functional properties. From multitude of CD experiments in different environments including among others also model membranes of diverse lipid compositions and corresponding patch clamp experiments, we can draw several important conclusions.

The individual synthetic peptides, corresponding to the three TMS, self-associate after the interaction with lipid vesicles. Moreover, all studied TMS are able to span the DPhPC/DPhPG membrane, since TMS6, TMS3 and TMS1 show ion channel activity. However, no direct correlation between the secondary structure of the TMS and functional properties was discovered. Furthermore, the properties of these slightly cation selective ion channels are to some extent analogical to the properties of full-length MntH protein: Manganese as physiological substrate of MntH is necessary for TMS3 channel formation. Manganese also modulate TMS6 channel function, the function of some TMS channels is pH dependent and His^{211} plays an important role in TMS6 channel- as well as full-length protein- function. Strikingly, although all transmembrane segments studied were able to form ion channels under certain experimental conditions, the TMS 1+3 or TMS 1+6 mixtures under the same experimental conditions were not.

Naturally, it is obvious that several interesting and fundamental questions arising from our results still wait to be answered:

First of all, how many other TMS of *E. coli* MntH show ion channel activity? By analogy to UCP2 carrier containing only two channel forming TMS of total six [97], we can expect that the number of TMS with ion channel activity is limited. Hence, it can be suggested that channel forming TMS domains are restricted to the functionally important TMS of the membrane transport proteins. However, this hypothesis remains to be verified.

Furthermore, it has been shown that selected TMS of *E. coli* MntH form cation selective channels, but further research should address the question to what extent this peptide-specific activity represents a functional aspect of full-length secondary-active transport protein. Regarding to certain similarity between ion-channels and transporter

[105] and especially to properties of Nramp/MntH, it should be certainly interesting to establish, whether specific structural parallels between those two exist.

Last but not least, the structure of the TMS channels needs to be verified. Our study suggested the approximate number of helices forming an active channel. This number of monomers forming a channel should be confirmed. Moreover the possible interaction between the monomers and specific lipids should be studied.

It is unfortunately evident that some of these questions cannot be answered without the knowledge of corresponding 3D structures.

References

[1] H.Gunshin, B.Mackenzie, U.V.Berger, Y.Gunshin, M.F.Romero, W.F.Boron, S.Nussberger, J.L.Gollan, and M.A.Hediger, Cloning and characterization of a mammalian proton-coupled metal-ion transporter, Nature 388 (1997) 482-488.

[2] N.Jabado, A.Jankowski, S.Dougaparsad, V.Picard, S.Grinstein, and P.Gros, Natural resistance to intracellular infections: natural resistance- associated macrophage protein 1 (Nramp1) functions as a pH-dependent manganese transporter at the phagosomal membrane, J. Exp. Med. 192 (2000) 1237-1248.

[3] M.F.Cellier, I.Bergevin, E.Boyer, and E.Richer, Polyphyletic origins of bacterial Nramp transporters, Trends Genet. 17 (2001) 365-370.

[4] B.Alberts, A.Johnson, J.Lewis, M.Raff, K.Roberts, and P.Walter, Molecular Biology of the Cell 4th Ed., Garland Science, New York and London, 2002.

[5] H.F.Lodish, A.Berk, Ch.A.Kaiser, M.Krieger, M.P.Scott, A.Bretscher, H.L.Ploegh, and P.Matsudaira, Molecular Cell Biology , Freeman, W.H., 2007.

[6] N.Nelson, Metal ion transporters and homeostasis, EMBO J. 18 (1999) 4361-4371.

[7] M.A.Hediger, Membrane permeability. The diversity of transmembrane transport processes, Curr. Opin. Cell Biol 9 (1997) 543-546.

[8] D.J.Eide, The molecular bioloy of metal ion transport in Saccharomyces cerevisiae, Annu. Rev. Nutr. 18 (1998) 441-469.

[9] D.Radisky and J.Kaplan, Regulation of transition metal transport across the yeast plasma membrane, J. Biol. Chem. 274 (1999) 4481-4484.

[10] J.J.R.Fraústo da Silva and R.J.P.Williams, The Biological Chemistry of the Elements: The Inorganic Chemistry of Life, Oxford University Press, 2001.

[11] F.Supek, L.Supekova, H.Nelson, and N.Nelson, Function of metal-ion homeostasis in the cell division cycles, mitochondrial protein processing, sensitivity to mycobacterial infection and brain function, J. Exp. Biol. 200 (pt2) (1997) 321-330.

[12] D.G.Kehres, A.Janakiraman, J.M.Slauch, and M.E.Maguire, SitABCD is the alkaline Mn(2+) transporter of Salmonella enterica serovar Typhimurium, J. Bacteriol. 184 (2002) 3159-3166.

[13] K.M.Papp, D.Kehres, and M.Maguire, Manganese and Iron Transport by Prokaryotic Nramp Family Transporters, in: M.Cellier and P.Gros (Eds.), The Nramp Family, Kluver Academic/Plenum Publishers, New York, 2004, pp.154-172.

[14] A.Sigel and H.Sigel, Metal Ions in Biological Systems, CRC Press, 1999.

[15] D.G.Kehres, M.L.Zaharik, B.B.Finlay, and M.E.Maguire, The NRAMP proteins of Salmonella typhimurium and Escherichia coli are selective manganese transporters involved in the response to reactive oxygen, Mol. Microbiol. 36 (2000) 1085-1100.

[16] G.C.Cotzias, P.S.Papavasiliou, R.Gellene, and R.B.Aronson, Parkinsonism and DOPA, Trans. Assoc. Am Physicians 81 (1968) 171-183.

[17] P.Courville, E.Urbankova, C.Rensing, R.Chaloupka, M.Quick, and M.Cellier, Functional study of Escherichia coli proton-dependent manganese transport, Biochem. Cell Biol. 84 (2006) 1058-1058.

[18] J.R.Forbes and P.Gros, Divalent-metal transport by NRAMP proteins at the interface of host- pathogen interactions, Trends Microbiol. 9 (2001) 397-403.

[19] G.Westin and W.Schaffner, A zinc-responsive factor interacts with a metal-regulated enhancer element (MRE) of the mouse metallothionein-I gene, EMBO J. 7 (1988) 3763-3770.

[20] H.K.Rudolph, A.Antebi, G.R.Fink, C.M.Buckley, T.E.Dorman, J.LeVitre, L.S.Davidow, J.I.Mao, and D.T.Moir, The yeast secretory pathway is perturbed by mutations in PMR1, a member of a Ca2+ ATPase family, Cell 58 (1989) 133-145.

[21] M.Ghislain, A.Goffeau, D.Halachmi, and Y.Eilam, Calcium homeostasis and transport are affected by disruption of cta3, a novel gene encoding Ca2(+)-ATPase in Schizosaccharomyces pombe, J Biol Chem. 265 (1990) 18400-18407.

[22] K.W.Cunningham and G.R.Fink, Calcineurin-dependent growth control in Saccharomyces cerevisiae mutants lacking PMC1, a homolog of plasma membrane Ca2+ ATPases, J Cell Biol 124 (1994) 351-363.

[23] A.Herchuelz and W.J.Malaisse, Regulation of calcium fluxes in rat pancreatic islets: dissimilar effects of glucose and of sodium ion accumulation, J Physiol 302 (1980) 263-280.

[24] M.Crompton, R.Moser, H.Ludi, and E.Carafoli, The interrelations between the transport of sodium and calcium in mitochondria of various mammalian tissues, Eur. J Biochem 82 (1978) 25-31.

[25] Y.Ohsumi and Y.Anraku, Calcium transport driven by a proton motive force in vacuolar membrane vesicles of Saccharomyces cerevisiae, J Biol Chem. 258 (1983) 5614-5617.

[26] E.K.Rooney and J.D.Gross, ATP-driven Ca2+/H+ antiport in acid vesicles from Dictyostelium, Proc. Natl. Acad. Sci U. S. A 89 (1992) 8025-8029.

[27] E.Lesuisse, F.Raguzzi, and R.R.Crichton, Iron uptake by the yeast Saccharomyces cerevisiae: involvement of a reduction step, J Gen. Microbiol. 133 (1987) 3229-3236.

[28] L.A.Gaither and D.J.Eide, Eukaryotic zinc transporters and their regulation, BioMetals 14 (2001) 251-270.

[29] L.E.Williams, J.K.Pittman, and J.L.Hall, Emerging mechanisms for heavy metal transport in plants, Biochim. Biophys Acta 1465 (2000) 104-126.

[30] H.Zhao and D.Eide, The ZRT2 gene encodes the low affinity zinc transporter in Saccharomyces cerevisiae, J Biol Chem. 271 (1996) 23203-23210.

[31] D.Eide, M.Broderius, J.Fett, and M.L.Guerinot, A novel iron-regulated metal transporter from plants identified by functional expression in yeast, Proc. Natl. Acad. Sci U. S. A 93 (1996) 5624-5628.

[32] M.L.Guerinot, The ZIP family of metal transporters, Biochim. Biophys Acta 1465 (2000) 190-198.

[33] S.Vidal, M.L.Tremblay, G.Govoni, S.Gauthier, G.Sebastiani, D.Malo, E.Skamene, M.Olivier, S.Jothy, and P.Gros, The Ity/Lsh/Bcg locus: natural resistance to infection with intracellular parasites is abrogated by disruption of the Nramp1 gene, J. Exp. Med. 182 (1995) 655-666.

[34] F.Supek, L.Supekova, H.Nelson, and N.Nelson, A yeast manganese transporter related to the macrophage protein involved in conferring resistance to mycobacteria, Proc. Natl. Acad. Sci. U. S. A 93 (1996) 5105-5110.

[35] M.F.Cellier, G.Prive, A.Belouchi, T.Kwan, V.Rodrigues, W.Chia, and P.Gros, Nramp defines a family of membrane proteins, Proc. Natl. Acad. Sci. U. S. A 92 (1995) 10089-10093.

[36] H.Makui, E.Roig, S.T.Cole, J.D.Helmann, P.Gros, and M.F.Cellier, Identification of the Escherichia coli K-12 Nramp orthologue (MntH) as a selective divalent metal ion transporter, Mol. Microbiol. 35 (2000) 1065-1078.

[37] J.R.Forbes and P.Gros, Iron, manganese, and cobalt transport by Nramp1 (Slc11a1) and Nramp2 (Slc11a2) expressed at the plasma membrane, Blood 102 (2003) 1884-1892.

[38] E.Richer, P.Courville, I.Bergevin, and M.F.Cellier, Horizontal gene transfer of "prototype" Nramp in bacteria, J. Mol. Evol. 57 (2003) 363-376.

[39] M.E.Portnoy, X.F.Liu, and V.C.Culotta, Saccharomyces cerevisiae expresses three functionally distinct homologues of the Nramp family of metal transporters, Mol. Cell. Biol. 20 (2000) 7893-7902.

[40] P.Courville, R.Chaloupka, and M.F.M.Cellier, Recent progress in structure-function analyses of Nramp proton-dependent metal-ion transporters, Biochem. Cell Biol. 84 (2006) 960-978.

[41] M.F.Cellier, G.Govoni, S.Vidal, T.Kwan, N.Groulx, J.Liu, F.Sanchez, E.Skamene, E.Schurr, and P.Gros, Human natural resistance-associated macrophage protein: cDNA cloning, chromosomal mapping, genomic organization, and tissue-specific expression, J. Exp. Med. 180 (1994) 1741-1752.

[42] J.E.Plant, J.M.Blackwell, A.D.O'Brien, D.J.Bradley, and A.A.Glynn, Are the Lsh and Ity disease resistance genes at one locus on mouse chromosome 1?, Nature 297 (1982) 510-511.

[43] S.Gruenheid, E.Pinner, M.Desjardins, and P.Gros, Natural resistance to infection with intracellular pathogens: the Nramp1 protein is recruited to the membrane of the phagosome, J. Exp. Med. 185 (1997) 717-730.

[44] G.Govoni, S.Gauthier, F.Billia, N.N.Iscove, and P.Gros, Cell-specific and inducible Nramp1 gene expression in mouse macrophages in vitro and in vivo, J. Leukoc. Biol. 62 (1997) 277-286.

[45] M.F.Cellier, C.Shustik, W.Dalton, E.Rich, J.Hu, D.Malo, E.Schurr, and P.Gros, Expression of the human NRAMP1 gene in professional primary phagocytes: studies in blood cells and in HL-60 promyelocytic leukemia, J. Leukoc. Biol. 61 (1997) 96-105.

[46] S.M.Vidal, D.Malo, K.Vogan, E.Skamene, and P.Gros, Natural resistance to infection with intracellular parasites: isolation of a candidate for Bcg, Cell 73 (1993) 469-485.

[47] A.Cohen, H.Nelson, and N.Nelson, Metal-Ion Transporters: From Yeast to Human Diseases, in: M.Cellier and P.Gros (Eds.), The Nramp Family, Kluver Academic/Plenum Publishers, New York, 2004.

[48] L.Abel, F.O.Sanchez, J.Oberti, N.V.Thuc, L.V.Hoa, V.D.Lap, E.Skamene, P.H.Lagrange, and E.Schurr, Susceptibility to leprosy is linked to the human NRAMP1 gene, J. Infect. Dis. 177 (1998) 133-145.

[49] R.Bellamy, C.Ruwende, T.Corrah, K.P.McAdam, H.C.Whittle, and A.V.Hill, Variations in the NRAMP1 gene and susceptibility to tuberculosis in West Africans, N. Engl. J. Med. 338 (1998) 640-644.

[50] S.Gruenheid, M.Cellier, S.Vidal, and P.Gros, Identification and characterization of a second mouse *Nramp* gene, Genomics 25 (1995) 514-525.

[51] S.Vidal, A.Belouchi, M.Cellier, B.Beatty, and P.Gros, Cloning and characterization of a second human NRAMP gene on chromosome 12q13, Mammalian Genome 6 (1995) 224-230.

[52] M.D.Fleming, C.C.Trenor, III, M.A.Su, D.Foernzler, D.R.Beier, W.F.Dietrich, and N.C.Andrews, Microcytic anaemia mice have a mutation in Nramp2, a candidate iron transporter gene, Nat. Genet. 16 (1997) 383-386.

[53] A.C.Chua and E.H.Morgan, Effects of iron deficiency and iron overload on manganese uptake and deposition in the brain and other organs of the rat, Biol. Trace Elem. Res. 55 (1996) 39-54.

[54] M.Tabuchi, T.Yoshimori, K.Yamaguchi, T.Yoshida, and F.Kishi, Human NRAMP2/DMT1, which mediates iron transport across endosomal membranes, is localized to late endosomes and lysosomes in HEp-2 cells, J. Biol. Chem. 275 (2000) 22220-22228.

[55] E.Luk, L.Jensen, and V.C.Culotta, The Role of Yeast Nramp Metal Transporter in Manganese and Iron Homeostasis, in: M.Cellier and P.Gros (Eds.), The Nramp Family, Kluver Academic/Plenum Publishers, New York, 2004.

[56] X.Z.Chen, J.B.Peng, A.Cohen, H.Nelson, N.Nelson, and M.A.Hediger, Yeast SMF1 mediates H(+)-coupled iron uptake with concomitant uncoupled cation currents, J. Biol. Chem. 274 (1999) 35089-35094.

[57] X.F.Liu, F.Supek, N.Nelson, and V.C.Culotta, Negative control of heavy metal uptake by the Saccharomyces cerevisiae BSD2 gene, J. Biol. Chem. 272 (1997) 11763-11769.

[58] A.H.West, D.J.Clark, J.Martin, W.Neupert, F.Hartl, and A.L.Horwich, Two related genes encoding extremely hydrophobic proteins suppress a lethal mutation in the yeast mitochondrial processing enhancing protein, J. Biol. Chem. 267 (1992) 24625-24633.

[59] A.Cohen, H.Nelson, and N.Nelson, The Family of SMF Metal Ion Transporters in Yeast Cells, J. Biol. Chem. 275 (2000) 33388-33394.

[60] P.Courville, E.Urbankova, C.Rensing, R.Chaloupka, M.Quick, and M.F.Cellier, Solute Carrier 11 Cation Symport Requires Distinct Residues in Transmembrane Helices 1 and 6, J. Biol. Chem. 283 (2008) 9651-9658.

[61] E.Richer, P.Courville, and Cellier M.F.M., Evolutionary Analysis of Nramp Family, in: M.Cellier and P.Gros (Eds.), The Nramp family, Landes Bioscience, Georgetown, TX, 2003.

[62] P.Courville, R.Chaloupka, F.Veyrier, and M.F.Cellier, Determination of Transmembrane Topology of the Escherichia coli Natural Resistance-associated Macrophage Protein (Nramp) Ortholog, J. Biol. Chem. 279 (2004) 3318-3326.

[63] R.Chaloupka, P.Courville, F.Veyrier, B.Knudsen, T.A.Tompkins, and M.F.Cellier, Identification of functional amino acids in the Nramp family by a combination of evolutionary analysis and biophysical studies of metal and proton cotransport in vivo, Biochemistry 44 (2005) 726-733.

[64] S.H.White, A.S.Ladokhin, S.Jayasinghe, and K.Hristova, How membranes shape protein structure, J. Biol. Chem. 276 (2001) 32395-32398.

[65] N.Bordag and S.Keller, [alpha]-Helical transmembrane peptides: A "Divide and Conquer" approach to membrane proteins, Chemistry and Physics of Lipids 163 (2010) 1-26.

[66] S.H.White and W.C.Wimley, Membrane protein folding and stability: physical principles, Annu. Rev. Biophys. Biomol. Struct. 28 (1999) 319-365.

[67] R.E.Jacobs and S.H.White, The nature of the hydrophobic binding of small peptides at the bilayer interface: implications for the insertion of transbilayer helices, Biochemistry 28 (1989) 3421-3437.

[68] J.L.Popot and D.M.Engelman, Membrane protein folding and oligomerization: the two-stage model, Biochemistry 29 (1990) 4031-4037.

[69] J.L.Popot, S.E.Gerchman, and D.M.Engelman, Refolding of bacteriorhodopsin in lipid bilayers. A thermodynamically controlled two-stage process, J Mol. Biol 198 (1987) 655-676.

[70] H.Furthmayr and V.T.Marchesi, Subunit structure of human erythrocyte glycophorin A, Biochemistry 15 (1976) 1137-1144.

[71] T.W.Kahn and D.M.Engelman, Bacteriorhodopsin can be refolded from two independently stable transmembrane helices and the complementary five-helix fragment, Biochemistry 31 (1992) 6144-6151.

[72] K.D.Ridge, S.S.Lee, and L.L.Yao, In vivo assembly of rhodopsin from expressed polypeptide fragments, Proc. Natl. Acad. Sci U. S. A 92 (1995) 3204-3208.

[73] J.Corbin, H.H.Wang, and M.P.Blanton, Identifying the cholesterol binding domain in the nicotinic acetylcholine receptor with [125I]azido-cholesterol, Biochim. Biophys Acta 1414 (1998) 65-74.

[74] D.Marsh, Peptide models for membrane channels, Biochem. J. 315 (Pt 2) (1996) 345-361.

[75] R.E.Galardy and Z.P.Kortylewicz, Synthesis of a docosapeptide comprising the hydrophobic membrane spanning region of glycophorin A, Int. J Pept. Protein Res. 26 (1985) 33-48.

[76] J.F.Hunt, T.N.Earnest, O.Bousche, K.Kalghatgi, K.Reilly, C.Horvath, K.J.Rothschild, and D.M.Engelman, A biophysical study of integral membrane protein folding, Biochemistry 36 (1997) 15156-15176.

[77] T.Lazarova, K.A.Brewin, K.Stoeber, and C.R.Robinson, Characterization of peptides corresponding to the seven transmembrane domains of human adenosine A2a receptor, Biochemistry 43 (2004) 12945-12954.

[78] J.F.Hunt, P.Rath, K.J.Rothschild, and D.M.Engelman, Spontaneous, pH-dependent membrane insertion of a transbilayer alpha-helix, Biochemistry 36 (1997) 15177-15192.

[79] A.M.Duarte, C.P.van Mierlo, and M.A.Hemminga, Molecular dynamics study of the solvation of an alpha-helical transmembrane peptide by DMSO, J Phys. Chem. B 112 (2008) 8664-8671.

[80] D.Roccatano, G.Colombo, M.Fioroni, and A.E.Mark, Mechanism by which 2,2,2-trifluoroethanol/water mixtures stabilize secondary-structure formation in peptides: a molecular dynamics study, Proc. Natl. Acad. Sci U. S. A 99 (2002) 12179-12184.

[81] H.Li, F.Li, H.Sun, and Z.M.Qian, Membrane-inserted conformation of transmembrane domain 4 of divalent-metal transporter, Biochem. J. 372 (2003) 757-766.

[82] H.Li, F.Li, Z.M.Qian, and H.Sun, Structure and topology of the transmembrane domain 4 of the divalent metal transporter in membrane-mimetic environments, Eur. J. Biochem. 271 (2004) 1938-1951.

[83] R.Xue, S.Wang, H.Qi, Y.Song, C.Wang, and F.Li, Structure analysis of the fourth transmembrane domain of Nramp1 in model membranes, BBA-Biomembranes 1778 (2008) 1444-1452.

[84] R.Xue, S.Wang, H.Qi, Y.Song, S.Xiao, C.Wang, and F.Li, Structure and topology of Slc11a1(164-191) with G169D mutation in membrane-mimetic environments, Journal of Structural Biology 165 (2009) 27-36.

[85] R.Renthal, An unfolding story of helical transmembrane proteins, Biochemistry 45 (2006) 14559-14566.

[86] M.A.Lemmon, J.M.Flanagan, J.F.Hunt, B.D.Adair, B.J.Bormann, C.E.Dempsey, and D.M.Engelman, Glycophorin A dimerization is driven by specific interactions between transmembrane alpha-helices, J Biol Chem. 267 (1992) 7683-7689.

[87] W.C.Wigley, S.Vijayakumar, J.D.Jones, C.Slaughter, and P.J.Thomas, Transmembrane domain of cystic fibrosis transmembrane conductance regulator: design, characterization, and secondary structure of synthetic peptides m1-m6, Biochemistry 37 (1998) 844-853.

[88] R.A.Melnyk, A.W.Partridge, and C.M.Deber, Retention of native-like oligomerization states in transmembrane segment peptides: application to the Escherichia coli aspartate receptor, Biochemistry 40 (2001) 11106-11113.

[89] S.O.Smith, D.Song, S.Shekar, M.Groesbeek, M.Ziliox, and S.Aimoto, Structure of the transmembrane dimer interface of glycophorin A in membrane bilayers, Biochemistry 40 (2001) 6553-6558.

[90] K.R.MacKenzie, J.H.Prestegard, and D.M.Engelman, A transmembrane helix dimer: structure and implications, Science 276 (1997) 131-133.

[91] M.M.Javadpour, M.Eilers, M.Groesbeek, and S.O.Smith, Helix packing in polytopic membrane proteins: role of glycine in transmembrane helix association, Biophys. J. 77 (1999) 1609-1618.

[92] M.Eilers, S.C.Shekar, T.Shieh, S.O.Smith, and P.J.Fleming, Internal packing of helical membrane proteins, Proc. Natl. Acad. Sci U. S. A 97 (2000) 5796-5801.

[93] S.O.Smith, M.Eilers, D.Song, E.Crocker, W.Ying, M.Groesbeek, G.Metz, M.Ziliox, and S.Aimoto, Implications of threonine hydrogen bonding in the glycophorin A transmembrane helix dimer, Biophys. J. 82 (2002) 2476-2486.

[94] K.R.MacKenzie and D.M.Engelman, Structure-based prediction of the stability of transmembrane helix-helix interactions: the sequence dependence of glycophorin A dimerization, Proc. Natl. Acad. Sci. U. S. A 95 (1998) 3583-3590.

[95] S.Oiki, W.Danho, and M.Montal, Channel protein engineering: synthetic 22-mer peptide from the primary structure of the voltage-sensitive sodium channel forms ionic channels in lipid bilayers, Proc. Natl. Acad. Sci. U. S. A 85 (1988) 2393-2397.

[96] M.Oblatt-Montal, G.L.Reddy, T.Iwamoto, J.M.Tomich, and M.Montal, Identification of an ion channel-forming motif in the primary structure of CFTR, the cystic fibrosis chloride channel, Proc. Natl. Acad. Sci. U. S. A 91 (1994) 1495-1499.

[97] H.Yamaguchi, M.Jelokhani-Niaraki, and H.Kodama, Second transmembrane domain of human uncoupling protein 2 is essential for its anion channel formation, FEBS Lett. 577 (2004) 299-304.

[98] D.Langosch, K.Hartung, E.Grell, E.Bamberg, and H.Betz, Ion channel formation by synthetic transmembrane segments of the inhibitory glycine receptor--a model study, Biochim. Biophys Acta 1063 (1991) 36-44.

[99] G.L.Reddy, T.Iwamoto, J.M.Tomich, and M.Montal, Synthetic peptides and four-helix bundle proteins as model systems for the pore-forming structure of channel proteins. II. Transmembrane segment M2 of the brain glycine receptor is a plausible candidate for the pore-lining structure, J Biol Chem. 268 (1993) 14608-14615.

[100] D.Gerber, N.Sal-Man, and Y.Shai, Two motifs within a transmembrane domain, one for homodimerization and the other for heterodimerization, J Biol Chem. 279 (2004) 21177-21182.

[101] A.Bennasroune, M.Fickova, A.Gardin, S.rrig-Grosch, D.Aunis, G.Cremel, and P.Hubert, Transmembrane peptides as inhibitors of ErbB receptor signaling, Mol. Biol Cell 15 (2004) 3464-3474.

[102] N.Sal-Man, D.Gerber, and Y.Shai, Hetero-assembly between all-L- and all-D-amino acid transmembrane domains: forces involved and implication for inactivation of membrane proteins, J Mol. Biol 344 (2004) 855-864.

[103] N.Sal-Man, D.Gerber, and Y.Shai, The identification of a minimal dimerization motif QXXS that enables homo- and hetero-association of transmembrane helices in vivo, J Biol Chem. 280 (2005) 27449-27457.

[104] A.Su, S.Mager, S.L.Mayo, and H.A.Lester, A multi-substrate single-file model for ion-coupled transporters, Biophys. J. 70 (1996) 762-777.

[105] L.J.DeFelice and T.Goswami, Transporters as channels, Annu. Rev. Physiol 69 (2007) 87-112.

[106] A.Accardi and C.Miller, Secondary active transport mediated by a prokaryotic homologue of ClC Cl- channels, Nature 427 (2004) 803-807.

[107] Y.Nevo and N.Nelson, The NRAMP family of metal-ion transporters, Biochim. Biophys. Acta 1763 (2006) 609-620.

[108] H.Li, J.D.Gu, and H.Sun, Structure, topology and assembly of a 32-mer peptide corresponding to the loop 3 and transmembrane domain 4 of divalent metal transporter (DMT1) in membrane-mimetic environments, J. Inorg. Biochem. 102 (2008) 1257-1266.

[109] S.Xiao, J.Li, Y.Wang, C.Wang, R.Xue, S.Wang, and F.Li, Identification of an "[alpha]-helix-extended segment-[alpha]-helix" conformation of the sixth transmembrane domain in DMT1, BBA-Biomembranes In Press, Uncorrected Proof () -

[110] H.Qi, L.Yang, R.Xue, Y.Song, S.Wang, and F.Li, The third and fourth transmembrane domains of Slc11a1: Comparison of their structures and positioning in phospholipid model membranes, Biopolymers 92 (2009) 52-64.

[111] S.Lam-Yuk-Tseung, G.Govoni, J.Forbes, and P.Gros, Iron transport by Nramp2/DMT1: pH regulation of transport by 2 histidines in transmembrane domain 6, Blood 101 (2003) 3699-3707.

[112] H.A.Haemig and R.J.Brooker, Importance of conserved acidic residues in MntH, the Nramp homolog of Escherichia coli, J. Membr. Biol. 201 (2004) 97-107.

[113] D.O.Daley, M.Rapp, E.Granseth, K.Melen, D.Drew, and H.G.von, Global topology analysis of the Escherichia coli inner membrane proteome, Science 308 (2005) 1321-1323.

[114] A.Cohen, Y.Nevo, and N.Nelson, The first external loop of the metal ion transporter DCT1 is involved in metal ion binding and specificity, Proc. Natl. Acad. Sci. U. S. A 100 (2003) 10694-10699.

[115] K.R.MacKenzie, Folding and Stability alpha-Helical Integral Membrane Proteins, Chemical Reviews 106 (2006) 1931-1977.

[116] E.Screpanti and C.Hunte, Discontinuous membrane helices in transport proteins and their correlation with function, J. Struct. Biol. 159 (2007) 261-267.

[117] E.Neher and B.Sakmann, Single-channel currents recorded from membrane of denervated frog muscle fibres, Nature 260 (1976) 799-802.

[118] E.Neher, B.Sakmann, and J.H.Steinbach, The extracellular patch clamp: a method for resolving currents through individual open channels in biological membranes, Pflugers Arch. 375 (1978) 219-228.

[119] O.P.Hamill, A.Marty, E.Neher, B.Sakmann, and F.J.Sigworth, Improved patch-clamp techniques for high-resolution current recording from cells and cell-free membrane patches, Pflugers Arch. 391 (1981) 85-100.

[120] D.J.Aidley and P.R.Stanfield, Ion Channels: Molecules in Action, Cambridge University Press, Cambridge, 1996.

[121] R.Coronado and R.Latorre, Phospholipid bilayers made from monolayers on patch-clamp pipettes, Biophys. J. 43 (1983) 231-236.

[122] G.Boheim, W.Hanke, F.J.Barrantes, H.Eibl, B.Sakmann, G.Fels, and A.Maelicke, Agonist-activated ionic channels in acetylcholine receptor reconstituted into planar lipid bilayers, Proc. Natl. Acad. Sci U. S. A 78 (1981) 3586-3590.

[123] I.R.Mellor and M.S.Sansom, Ion-channel properties of mastoparan, a 14-residue peptide from wasp venom, and of MP3, a 12-residue analogue, Proc. R. Soc Lond B Biol Sci 239 (1990) 383-400.

[124] M.S.Sansom, The biophysics of peptide models of ion channels, Prog. Biophys Mol. Biol 55 (1991) 139-235.

[125] P.Balaram, K.Krishna, M.Sukumar, I.R.Mellor, and M.S.Sansom, The properties of ion channels formed by zervamicins, Eur. Biophys J 21 (1992) 117-128.

[126] B.Hille, Ion Channels of Excitable Membranes, Sinauer Associates, Inc., 2001.

[127] R.A.Robinson and R.H.Stokes, Electrolyte Solutions, Butterworths, London, 1970.

[128] S.M.Kelly, T.J.Jess, and N.C.Price, How to study proteins by circular dichroism, Biochim. Biophys Acta 1751 (2005) 119-139.

[129] S.Harding and B.Chowdhry, Protein-Ligand Interactions: Structure and Spectroscopy, Oxford University Press, Oxford, England, 2001.

[130] T.E.Creighton, Protein folding: does diffusion determine the folding rate?, Curr. Biol 7 (1997) R380-R383.

[131] K.Park, A.Perczel, and G.D.Fasman, Differentiation between transmembrane helices and peripheral helices by the deconvolution of circular dichroism spectra of membrane proteins, Protein Sci. 1 (1992) 1032-1049.

[132] L.Whitmore and B.A.Wallace, DICHROWEB, an online server for protein secondary structure analyses from circular dichroism spectroscopic data, Nucleic Acids Res. 32 (2004) W668-W673.

[133] G.D.Fasman, Circular Dichroism and Conformational Analysis of Biomolecules, Plenum Press, New York, USA , 1996.

[134] N.Sreerama, R.W.Woody, and P.R.Callis, Theoretical-Study of the Crystal-Field Effects on the Transition Dipole-Moments in Methylated Adenines, J. Phys. Chem. 98 (1994) 10397-10407.

[135] B.A.Wallace, J.G.Lees, A.J.Orry, A.Lobley, and R.W.Janes, Analyses of circular dichroism spectra of membrane proteins, Protein Sci. 12 (2003) 875-884.

[136] S.Lindsay, High Performance Liquid Chromatogaphy, Wiley, West Sassex, England, 1992.

[137] L.R.Snyder, J.J.Kirkland, and J.W.Dolan, Introduction to Modern Liquid Chromatography, Wiley, Hoboken, New Jersey, 2010.

[138] L.Zhong and W.C.Johnson, Jr., Environment affects amino acid preference for secondary structure, Proc. Natl. Acad. Sci U. S. A 89 (1992) 4462-4465.

[139] P.Burkhard, J.Stetefeld, and S.V.Strelkov, Coiled coils: a highly versatile protein folding motif, Trends Cell Biol 11 (2001) 82-88.

[140] V.Nunukova, E.Urbankova, M.Jelokhani-Niaraki, and R.Chaloupka, Ion Channel Activity of Transmembrane Segment 3 of E. coli MntH in the Presence of Manganese, WDS'08 Proceedings of Contributed Papers Part III (2008) 147-151.

[141] B.Mackenzie, M.L.Ujwal, M.H.Chang, M.F.Romero, and M.A.Hediger, Divalent metal-ion transporter DMT1 mediates both H+ -coupled Fe2+ transport and uncoupled fluxes, Pflugers Arch. 451 (2006) 544-558.

[142] J.Taira, M.Jelokhani-Niaraki, S.Osada, F.Kato, and H.Kodama, Ion-Channel Formation Assisted by Electrostatic Interhelical Interactions in Covalently Dimerized Amphiphilic Helical Peptides, Biochemistry 47 (2008) 3705-3714.

[143] L.Yang, T.A.Harroun, T.M.Weiss, L.Ding, and H.W.Huang, Barrel-Stave Model or Toroidal Model? A Case Study on Melittin Pores, Biophys. J. 81 (2001) 1475-1485.

[144] B.Hoffmann, A.Stockl, M.Schlame, K.Beyer, and M.Klingenberg, The reconstituted ADP/ATP carrier activity has an absolute requirement for cardiolipin as shown in cysteine mutants, J. Biol. Chem. 269 (1994) 1940-1944.

[145] M.Jelokhani-Niaraki, R.S.Hodges, J.E.Meissner, U.E.Hassenstein, and L.Wheaton, Interaction of Gramicidin S and its Aromatic Amino Acid Analogues with Phospholipid Membranes, Biophys. J. (2008) biophysj-

[146] D.C.Gadsby, Ion transport: spot the difference, Nature 427 (2004) 795-797.

[147] H.Xu, J.Jin, L.J.DeFelice, N.C.Andrews, and D.E.Clapham, A spontaneous, recurrent mutation in divalent metal transporter-1 exposes a calcium entry pathway, PLoS Biol. 2 (2004) 378-386.

Appendix 1: Additional CD spectra and deconvolution analysis of TMS1 and peptide mixtures

Table 1 Deconvolution analysis of TMS1 spectra in different environments

	Secondary structure [%]			
	α−helix	β−strand	Turns	Unordered
buffer	7.0	35.5	22.5	35.0
+ 2 mM $MnCl_2$	7.2	35.8	23.1	33.9
50% TFE	25.8	24.5	20.8	29.0
+ 2 mM $MnCl_2$	38.0	16.1	28.7	17.4
1 mM SDS	23.7	31.9	16.3	28.1
+ 2 mM $MnCl_2$	25.7	29.5	17.8	27.1
8 mM SDS	27.4	29.9	15.4	27.3
+ 2 mM $MnCl_2$	29.9	25.2	18.2	26.6
20 mM SDS	27.6	28.8	16.5	27.1
+ 2 mM $MnCl_2$	30.4	24.6	18.7	26.3

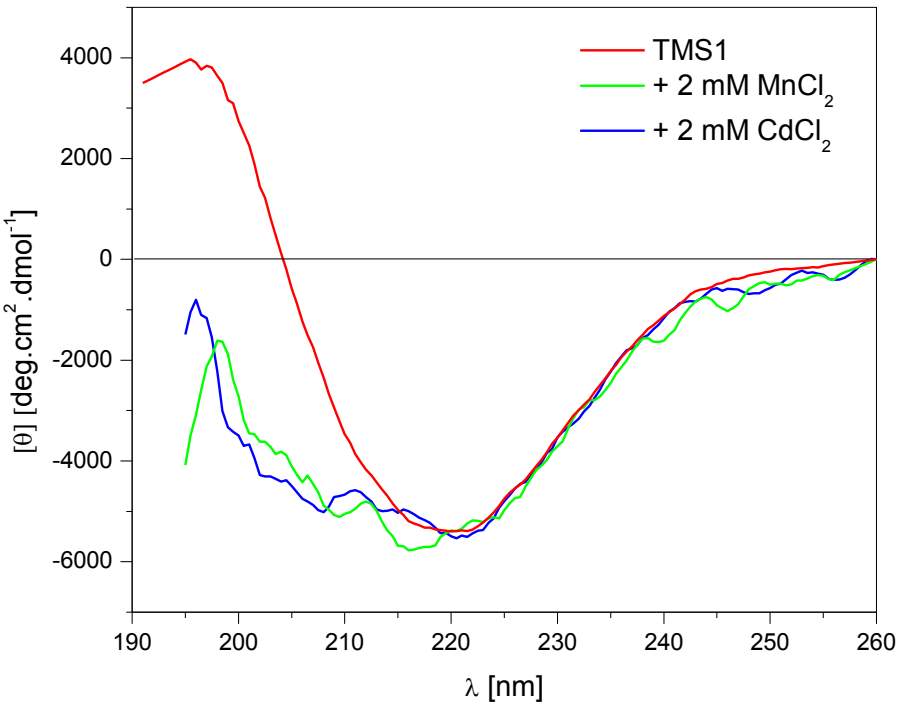

Figure 1 CD spectra of TMS1 in POPC/POPG vesicles

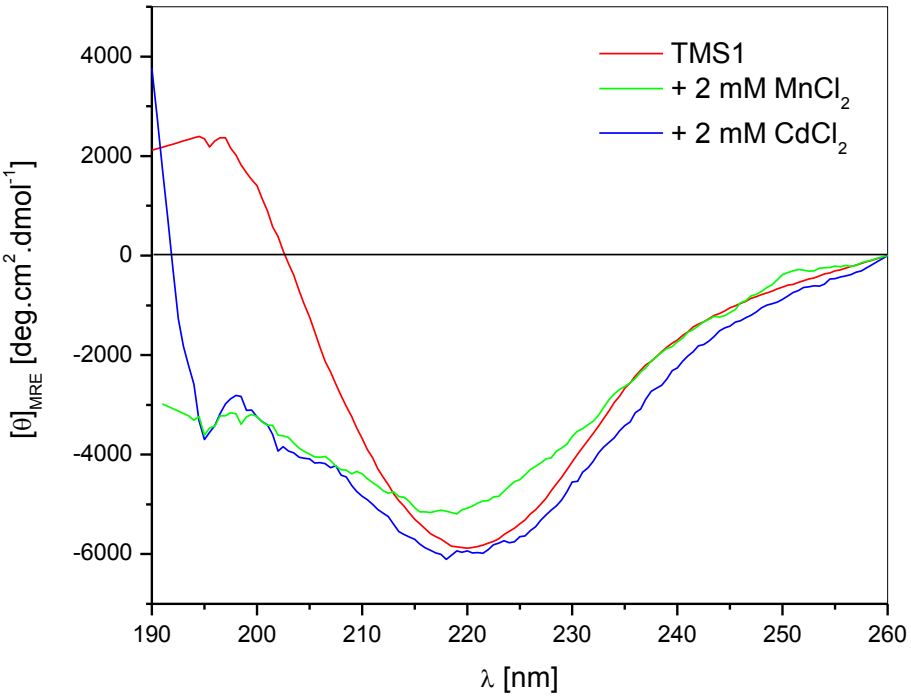

Figure 2 CD spectra of TMS1 in *E. coli* polar lipid extract vesicles

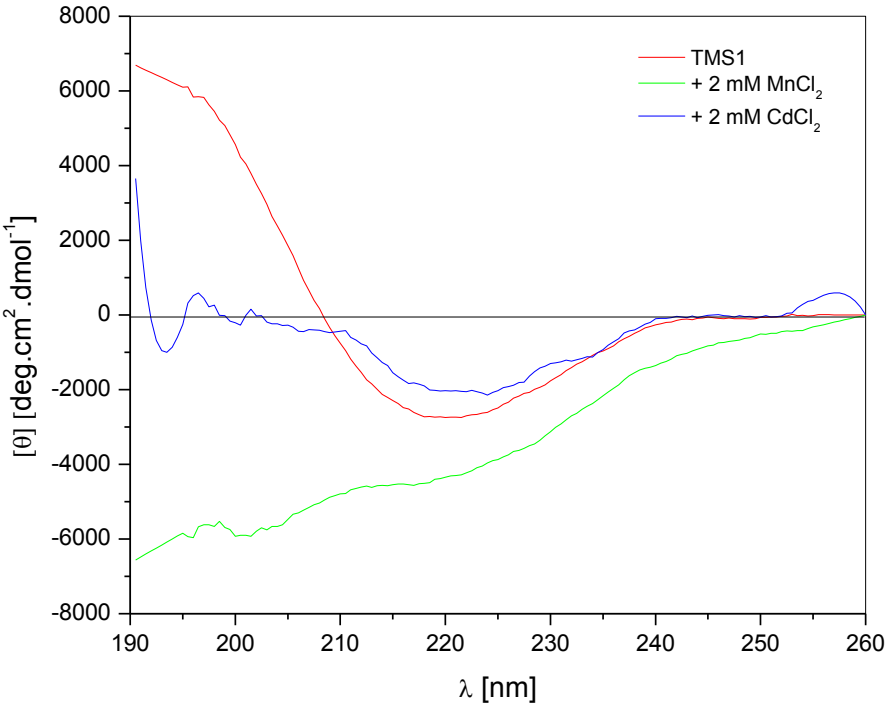

Figure 3 CD spectra of TMS1 in POPE/POPG vesicles

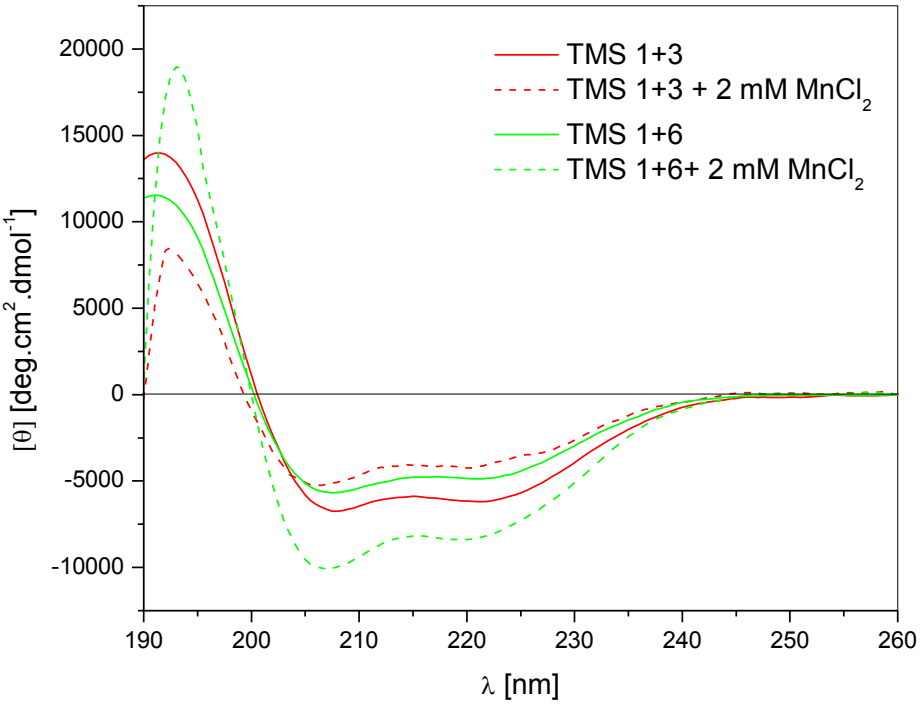

Figure 4 CD spectra of the mixtures TMS 1+3 and TMS 1+6 in 50% TFE

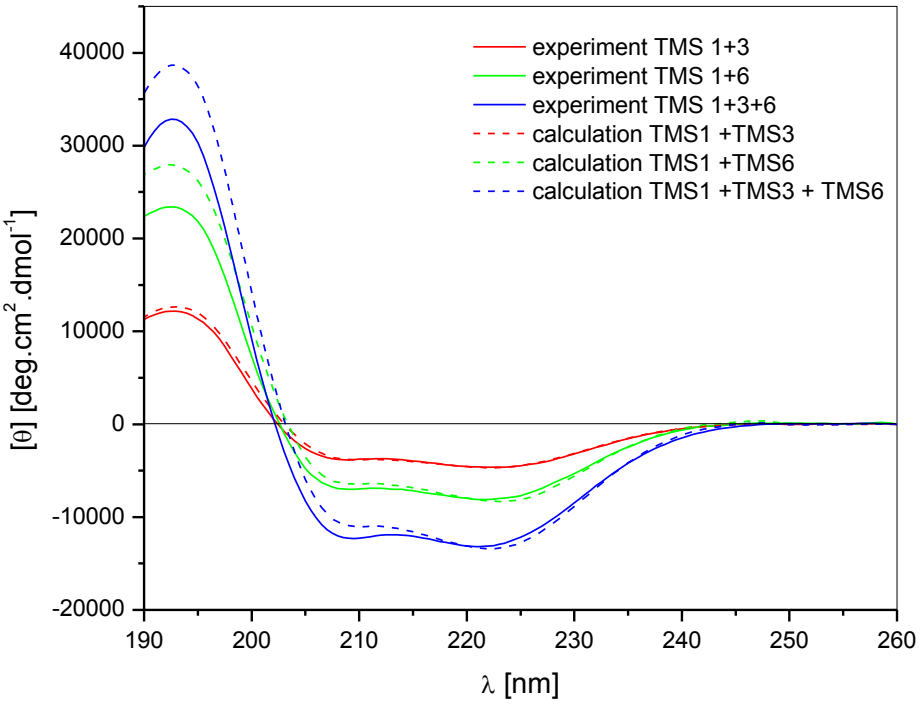

Figure 5 CD spectra from experiment vs. calculated data from segments TMS1, TMS3 and TMS6 in SDS at CMC**.** Calculated data are normalized to 220 nm to the experimental spectra.

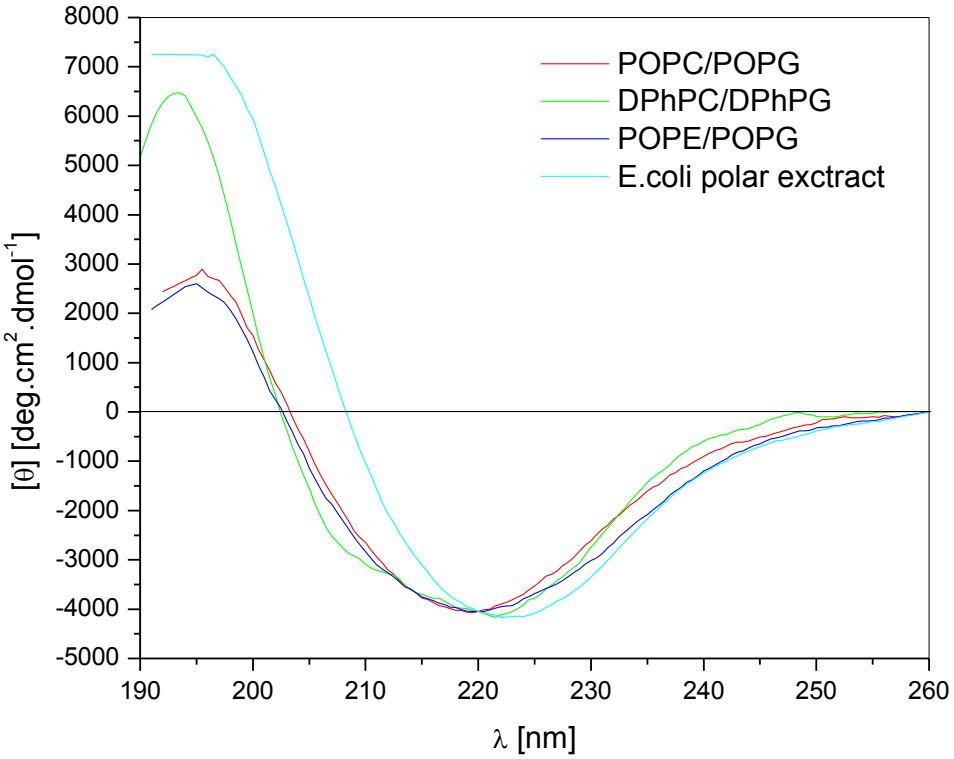

Figure 6 CD spectra of the mixture TMS 1+3 in all lipid systems. Spectra are normalize to 220 nm

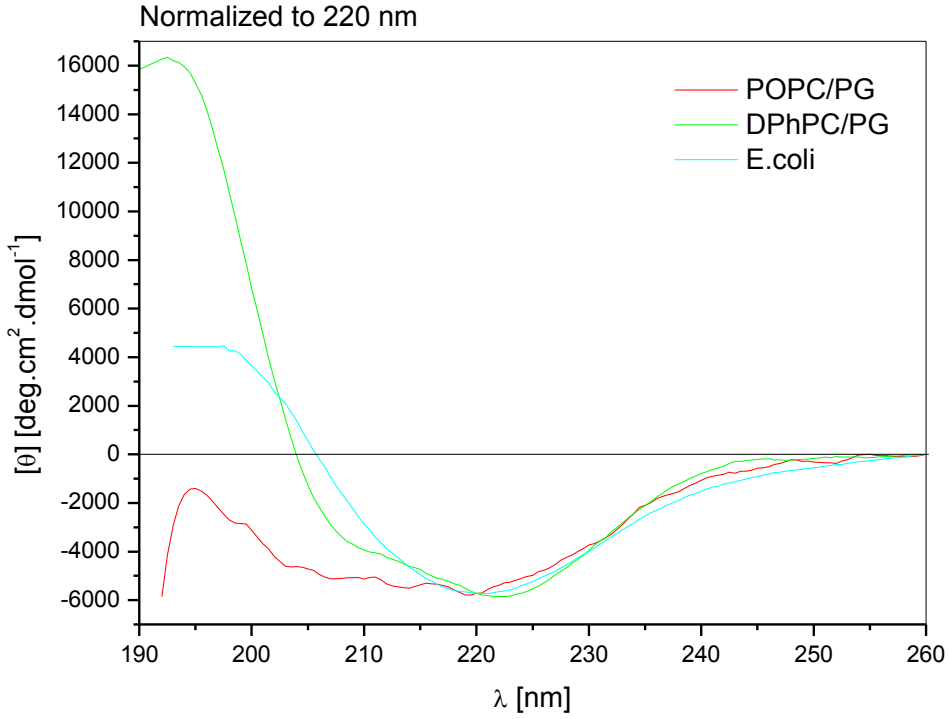

Figure 7 CD spectra of the mixture TMS 1+6 in all lipid systems. Spectra are normalize to 220 nm

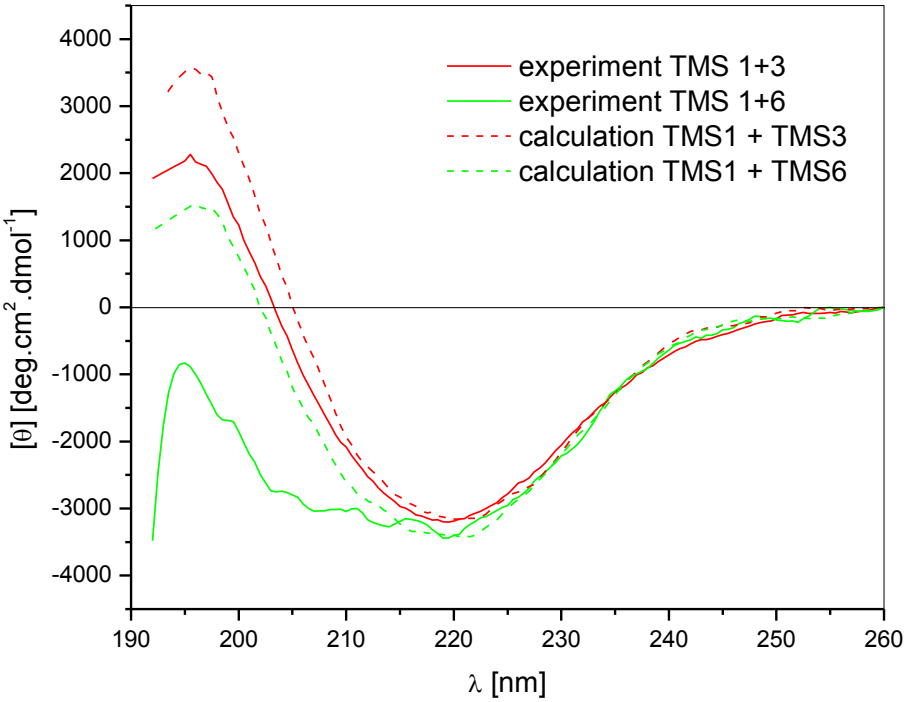

Figure 8 CD spectra from experiment vs. calculated data from segments TMS1, TMS3 and TMS6 in POPC/POPG vesicles. Calculated data are normalized to 220 nm to the experimental spectra.

Table 2 Deconvolution analysis of spectra of segment mixtures TMS 1+3 and TMS 1+6 in buffer and lipid vesicles

		Secondary structure [%]			
		α−helix	β−strand	Turns	Unordered
buffer	TMS 1+3	6.8	37.0	22.9	33.3
	+ 2 mM $MnCl_2$	6.7	36.8	22.5	34.0
	TMS 1+6	7.3	34.7	22.8	35.2
	+ 2 mM $MnCl_2$	6.7	36.9	22.5	33.9
E. coli polar extract	TMS 1+3	12.1	36.5	22.9	28.5
	+ 2 mM $MnCl_2$	13.2	32.4	23.3	31.1
	TMS 1+6	12.6	32.2	23.7	31.5
	+ 2 mM $MnCl_2$	10.0	30.8	23.7	35.5
DPhPC/DPhPG	TMS 1+3	13.6	33.5	21.7	31.2
	+ 2 mM $MnCl_2$	10.4	35.5	22.4	31.8
	TMS 1+6	18.4	33.6	19.1	29.0
	+ 2 mM $MnCl_2$	14.9	30.3	24.5	30.2
POPC/POPG	TMS 1+3	9.8	35.1	23.2	31.8
	+ 2 mM $MnCl_2$	9.3	35.4	23.1	32.3
	TMS 1+6	9.1	34.1	22.4	34.5
	+ 2 mM $MnCl_2$	10.5	34.7	22.9	31.9

Appendix 2: Additional CD spectra and deconvolution analysis of TMS3

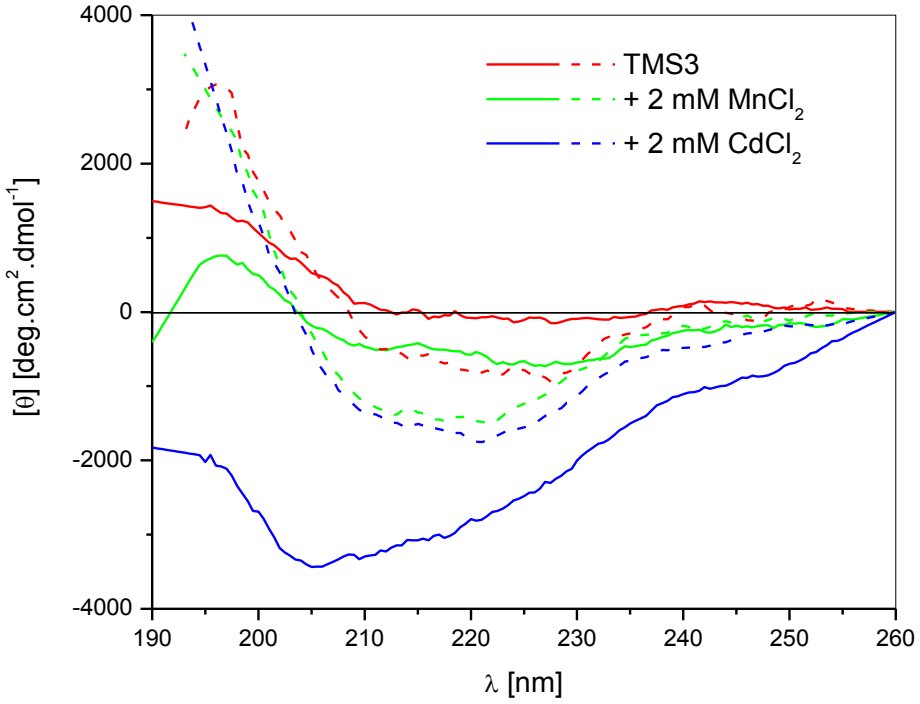

Figure 9 CD spectra of TMS3 in lipid vesicles with metal ions: DPhPC/DPhPG (solid lines) and POPC/POPG (dashed lines)

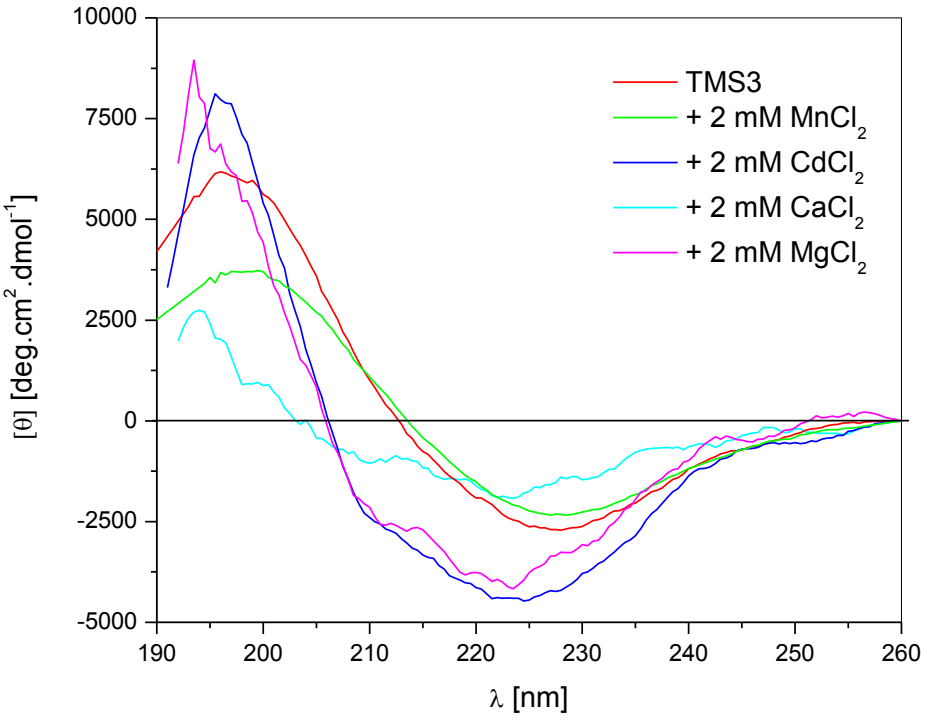

Figure 10 CD spectra of TMS3 in *E. coli* polar lipid extract SUV with different metal ions

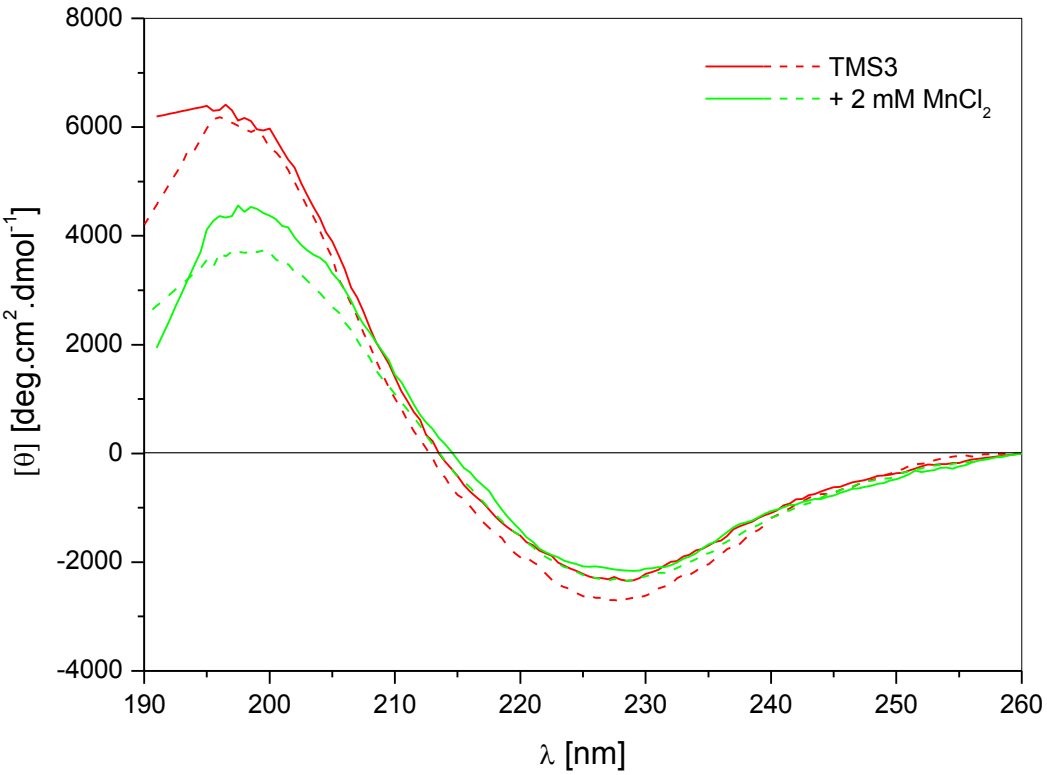

Figure 11 CD spectra of TMS3 in different temperatures: 25°C (dashed line) and 40°C (solid line)

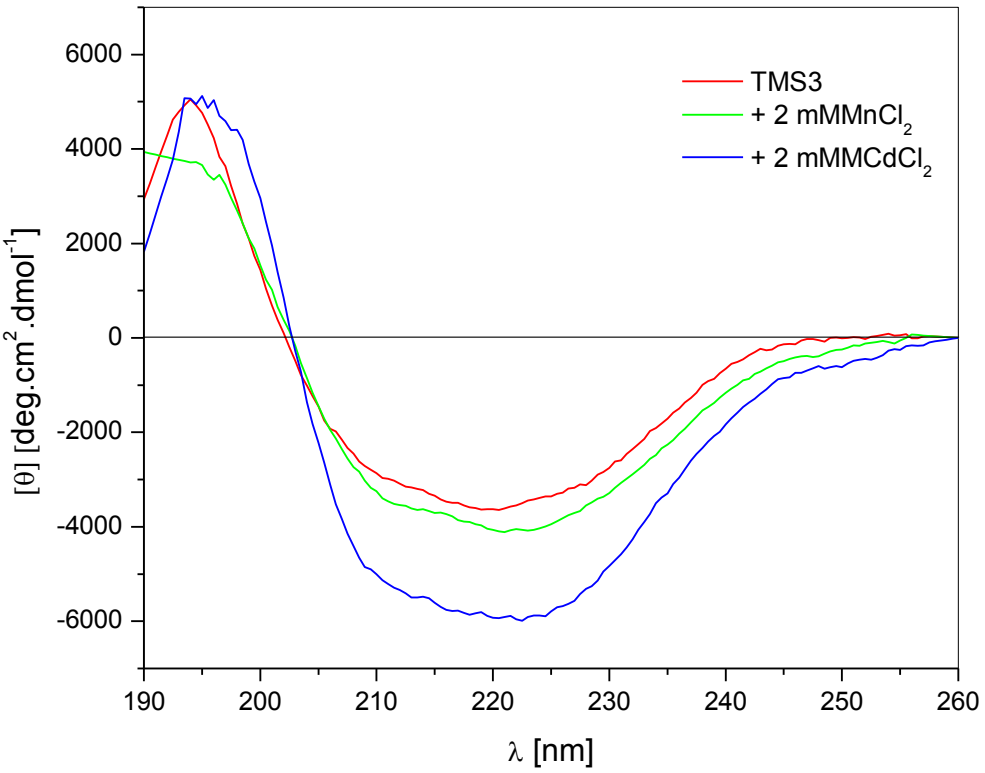

Figure 12 CD spectra of TMS3 in POPE/POPG vesicles with metal ions

Table 3 Deconvolution analysis of TMS3 spectra in TFE and SDS

	Secondary structure [%]			
	α−helix	β−strand	Turns	Unordered
3.5% TFE	6.7	39.8	22.4	31.3
+ 2 mM $MnCl_2$	9.7	36.7	24.7	28.9
25% TFE	11.8	35.8	22.0	30.6
+ 2 mM $MnCl_2$	11.8	35.1	22.8	30.3
50% TFE	27.2	25.0	20.0	27.8
+ 2 mM $MnCl_2$	29.9	24.7	18.3	27.1
1 mM SDS	51.5	9.3	17.5	21.8
+ 2 mM $MnCl_2$	50.3	11.7	15.7	22.4
8 mM SDS	52.0	12.9	14.2	20.9
+ 2 mM $MnCl_2$	50.2	12.8	15.7	21.3
20 mM SDS	41.1	17.6	16.6	24.7
+ 2 mM $MnCl_2$	37.2	21.1	15.1	26.5

Appendix 3: Additional CD spectra and deconvolution analysis of TMS6 peptides

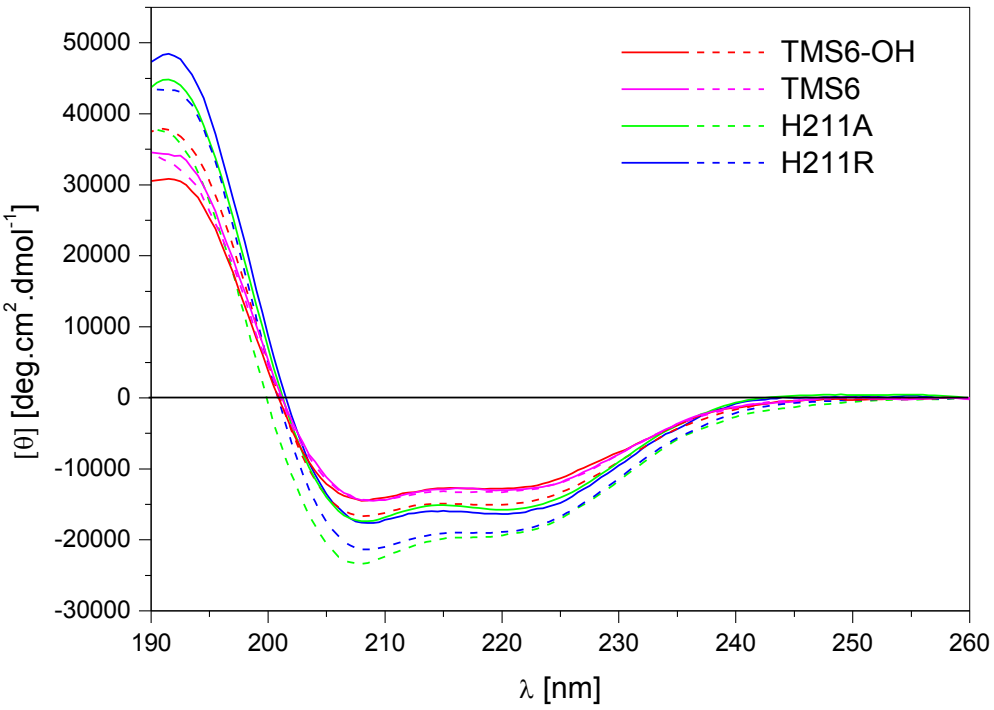

Figure 13 CD spectra of TMS6 peptides in 50 % TFE**.** Solid lines show spectra without manganese and dashed lines show spectra in the presence of 2 mM MnCl2. The spectra represent the average of two independent experiments.

Table 4 Deconvolution analysis of TMS6 peptides spectra in 50% TFE

	Secondary structure [%]			
	α−helix	β−strand	Turns	Unordered
TMS6-OH	41.2	16.6	17.3	24.9
+ 2 mM $MnCl_2$	46.4	15.0	15.8	22.9
TMS6	46.3	13.6	15.8	24.3
+ 2 mM $MnCl_2$	40.6	17.5	15.8	26.2
H211A	51.1	12.0	13.9	23.1
+ 2 mM $MnCl_2$	55.6	3.7	16.7	24.1
H211R	52.7	12.2	13.2	21.9
+ 2 mM $MnCl_2$	56.9	5.6	15.3	22.2

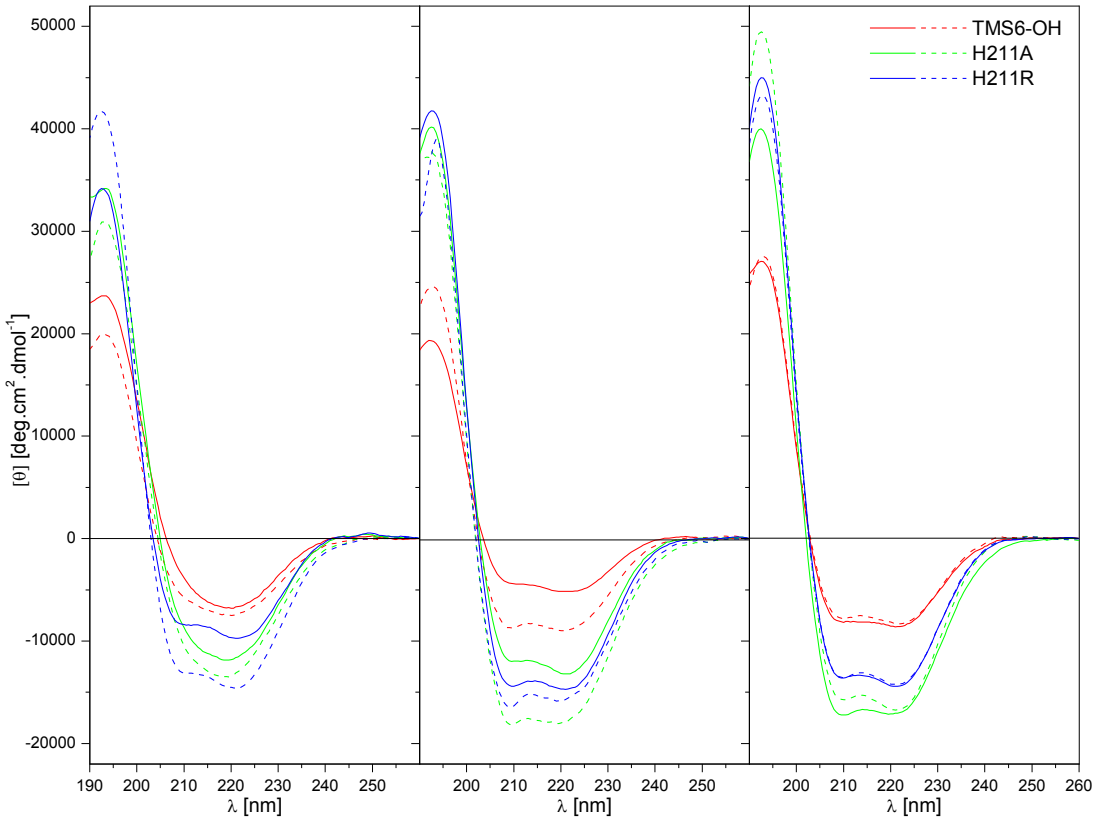

Figure 14 CD spectra of TMS6-OH and mutants in different concentrations of SDS

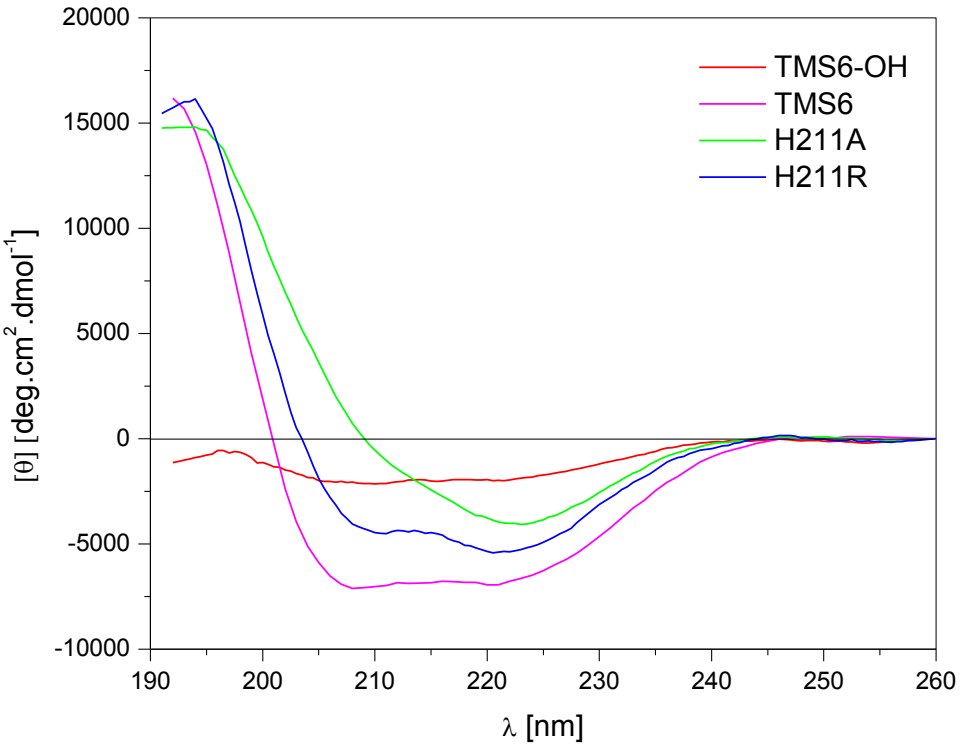

Figure 15 CD spectra of TMS6 peptides in POPC/POPG vesicles

Table 5 Deconvolution analysis of TMS6 peptides spectra in SDS

		Secondary structure [%]			
		α−helix	β−strand	Turns	Unordered
1 mM SDS	TMS6-OH	18.3	38.2	15.2	28.2
	+ 2 mM $MnCl_2$	22.7	31.7	18.0	27.7
	H211A	29.5	30.1	12.7	27.8
	+ 2 mM $MnCl_2$	31.6	26.5	16.3	25.6
	H211R	37.7	23.7	14.6	24.0
	+ 2 mM $MnCl_2$	46.9	17.8	13.6	21.7
8 mM SDS	TMS6-OH	22.2	32.8	16.9	28.1
	+ 2 mM $MnCl_2$	31.7	24.2	17.7	26.5
	H211A	54.4	9.5	15.0	21.1
	+ 2 mM $MnCl_2$	53.0	9.4	14.9	22.6
	H211R	50.8	13.9	13.7	21.7
	+ 2 mM $MnCl_2$	54.9	5.0	19.6	20.5
20 mM SDS	TMS6-OH	31.3	25.6	16.9	26.2
	+ 2 mM $MnCl_2$	32.2	24.8	17.2	25.9
	H211A	44.2	18.4	14.5	22.8
	+ 2 mM $MnCl_2$	56.3	10.7	13.3	19.7
	H211R	50.4	14.9	14.3	20.4
	+ 2 mM $MnCl_2$	50.0	14.5	14.5	21.1

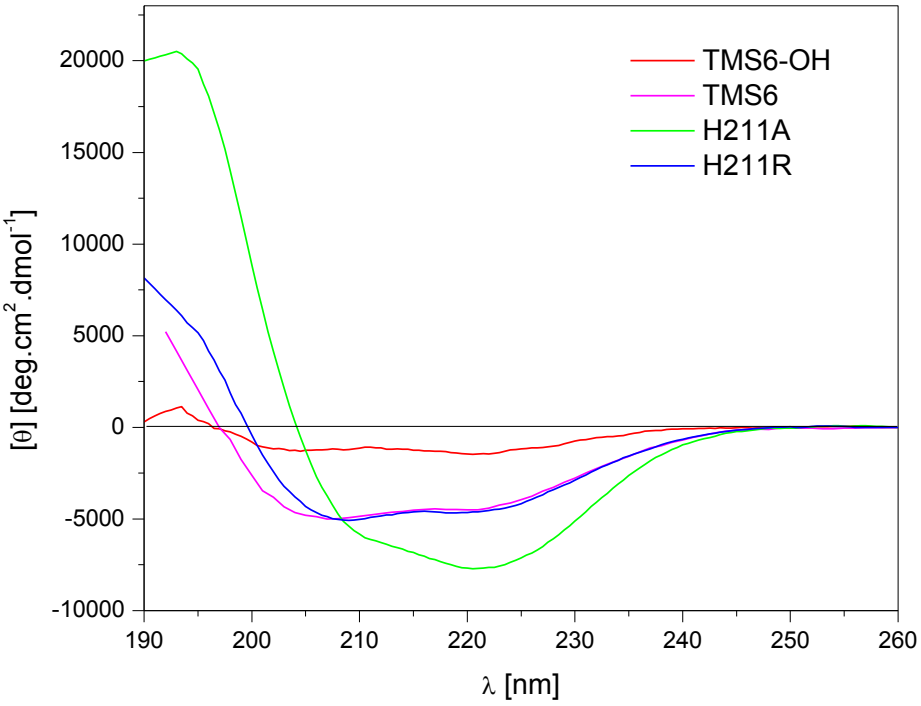

Figure 16 CD spectra of TMS6 peptides in *E. coli* polar lipid extract

Table 6 Deconvolution analysis of TMS6 peptides spectra in *E. coli* polar lipid extract

	Secondary structure [%]			
	α−helix	β−strand	Turns	Unordered
TMS6-OH	7.9	34.4	22.9	32.7
+ 2 mM $MnCl_2$	10.4	29.9	24.2	35.5
+ 2 mM $CdCl_2$	12.2	18.7	28.1	31.0
TMS6	16.3	28.1	25.2	30.5
+ 2 mM $MnCl_2$	13.1	29.4	24.8	32.6
H211A	24.0	30.2	17.7	28.0
+ 2 mM $MnCl_2$	18.5	26.1	22.9	32.5
+ 2 mM $CdCl_2$	8.7	36.2	24.6	30.5
H211R	13.3	31.6	21.1	32.0
+ 2 mM $MnCl_2$	11.4	32.3	23.8	32.5
+ 2 mM $CdCl_2$	10.5	31.7	25.3	32.6

Appendix 4: List of publications

Publications:

Nunukova V. Urbankova E., Jelokhani-Niaraki M., Chloupka R., Ion channel activity of transmembrane segment 6 of Escherichia coli proton-dependent manganese transporter, Biopolymers, 93(8): pp. 718-726, 2010

WDS 2008 ISBN 978-80-7378067-8

V. Nunukova, E.Urbankova, R.Chaloupka, M. Jelokhani-Niaraki, Ion Channel Activity of Transmembrane Segment 3 of E. coli MntH in the Presence of Manganese, in *WDS'08 Proceedings of Contributed Papers: Part III – Physics* (eds. J. Safrankova and J. Pavlu), Prague Matfyzpress, pp. 147-151, 2008

Published abstract:

Nunukova V., Jelokhani-Niaraki M., Urbankova E., Chloupka R., Biophysical properties of transmembrane segment 6 of E. coli MntH transporter, Biophysical Journal, Volume 96, Issue 3, Supplement 1, February 2009, Page 327a

Poster presentations:

April 24th-26th, 2009; Toronto, Ontario Canada, Chemical Biophysics Symposium 2009: Biophysical properties of transmembrane segment 6 of E. coli MntH transporter

February 28th- March 4th, 2009; Boston, USA, Biophysical Society 52nd Annual Meeting: Biophysical properties of transmembrane segment 6 of E. coli MntH transporter

February 15th-19th, 2008; Linz, Austria X. Annual Winter Workshop: Transmembrane segment 3 of *Escherichia coli* Nramp Ortholog forms ion channels in model membranes in the presence of manganese